UNIVERSITY OF TRENTO

Department of Mathematics

Doctoral School in Mathematics

Ph.D. Thesis

Different approaches to epidemics modelling: from theoretical analysis to real data

Advisor:

Prof. Andrea Pugliese

Candidate:

Sara Sottile

Academic Year 2021 - 2022

Abstract

This work aims at presenting different approaches to epidemics modelling. It consists of two main topics, which cover both theoretical and computational approaches to the development and analysis of mathematical models of infectious diseases.

The first half regards the formulation and the analysis of SAIRS (Susceptible - Asyptomatics infected - Infected symptomatic - Recovered - Susceptible) epidemic models, including the possibility of vaccination. In such a model, the presence of asymptomatic cases allows for a wider circulation of the disease in the population, since they often remain unidentified. The model is formulated as a system of ordinary differential equations (ODEs), for which we provided a complete global stability analysis. In particular, the rigorous proof of the global stability for the endemic equilibrium is a challenging mathematical problem, which we solved combining two different approaches: the classical Lyapunov stability theorem, and a geometric approach, which generalises the Poincaré-Bendixon theorem. Afterwards, the model has been generalised using heterogeneous networks, which may describe different groups of individuals or different cities. Thus, the role of asymptomatic and symptomatic infectious individuals is explicitly considered in the transmission pattern of the disease among the groups in which the population is divided. For this model, the global stability analysis has been developed using the graph-theoretic approach to find Lyapunov functions.

The second part of the thesis covers simulations based approaches to modelling heterogeneous humans interactions in epidemics. The first example we provide is an application with synthetic data. We investigate a stochastic SIR (Susceptible - Infected symptomatic - Recovered) dynamics on a network, by using a specialised version of the Gillespie algorithm. We provide a theoretical result on the probability of the extinction of the disease. Then, we demonstrate how important epidemic indices change as a function of the contagiousness of the disease and the connectivity of the network. The other two examples we show consist of real data applications. Both regard the cost-benefit analysis of the introduction of new influenza vaccines. The first one analysed the Italian scenario of the introduction of the Laive attenuated influenza vaccine quadrivalent (LAIVq) vaccine in the paediatric age (2-6 years). The second one analysed the Spanish scenario of the introduction of the Adjuvanted QIV (aQIV) vaccine in the older population (65+ years). Both analyses have been performed using a multi-group SEIR (Susceptible - Exposed - Infected - Recovered) epidemiological model divided by age classes. The real data used regard the demography, the disease related data and costs of the events in the considered country.

Acknowledgements

First and foremost, I would like to express my gratitude to my supervisor Prof. Andrea Pugliese, for his guidance, his continuous support, and patience through my Ph.D. studies.

Secondly, I would also like to thank Mattia Sensi, who has been a great source of support during these years. I am very grateful for his partnership, but most important, his friendship. Thirdly, I would like to thank Stefania Ottaviano for our collaboration over the last two years. Moreover, I am also thankful to all the other co-authors of my works.

Furthermore, I would like to thank the Ph.D. students at the University of Trento, for their friendship during the time we spent together. I am glad to have found not only colleagues but true friends during my permanence in Trento.

Finally, during these years I had also the strong support of my family and my friends outside the academia. I would like to thank not only my longtime friends for always being there, but also all the friends met during the university years. I need to thank my father and sister, who always encouraged me during all my studies and research.

Most importantly, I want to dedicate this thesis to my mother, who passed me on the love for mathematics. I hope she can be proud of my results.

Contents

1. Introduction

Starting with the research of Kermack and McKendrick [1], in the last century a huge amount of mathematical epidemic models have been formulated, analysed and applied to a variety of infectious diseases. The recent Covid-19 pandemic has demonstrated the extent to which the study of mathematical models of infectious disease is crucial to provide particularly effective tools to help policy-makers combat the spread of the disease. Many large scale data-driven simulations have been used to examine and forecast aspects of the current epidemic spreading [2, 3], as well as in other past epidemics [4, 5, 6]. However, the study of theoretical epidemic models able to catch the salient transmission patterns of an epidemic, but that are yet mathematical tractable, offers essential insight to understand the qualitative behaviour of the epidemic, and provides useful information for control policies.

1.1 The stability analysis problem

The most common mathematical approach to the subject of epidemics is the so called compartmental approach. This approach considers the population partitioned into compartments with respect to an ongoing epidemic. Usually, the evolution of infectious disease is formulated in terms of systems of ordinary differential equations (ODEs) [7, 8]. These models are named for the compartments involved and their evolution, such as SIR (Susceptible – Infected – Recovered), SIRS (Susceptible – Infected – Recovered – Susceptible), SEIR (Susceptible – Exposed – Infected – Recovered), and so on. The classical first step in the analysis of an epidemic model is the search for equilibria points, defined as the constant solutions of the model. Usually, epidemic models admit a single disease-free equilibrium and one or more endemic equilibria, characterised by a positive number of infected individuals. These models may exhibit various long-term behaviours, depending on the stability of such equilibria or on the existence of periodic solutions [9]. For models which do not admit periodic solutions, we may still observe different asymptotic behaviour. The simplest case occurs when the model admits at most two equilibria in the biologically relevant region, and their existence and stability depend on a threshold quantity, called basic reproduction number [10]. More complicated cases are, for examples, models where the endemic equilibria lose stability through Hopf bifurcation, or models with multiple endemic equilibria, possibly arising through the presence of a backward bifurcation [11]. However, also in the simplest cases determining the asymp-

totic behaviour could be arduous. The rigorous proof of global stability, especially for the positive endemic equilibrium, is a challenging mathematical problem for many disease models due to their complexity and high dimension [12]. The classical, and most commonly used method for global asymptotic stability (GAS) analysis is provided by the Lyapunov stability theorem and LaSalle's invariance principle. These approaches have been successfully applied, for example, to the SIR, SEIR and SIRS models (see, e.g. [12, 13, 14]). Unfortunately, it is often difficult to construct such Lyapunov functions and no general method is available. However, some classes of Lyapunov functions have proven useful. For example, a well known form of Lyapunov functions used in the literature of mathematical biology is

$$V(x) = \sum_{i=1,\dots,n} c_i x_i^* \left(\frac{x_i}{x_i^*} - 1 - \ln \frac{x_i}{x_i^*} \right),$$

coming from the first integral of a Lotka–Volterra system [15, 16]. Shuai and van den Driessche [12] have presented some general methods for building Lyapunov functions for epidemic models: a matrix-theoretic method using the Perron eigenvector, applied to prove the global stability of the disease-free equilibrium and a graph-theoretical method, discussed below, to prove the global stability of the endemic equilibrium.

Other techniques have appeared in literature and were successfully applied to prove global stability arguments for various epidemic models. For example, the Li–Muldowney geometric approach [17, 18] was used to determine the global asymptotic stability of the SEIR and SEIRS models [19, 20, 21], of some epidemic models with bi-linear incidence [22], as well as of SIR and SEIR epidemic models with information dependent vaccination [23, 24]. Applications of Li–Muldowney geometric approach can also be found in population dynamics [25].

The stability analysis get more complicated as we relax the assumptions on the model, e.g. if we consider heterogeneity in the interactions. As in the homogeneous mixing case, the stability analysis of the equilibrium points of the system under investigation allows to understand its long-term behaviour and, hence, to obtain some insight into how the prevalence of an endemic disease depends on the parameters of the model [26] and, in this case, also on the network topology. The problem of existence and global stability, especially for the endemic equilibrium, for many complex multi-group models remains an open question, or requires cumbersome conditions [27]. In this framework, Guo et al. [28, 29] and Li and Shuai [30] developed a graph-theoretic method to find Lyapunov functions for some multi-group epidemic models which has allowed to obtain various results on the global dynamics of SIRS-type models [31, 32] and SEIRS-type models [33]. In this thesis, an example is provided in Chapter 3.

The investigation of the global stability has not only a theoretical mathematical interests. Indeed, understanding the behaviour of a relatively simple epidemic models can be useful also for interpreting results from data-driven models [34].

1.2 The role of asymptomatic infections

Unlike the more famous and studied epidemic models, much less attention has been paid to SAIR(S)-type models, i.e. models that include asymptomatic infections. Thus, we think that a deeper understanding of these kind of models is needed, and could prove to be very useful in the epidemiological field. Indeed, in various communicable diseases, such as influenza, cholera, shigella and Covid-19, an understanding of the infection transmission by asymptomatic individuals may be crucial in determining the overall pattern of the epidemic dynamics [35, 36]. In our interpretation an SAIRS models differs from SEIRS models, since individuals in A can transmit the infection. It differs from models that distinguish between severe and mild infections, since individuals from A may other enter I or directly recover entering R; in this sense, the class A includes both pre-symptomatic and asymptomatic infected, considered in several models for Covid-19 infections (see, for instance, [3]).

Although models incorporating asymptomatic individuals already exist in the literature [37, 38, 35], they have not been analytically investigated as thoroughly as more famous compartmental models. Since these types of models have been receiving much more attention lately, we believe they deserve a deeper understanding from a theoretical point of view. Thus, we aim to partially fill this gap and provide a stability analysis of both the SAIRS epidemic model and its multi-group counterpart, presented in the first two chapters of this work. We remark that our primary aim is to provide a global stability analysis under different mathematical assumptions to study some variations of the original SAIRS model, which is lacking in the literature. However, we think that this study may reveal useful also for data-driven models, in which the assumptions considered should be those that best fit the disease under investigation and the available medical knowledge.

1.3 Heterogeneity in epidemic models

Classic epidemiological models are generally based on the assumption of the "mass-mixing", which means all the individuals have a uniform contact pattern. While such an assumption considerably simplifies the models, it can be more realistic to take into account heterogeneous interactions among the population.

Heterogeneity may enter in several aspects of disease transmission processes [39, 40, 41], such as spatial distribution of populations, different susceptibility among age groups or different social behaviour among groups for sexually transmitted diseases.

One of the simplest techniques of introducing heterogeneity effects is to divide the population into sub-populations [42], which describe different cities, species, or age groups. In this context, individuals are subdivided into groups, but are identical within each group and assumed to be homogeneously mixing within the compartment, and equally connected outwards the compartments.

These kind of models, although more complex than models for a homogeneously mixing population, are still amenable theoretical analysis. An example of this kind is

presented in Section 3.1.

However, the heterogeneity presented by such models is limited. Indeed, in practice, some individuals have more social interactions than others, and contacts with family members, friends, and co-workers are much more likely than interactions with any other random person in the population. With the advent of increasing computational power and the availability of specific data, models which describe contacts between individuals are becoming more popular. In this setting, graph theory and network theory are used to describe these interactions. In this framework, individuals are modelled as the nodes of the network and the edges represent their contacts. The theoretical analysis of epidemic spreading in heterogeneous networks require the development of novel techniques, described e.g. in [43]. A disadvantage of such models is that a complete description of a population would require the knowledge of every individual and its relationships, which is not possible. The use of synthetic networks can be helpful to understand the interplay between network properties and disease characteristics on the spread [44]. Towards this aim, in Section 4.1 we analyse (using both theoretical methods and analysis of simulation results) SIR epidemics on scale-free networks to infer how properties of an epidemic (e.g. probability of a major epidemic, infected fraction, infection peak) depend on network structure and node of epidemic introduction.

1.4 Public health analysis using mathematical models

Starting from theoretical models, the mathematical research in epidemic spreading offers the possibility to investigate real scenarios for public health analysis. In particular, it can provide guidance and advice to public health policymakers [45].

In recent years, thanks to the electronic data management and the availability of these data over the internet, surveillance of infectious diseases has become widespread. Digital traces also use data from volunteer users, e.g. *influenzanet* in Europe [46] or *Flu near you* in USA [47].

These ongoing developments have increased the application of mathematical models to design practical strategies for disease control. It could be a common thought that such analysis regard only critical situations, such as the outbreak of Ebola in Africa [48] or the emergence of COVID-19 as a global pandemic [3, 49]. However, the analysis of control strategies for well-known transmissible diseases remains useful to prevent the re-emergence of localised outbreak. In this context, some examples come from the seasonal influenza [50, 51] or sexually transmitted diseases [52, 53].

In particular, for disease for which a vaccination is available, one of the most important goal is the understanding of the efficient vaccination strategies for achieving herd immunity and disease elimination. A different problem concerns infections, such as influenza, where vaccination cannot lead to disease elimination because of viral mutations that ensure infection persistence over the seasons. In that case, the aim of vaccination is to decrease disease burden; the problem then becomes establishing the cost-effectiveness of vaccination strategies, or of the introduction of new vaccines. Such analysis are generally performed in terms of Quality-Adjusted Life Years gained and economic cost [54, 55].

Two examples of this kind are shown in Chapters 5 and 6 for different influenza vaccines and countries.

While models are therefore useful for public health policy questions, a major problem faced by scientists is the question of model choice. There is not an objective way to evaluate the quality of a model. More complex models could better fit real-world data than simpler models, however parameters can be practically unidentifiable, or anyway estimation can be unsuccessful. On the contrary, complexity can be important to include to understand whether uncertain factors are central to infection dynamics. In many cases, different model structures can appear reasonable to answer to the same problem. New developed methods in this field may help to build models from the best available information for any given policy question.

1.5 Outline

The original results presented in this thesis are based on the research outputs produced during the last three years.

The first theoretical part consists on two papers, both co-authored with Stefania Ottaviano and Mattia Sensi. The first one, published on the journal "*Nonlinear Analysis: Real World Applications*", focused on the analysis of SAIRS epidemic models with vaccination [56]. The global stability analysis of the model, formulated as a system of ODEs, is provided. In particular, we solved the problem of the global stability for the endemic equilibrium, combining two different approaches: the classical Lyapunov stability theorem, and a geometric approach, which generalises the Poincaré-Bendixon theorem. The second paper, submitted to the journal "*Mathematical Methods in the Applied Sciences*", is a generalisation of the previous model to multi-group compartmental models [57]. For this model, the global stability analysis has been developed using the graph-theoretic approach to find Lyapunov functions. These papers constitute Chapter 2 and Chapter 3 of this thesis, respectively.

The second part of the thesis regards some applications of modelling heterogeneity in humans interactions. Chapter 4 deals with spreading processes of infectious diseases over networks. In particular, we analyse a stochastic SIR model on scale-free random network. We first provide an approximate result on the probability of a minor epidemic, and later we validate it by running simulations on different instances of the model. These results are published on the "*Journal of Simulations*", in a paper co-authored with Ozan Kahramanoğulları and Mattia Sensi [58]. The last two chapters provide applications of epidemic models to public health policy. Both concern the cost-benefit analysis of the introduction of new influenza vaccines. The model used to perform the analysis is a SEIR multi-group model, in which groups represent the different age-classes of the population. In Chapter 5 it is analysed the Italian scenario of the introduction of the Laive attenuated influenza vaccine quadrivalent (LAIVq) vaccine in the paediatric age (2-6 years). This study has been carried on in collaboration with Caterina Rizzo, my supervisor Andrea Pugliese and Fasika Molla Abreha and has been published (in Italian) on the "*Journal of Preventive Medicine and Hygiene*" [59, Chapter 6]. Finally, Chapter

6 presents the scenario of introducing the Adjuvanted QIV (aQIV) vaccine in the older population (65+ years) in Spain. This work has been performed in collaboration with Anna Fochesato, Andrea Pugliese and researchers from the Evidera's team and published on the journal "*Vaccines*" [60].

2. Global stability of SAIRS epidemic models

2.1 Introduction and Outline

Once an infectious disease starts circulating in a population, the main goal is to contain its spread. Several control strategies may be applied to control a disease, such as detection and isolation of infectious individuals or vaccination. However, the detection of infectious individuals is far from being an easy task: various diseases, such as influenza, cholera, shigella or Covid-19, are often spread by asymptomatic individuals [35, 36, 37, 61]. These "asymptomatic" individuals, despite showing no symptoms, are able to transmit the infection (see e.g., [62, 63, 64, 65], where a considerable fraction of SARS-Cov-2 infections have been attributed to asymptomatic individuals). This is one of the main aspects that has allowed the virus to circulate widely in the population, since asymptomatic cases often remain unidentified and presumably have more contacts than symptomatic cases, since lack of symptoms often implies a lack of quarantine. Hence, the contribution of the so-called "silent spreaders" to the infection transmission dynamics should be considered in mathematical epidemic models. Models that incorporate an asymptomatic compartment already exist in literature [35, 37, 38], but have not been analytically studied as thoroughly as more famous compartmental models. In this chapter, we consider an SAIRS (Susceptible - Asymptomatic infected - symptomatic Infected - Recovered - Susceptible) model based on the one proposed in [61, Sec. 2], in which the authors provide only a local stability analysis. An SAIR-type model is studied in [66] with application to SARS-CoV-2. After a global stability analysis of the model, the authors present a method to estimate the parameters. They apply the estimation method to Covid-related data from several countries, demonstrating that the predicted epidemic trajectories closely match actual data. The global stability analysis in [66] regards only a simplified version of the model in [61]: first, recovered people do not lose their immunity; moreover, the infection rates of the asymptomatic and symptomatic individuals are equal, as well as their recovery rates, while in [61] these parameters are considered to be potentially different. Thus, the main scope of our work is to provide a global stability analysis of the model proposed in [61], and for some variations thereof. In addition, we include in our model the possibility of vaccination. In the investigation of global stability, we answer an open problem left in [66]. In particular, we study the

global asymptotic stability (GAS) of the disease-free equilibrium (DFE) and provide results related to the global asymptotic stability of the endemic equilibrium (EE) for many variations of the model, as we will explain in detail later.

In our model, the total population N is partitioned into four compartments, namely S, A, I, R, which represent the fraction of Susceptible, Asymptomatic infected, symptomatic Infected and Recovered individuals, respectively, such that $N = S + A + I + R$. The infection can be transmitted to a susceptible through a contact with either an asymptomatic infectious individual, at rate β_A, or a symptomatic individual, at rate β_I. This aspect differentiates an SAIR-type model from the more used and studied SEIR-type model, where once infected a susceptible individual enters an intermediate stage called "Exposed" (E), but a contact between a person in state E and one in state S does not lead to an infection.

In this context instead, once infected, all susceptible individuals enter an asymptomatic state, indicating in any case a delay between infection and symptom onset. We include in the asymptomatic class both individuals who will never develop the symptoms and pre-symptomatic who will eventually become symptomatic. The pre-symptomatic phase seems to have a relevant role in the transmission: for example, in the case of Covid-19, empirical evidence shows that the serial interval tends to be shorter than the average incubation period, suggesting that a significant proportion of secondary transmission can occur prior to symptoms onset [3]; the importance of the pre-symptomatic phase in the transmission is underlined also for other diseases, such as dengue [67], and H1N1 influenza [68].

From the asymptomatic compartment, an individual can either progress to the class of symptomatic infectious I, at rate α, or recover without ever developing symptoms, at rate δ_A. An infected individuals with symptoms can recover at a rate δ_I. We assume that the recovered individuals do not obtain a long-life immunity and can return to the susceptible state after an average time $1/\gamma$. We also assume that a proportion ν of susceptible individuals receive a dose of vaccine which grants them a temporary immunity. We do not add a compartment for the vaccinated individuals, not distinguishing the vaccine-induced immunity from the natural one acquired after recovery from the virus. Moreover, we consider the vital dynamics of the entire population and, for simplicity, we assume that the rate of births and deaths are the same, equal to μ; we do not distinguish between natural deaths and disease-related deaths.

The chapter is organized as follows. In Sec. 2.2, we present the system of equations for the SAIRS model with vaccination, providing its positive invariant set. In Sec. 2.3, we determine the value of the basic reproduction number $\mathcal{R}_0$ and prove that if $\mathcal{R}_0 < 1$, the disease-free equilibrium (DFE) is globally asymptotically stable (GAS) and unstable if $\mathcal{R}_0 > 1$.

In Sec. 2.4, we discuss the uniform persistence of the disease, the existence and uniqueness of the endemic equilibrium (EE), and we investigate its stability properties. In particular, first we provide the local asymptotic stability of the EE, then we investigate its global asymptotic stability for some variations of the original model under study. We start by considering the open problem left in [66], where the global stability of

an SAIR model with vital dynamics is studied. The authors consider a disease which confers permanent immunity, meaning that the recovered individuals never return to the susceptible state. Moreover, they impose the restrictions $\beta_A = \beta_I$ and $\delta_A = \delta_I$, and leave the global stability of the endemic equilibrium when $\beta_A \neq \beta_I$ and $\delta_A \neq \delta_I$, as an open problem. Thus, in Sec. 2.5.1, we directly solve the open problem left in [66], by considering an SAIR model (i.e., $\gamma = 0$), with $\beta_A \neq \beta_I$ and $\delta_A \neq \delta_I$, including in addition the possibility of vaccination. We consider the basic reproduction number $\mathcal{R}_0$ for this model and prove that if $\mathcal{R}_0 > 1$ the EE is GAS. In Sec. 2.5.2, we study the GAS of the EE for an SAIRS model (i.e., $\gamma \neq 0$) with vaccination, with the restrictions $\beta_A = \beta_I$ and $\delta_A = \delta_I$, proving that if $\mathcal{R}_0 > 1$ the EE is GAS. Thus, we extend the global analysis in [66] to a model including vaccination and loss of immunity. In Sec. 2.5.3, we investigate the global stability of the SAIRS model with $\beta_A \neq \beta_I$ or $\delta_A \neq \delta_I$, i.e., the model proposed in [61], with in addition the possibility of vaccination. In this case, we use a geometric approach to global stability for nonlinear autonomous systems due to Lu and Lu [69], that generalises the criteria developed by Li and Muldowney [17, 18]. We prove that if $\mathcal{R}_0 > 1$ and $\beta_A < \delta_I$, the EE is GAS.

In Sec. 2.6, we are able to prove the GAS of the DFE also in the case $\mathcal{R}_0 = 1$, assuming that no vaccination campaign is in place. In Sec. 2.7, we validate our analytical results via several numerical simulations and deeper explore the role of parameters.

2.2 The SAIRS model with vaccination

We consider an extension of the SAIRS model presented in [61].

The system of ODEs which describes the model is given by

$$\begin{aligned}
\frac{dS(t)}{dt} &= \mu - \Big(\beta_A A(t) + \beta_I I(t)\Big) S(t) - (\mu + \nu) S(t) + \gamma R(t), \\
\frac{dA(t)}{dt} &= \Big(\beta_A A(t) + \beta_I I(t)\Big) S(t) - (\alpha + \delta_A + \mu) A(t), \\
\frac{dI(t)}{dt} &= \alpha A(t) - (\delta_I + \mu) I(t), \\
\frac{dR(t)}{dt} &= \delta_A A(t) + \delta_I I(t) + \nu S(t) - (\gamma + \mu) R(t),
\end{aligned} \tag{2.1}$$

with initial condition $(S(0), A(0), I(0), R(0))$ belonging to the set

$$\bar{\Gamma} = \{(S, A, I, R) \in \mathbb{R}^4_+ | S + A + I + R = 1\}, \tag{2.2}$$

where $\mathbb{R}^4_+$ is the non-negative orthant of $\mathbb{R}^4$. The flow diagram for system (2.1) is given in Figure 2.1.

Assuming initial conditions in $\bar{\Gamma}$, $S(t) + A(t) + I(t) + R(t) = 1$, for all $t \geq 0$; hence,

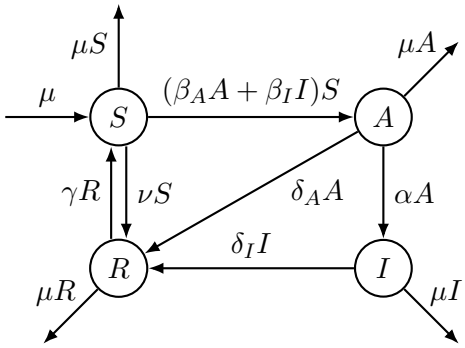

Figure 2.1: Flow diagram for system (2.1).

system (2.1) is equivalent to the following three-dimensional dynamical system

$$\begin{aligned}
\frac{dS(t)}{dt} &= \mu - \Big(\beta_A A(t) + \beta_I I(t)\Big)S(t) - (\mu + \nu + \gamma)S(t) + \gamma(1 - A(t) - I(t)),\\
\frac{dA(t)}{dt} &= \Big(\beta_A A(t) + \beta_I I(t)\Big)S(t) - (\alpha + \delta_A + \mu)A(t),\\
\frac{dI(t)}{dt} &= \alpha A(t) - (\delta_I + \mu)I(t),
\end{aligned} \tag{2.3}$$

with initial condition $(S(0), A(0), I(0))$ belonging to the set

$$\Gamma = \{(S, A, I) \in \mathbb{R}^3_+ | S + A + I \leq 1\}.$$

System (2.3) can be written in vector notation as

$$\frac{dx(t)}{dt} = f(x(t)),$$

where $x(t) = (S(t), A(t), I(t))$ and $f(x(t)) = (f_1(x(t)), f_2(x(t)), f_3(x(t)))$ is defined according to (2.3).

Theorem 2.2.1. *Γ is positively invariant set for system (2.3). That is, for all initial values $x(0) \in \Gamma$, the solution $x(t)$ of (2.3) will remain in Γ for all $t > 0$.*

Proof. A compact set C is invariant for the system $dx(t)/dt = f(x(t))$ if at each point $y \in \partial C$ (the boundary of C), the vector $f(y)$ is tangent or pointing into the set [70].

The boundary $\partial\Gamma$ consists of the following 4 hyperplanes:

$$\begin{aligned}
H_1 &= \{(S, A, I) \in \Gamma \mid S = 0\}, \qquad H_2 = \{((S, A, I) \in \Gamma \mid A = 0\},\\
H_3 &= \{(S, A, I) \in \Gamma \mid I = 0\}, \quad H_4 = \{(S, A, I) \in \Gamma \mid S + A + I = 1\}
\end{aligned}$$

whose respective outer normal vectors are:

$$\eta_1 = (-1, 0, 0), \qquad \eta_2 = (0, -1, 0), \qquad \eta_3 = (0, 0, -1), \qquad \eta_4 = (1, 1, 1).$$

Thus, let us consider a point $x \in \partial\Gamma$. To prove the statement, we distinguish among four cases.

Case 1: $S = 0$. Then, since $A + I \leq 1$

$$\langle f(x), \eta_1 \rangle = -\mu - \gamma(1 - A - I) \leq 0.$$

Case 2: $A = 0$. Then, since $S \geq 0$, $I \geq 0$

$$\langle f(x), \eta_2 \rangle = -\beta_I IS \leq 0.$$

Case 3: $I = 0$. Then, since $A \geq 0$

$$\langle f(x), \eta_3 \rangle = -\alpha A \leq 0.$$

Case 4: $S + A + I = 1$. Then, since $S \geq 0$, $A \geq 0$, $I \geq 0$

$$\langle f(x), \eta_4 \rangle = -\nu S - \delta_A A - \delta_I I \leq 0.$$

Thus, any solution that starts in $\partial\Gamma$ will remain inside Γ. □

2.3 Disease Elimination

In this section, we provide the value of the basic reproduction number, that is defined as the expected number of secondary infections produced by an index case in a completely susceptible population [71, 72]. This numerical value gives a measure of the potential for disease spread within a population [73]. Then, we investigate the stability properties of the disease-free equilibrium of the system (2.3), that is equal to

$$x_0 = (S_0, A_0, I_0) = \left(\frac{\mu + \gamma}{\mu + \nu + \gamma}, 0, 0 \right). \tag{2.4}$$

Lemma 2.3.1. *The basic reproduction number* $\mathcal{R}_0$ *of* (2.3) *is given by*

$$\mathcal{R}_0 = \left(\beta_A + \frac{\alpha\beta_I}{\delta_I + \mu} \right) \frac{\gamma + \mu}{(\alpha + \delta_A + \mu)(\nu + \gamma + \mu)}. \tag{2.5}$$

Proof. Let us use the next generation matrix method [74] to find $\mathcal{R}_0$. System (2.3) has 2 infected compartments, denoted by A and I. We can write

$$\frac{dA(t)}{dt} = \mathcal{F}_1(S(t), A(t), I(t)) - \mathcal{V}_1(S(t), A(t), I(t)),$$
$$\frac{dI(t)}{dt} = \mathcal{F}_2(S(t), A(t), I(t)) - \mathcal{V}_2(S(t), A(t), I(t)),$$

where

$$\mathcal{F}_1(S(t),A(t),I(t)) = \Big(\beta_A A(t) + \beta_I I(t)\Big)S(t), \quad \mathcal{V}_1(S(t),A(t),I(t)) = (\alpha+\delta_A+\mu)A(t),$$
$$\mathcal{F}_2(S(t),A(t),I(t)) = 0, \qquad \mathcal{V}_2(S(t),A(t),I(t)) = -\alpha A(t) + (\delta_I+\mu)I(t).$$

Thus, we obtain

$$F = \begin{pmatrix} \dfrac{\partial \mathcal{F}_1}{\partial A}(x_0) & \dfrac{\partial \mathcal{F}_1}{\partial I}(x_0) \\ \dfrac{\partial \mathcal{F}_2}{\partial A}(x_0) & \dfrac{\partial \mathcal{F}_2}{\partial I}(x_0) \end{pmatrix} = \begin{pmatrix} \beta_A S_0 & \beta_I S_0 \\ 0 & 0 \end{pmatrix}, \qquad \text{where } S_0 = \frac{\gamma+\mu}{\gamma+\mu+\nu}, \tag{2.6}$$

$$V = \begin{pmatrix} \dfrac{\partial \mathcal{V}_1}{\partial A}(x_0) & \dfrac{\partial \mathcal{V}_1}{\partial I}(x_0) \\ \dfrac{\partial \mathcal{V}_2}{\partial A}(x_0) & \dfrac{\partial \mathcal{V}_2}{\partial I}(x_0) \end{pmatrix} = \begin{pmatrix} \alpha+\delta_A+\mu & 0 \\ -\alpha & \delta_I+\mu \end{pmatrix}, \tag{2.7}$$

from which

$$V^{-1} = \begin{pmatrix} \dfrac{1}{\alpha+\delta_A+\mu} & 0 \\ \dfrac{\alpha}{(\alpha+\delta_A+\mu)(\delta_I+\mu)} & \dfrac{1}{\delta_I+\mu} \end{pmatrix}.$$

The next generation matrix is defined as $M := FV^{-1}$, that is

$$M = \begin{pmatrix} \dfrac{\beta_A S_0}{\alpha+\delta_A+\mu} + \dfrac{\alpha\beta_I S_0}{(\alpha+\delta_A+\mu)(\delta_I+\mu)} & \dfrac{\beta_I S_0}{\delta_I+\mu} \\ 0 & 0 \end{pmatrix}.$$

The basic reproduction number $\mathcal{R}_0$ is defined as the spectral radius of M, denoted by $\rho(M)$. Thus, with a direct computation, we obtain (2.5). □

In the following, we recall some results that we will use to prove the global asymptotic stability of the disease-free equilibrium x_0 of (2.3).

Lemma 2.3.2. *The matrix $(F-V)$ has a real spectrum. Moreover, if $\rho(FV^{-1}) < 1$, all the eigenvalues of $(F-V)$ are negative.*

Proof. From (2.6) and (2.7)

$$(F-V) = \begin{pmatrix} \beta_A S_0 - (\alpha+\delta_A+\mu) & \beta_I S_0 \\ \alpha & -(\delta_I+\mu) \end{pmatrix}. \tag{2.8}$$

Since $(F-V)$ is a 2×2 matrix whose off-diagonal elements have the same sign, it is easy to see that its eigenvalues are real. Indeed, for a generic matrix $A = \begin{pmatrix} a & b \\ c & d \end{pmatrix}$ with

$\text{sign}(b) = \text{sign}(c)$, the eigenvalues can be easily shown to be real by explicitly computing them:

$$\lambda_{1,2} = \frac{(a+d) \pm \sqrt{(a-d)^2 + 4bc}}{2},$$

and noticing that the radicand is the sum of two non-negative values. Now, if $\rho(FV^{-1}) = \mathcal{R}_0 < 1$ all eigenvalues of $(F - V)$ are negative as a consequence of [73, Lemma 2]. □

Theorem 2.3.3. *The disease-free equilibrium x_0 of (2.3) is locally asymptotically stable if $\mathcal{R}_0 < 1$, and unstable if $\mathcal{R}_0 > 1$.*

Proof. See [73, Theorem 1]. □

Theorem 2.3.4. *The disease-free equilibrium x_0 of (2.3) is globally asymptotically stable in Γ if $\mathcal{R}_0 < 1$.*

Proof. Since Γ is an invariant set for (2.3) and in view of Theorem 2.3.3, it is sufficient to show that for all $x(0) \in \Gamma$

$$\lim_{t\to\infty} A(t) = 0, \qquad \lim_{t\to\infty} I(t) = 0, \qquad \text{and} \qquad \lim_{t\to\infty} S(t) = S_0,$$

with S_0 as in (2.4). From the first equation of (2.3) follows that

$$\frac{dS(t)}{dt} \leq \mu + \gamma - (\mu + \nu + \gamma)S(t).$$

It easy to see that S_0 is a global asymptotically stable equilibrium for the comparison equation

$$\frac{dy(t)}{dt} = \mu + \gamma - (\mu + \nu + \gamma)y(t).$$

Then, for any $\varepsilon > 0$, there exists $\bar{t} > 0$, such that for all $t \geq \bar{t}$, it holds

$$S(t) \leq S_0 + \varepsilon, \tag{2.9}$$

hence

$$\limsup_{t\to\infty} S(t) \leq S_0. \tag{2.10}$$

Now, from (2.9) and second and third equation of (2.3), we have that for $t \geq \bar{t}$

$$\begin{aligned}
\frac{dA(t)}{dt} &\leq \Big(\beta_A A(t) + \beta_I I(t)\Big)(S_0 + \varepsilon) - (\alpha + \delta_A + \mu)A(t), \\
\frac{dI(t)}{dt} &= \alpha A(t) - (\delta_I + \mu)I(t).
\end{aligned}$$

Let us now consider the comparison system

$$\frac{dw_1(t)}{dt} = \Big(\beta_A w_1(t) + \beta_I w_2(t)\Big)(S_0 + \varepsilon) - (\alpha + \delta_A + \mu)w_1(t),$$
$$\frac{dw_2(t)}{dt} = \alpha w_1(t) - (\delta_I + \mu)w_2(t), \qquad w_1(\bar{t}) = A(\bar{t}), \quad w_2(\bar{t}) = I(\bar{t}),$$

that we can rewrite as

$$\frac{dw(t)}{dt} = (F_\varepsilon - V_\varepsilon)w(t),$$

where $w(t) = (w_1(t), w_2(t))^T$ and $F_\varepsilon - V_\varepsilon$ is the matrix in (2.8), computed in $x_0(\varepsilon) = (S_0 + \varepsilon, 0, 0)$. Let us note that if $\mathcal{R}_0 = \rho(FV^{-1}) < 1$, we can choose a sufficiently small $\varepsilon > 0$ such that $\rho(F_\varepsilon V_\varepsilon^{-1}) < 1$. Then, by applying Lemma 2.3.2 to $(F_\varepsilon - V_\varepsilon)$, we obtain that it has a real spectrum and all its eigenvalues are negative. It follows that $\lim_{t\to\infty} w(t) = 0$, whatever the initial conditions are (see, e.g., [75]), from which

$$\lim_{t\to\infty} A(t) = 0, \qquad \text{and} \qquad \lim_{t\to\infty} I(t) = 0.$$

Now, for any $\varepsilon > 0$ there exists $\bar{t}_1$ such that for any $t \geq \bar{t}_1$, $I(t) < \varepsilon$ and $A(t) < \varepsilon$. So, for $t \geq \bar{t}_1$ we have

$$\frac{dS(t)}{dt} \geq \mu - \varepsilon(\beta_A + \beta_I)S(t) - (\mu + \nu + \gamma)S(t) + \gamma(1 - 2\varepsilon).$$

It easy to see that $\dfrac{\mu + \gamma(1-2\varepsilon)}{\varepsilon(\beta_A + \beta_I) + (\mu + \nu + \gamma)}$ is a global asymptotically stable equilibrium for the comparison equation

$$\frac{dy(t)}{dt} = \mu - \varepsilon(\beta_A + \beta_I)y(t) - (\mu + \nu + \gamma)y(t) + \gamma(1 - 2\varepsilon).$$

Thus, for any $\zeta > 0$, there exists $\bar{t}_2 > 0$ such that for all $t \geq \bar{t}_2$,

$$S(t) \geq \frac{\mu + \gamma(1-2\varepsilon)}{\varepsilon(\beta_A + \beta_I) + (\mu + \nu + \gamma)} - \zeta.$$

Then, for any $\varepsilon > 0$, we have

$$\liminf_{t\to\infty} S(t) \geq \frac{\mu + \gamma(1-2\varepsilon)}{\varepsilon(\beta_A + \beta_I) + (\mu + \nu + \gamma)}.$$

Letting ε go to 0, we have $\liminf_{t\to\infty} S(t) \geq S_0$, that combined with (2.10) gives us

$$\lim_{t\to\infty} S(t) = S_0.$$

□

2.4 Existence and uniqueness of endemic equilibrium

In this section, we discuss the uniform persistence of the disease, the existence and uniqueness of an endemic equilibrium, and we investigate its stability properties.

We say that the disease is *endemic* if both the asymptomatic and infected fractions in the population remains above a certain positive level for a sufficiently large time. The notion of uniform persistence can be used to represent and analyse the endemic scenario [19]. In the following, with the notation $\mathring{\Theta}$, we indicate the interior of a set Θ.

Definition 1. *System* (2.3) *is said to be* uniformly persistent *if there exists a constant* $0 < \varepsilon < 1$ *such that any solution* $x(t) = (S(t), A(t), I(t))$ *with* $x(0) \in \mathring{\Gamma}$ *satisfies*

$$\min\{\liminf_{t\to\infty} S(t), \quad \liminf_{t\to\infty} A(t), \quad \liminf_{t\to\infty} I(t)\} \geq \varepsilon. \tag{2.11}$$

To address the uniform persistence of our system, we need the following result.

Lemma 2.4.1. *The DFE* x_0 *is the unique equilibrium of* (2.3) *on* $\partial\Gamma$.

Proof. Let us assume that $\bar{x} = (\bar{S}, \bar{A}, \bar{I})$ is an equilibrium of (2.3) on $\partial\Gamma$. Then, there are three possibilities:

Case 1: $\bar{S} = 0$. It follows from the second equation of (2.3) that $\bar{A} = 0$ and, consequently, from the third equation that $\bar{I} = 0$. Then, from the first equation of (2.3) we have $\gamma(\bar{A} + \bar{I}) = \mu + \gamma > 0$, and a contradiction occurs.

Case 2: $\bar{A} = 0$. It follows from the third equation of (2.3) that $\bar{I} = 0$, and from the first that $\bar{S} = S_0$.

Case 3: $\bar{I} = 0$. Analogously to Case 2, we find that $\bar{A} = 0$ and $\bar{S} = S_0$.

Case 4: $\bar{S} + \bar{A} + \bar{I} = 1$. By summing the equations in (2.3), we have $\delta_A \bar{A} + \delta_I \bar{I} + \nu \bar{S} = 0$, a contradiction.

By combining the above discussions the statement follows. □

Theorem 2.4.2. *If* $\mathcal{R}_0 > 1$, *system* (2.3) *is uniformly persistent and there exists at least one endemic equilibrium in* $\mathring{\Gamma}$.

Proof. By Lemma 2.4.1, the largest invariant set on $\partial\Gamma$ is the singleton $\{x_0\}$, which is isolated. If $\mathcal{R}_0 > 1$, we know from Theorem 2.3.3 that x_0 is unstable. Then, by using [76, Thm 4.3], and similar arguments in [19, Prop. 3.3], we can assert that the instability of x_0 implies the uniform persistence of (2.3). The uniform persistence and the positive invariance of the compact set Γ imply the existence of an endemic equilibrium in $\mathring{\Gamma}$ (see, e.g., [77, Thm 2.8.6] or [12, Thm. 2.2]). □

Lemma 2.4.3. *There exists an endemic equilibrium $x^* = (S^*, A^*, I^*)$ in $\mathring{\Gamma}$ for system (2.3) if and only if $\mathcal{R}_0 > 1$. Furthermore, this equilibrium is unique.*

Proof. We equate the right hand sides of (2.3) to 0, and assume $A^*, I^* \neq 0$. From the third equation we obtain

$$A^* = \frac{\delta_I + \mu}{\alpha} I^*, \tag{2.12}$$

and replace it in the second equation

$$\left(\beta_A \frac{\delta_I + \mu}{\alpha} + \beta_I\right) I^* S^* - (\alpha + \delta_A + \mu)\frac{\delta_I + \mu}{\alpha} I^* = 0.$$

Since $I^* \neq 0$, it follows that

$$S^* = \frac{(\alpha + \delta_A + \mu)(\delta_I + \mu)}{\beta_A(\delta_I + \mu) + \beta_I \alpha}. \tag{2.13}$$

Let us substitute the expressions (2.12) and (2.13) in the first equation, then we obtain

$$\mu - \left(\beta_A \frac{\delta_I + \mu}{\alpha} + \beta_I\right) \frac{(\alpha + \delta_A + \mu)(\delta_I + \mu)}{\beta_A(\delta_I + \mu) + \beta_I \alpha} I^* - (\mu + \nu + \gamma)\frac{(\alpha + \delta_A + \mu)(\delta_I + \mu)}{\beta_A(\delta_I + \mu) + \beta_I \alpha} + \gamma\left(1 - \frac{\delta_I + \mu}{\alpha} I^* - I^*\right) = 0,$$

which implies that

$$I^* = \frac{\mu - (\mu + \nu + \gamma)\dfrac{(\alpha + \delta_A + \mu)(\delta_I + \mu)}{\beta_A(\delta_I + \mu) + \beta_I \alpha} + \gamma}{\dfrac{1}{\alpha}(\beta_A(\delta_I + \mu) + \beta_I \alpha)\dfrac{(\alpha + \delta_A + \mu)(\delta_I + \mu)}{\beta_A(\delta_I + \mu) + \beta_I \alpha} + \gamma\dfrac{\delta_I + \mu}{\alpha} + \gamma}$$

$$= \frac{(\mu + \gamma)(\beta_A(\delta_I + \mu) + \beta_I \alpha) - (\mu + \nu + \gamma)(\alpha + \delta_A + \mu)(\delta_I + \mu)}{\dfrac{\beta_A(\delta_I + \mu) + \beta_I \alpha}{\alpha}\left((\alpha + \delta_A + \mu + \gamma)(\delta_I + \mu) + \gamma\alpha\right)}$$

$$= \frac{(\delta_I + \mu)\left((\mu + \gamma)\left(\beta_A + \beta_I \dfrac{\alpha}{\delta_I + \mu}\right) - (\mu + \nu + \gamma)(\alpha + \delta_A + \mu)\right)}{\dfrac{\beta_A(\delta_I + \mu) + \beta_I \alpha}{\alpha}\left((\alpha + \delta_A + \mu + \gamma)(\delta_I + \mu) + \gamma\alpha\right)}$$

$$= \frac{(\delta_I + \mu)(\mu + \nu + \gamma)(\alpha + \delta_A + \mu)\left(\dfrac{(\mu + \gamma)}{(\mu + \nu + \gamma)(\alpha + \delta_A + \mu)}\left(\beta_A + \beta_I \dfrac{\alpha}{\delta_I + \mu}\right) - 1\right)}{\dfrac{\beta_A(\delta_I + \mu) + \beta_I \alpha}{\alpha}\left((\alpha + \delta_A + \mu + \gamma)(\delta_I + \mu) + \gamma\alpha\right)}$$

$$= \frac{\alpha(\delta_I + \mu)(\mu + \nu + \gamma)(\alpha + \delta_A + \mu)}{(\beta_A(\delta_I + \mu) + \beta_I \alpha)\left((\alpha + \delta_A + \mu + \gamma)(\delta_I + \mu) + \gamma\alpha\right)}(\mathcal{R}_0 - 1). \tag{2.14}$$

The endemic equilibrium in $\mathring{\Gamma}$ exists if $A^* > 0$ and $I^* > 0$. We obtain that $I^* > 0$, and consequently $A^* > 0$, if and only if $\mathcal{R}_0 - 1 > 0$. □

Theorem 2.4.4. *The endemic equilibrium $x^* = (S^*, A^*, I^*)$ is locally asymptotically stable in $\mathring{\Gamma}$ for system (2.3) if $\mathcal{R}_0 > 1$.*

Proof. Note that the expression of (2.13) and (2.14) may be written as a function of $\mathcal{R}_0$; using the expression found in (2.5), we obtain

$$S^* = \frac{h_4}{\mathcal{R}_0}, \tag{2.15}$$

$$I^* = \frac{\alpha h_0 h_1 h_2 (\mathcal{R}_0 - 1)}{h_3(\beta_A h_2 + \beta_I \alpha)}, \tag{2.16}$$

where we have set $h_0 = \mu + \nu + \gamma$, $h_1 = \alpha + \delta_A + \mu$, $h_2 = \delta_I + \mu$, $h_3 = \gamma\alpha + (h_1 + \gamma)h_2$, $h_4 = \dfrac{\gamma + \mu}{h_0} \leq 1$. Moreover, we can compute

$$\beta_A A^* + \beta_I I^* = \frac{\beta_A h_2 + \beta_I \alpha}{\alpha} I^* = \frac{h_0 h_1 h_2 (\mathcal{R}_0 - 1)}{h_3}. \tag{2.17}$$

To determine the stability of the endemic equilibrium x^*, we need to compute the Jacobian matrix of (2.3) evaluated in x^*, that is

$$J_{|x^*} = \begin{pmatrix} -\dfrac{h_0 h_1 h_2 (\mathcal{R}_0 - 1)}{h_3} - h_0 & -\dfrac{\beta_A h_4}{\mathcal{R}_0} - \gamma & -\dfrac{\beta_I h_4}{\mathcal{R}_0} - \gamma \\ \dfrac{h_0 h_1 h_2 (\mathcal{R}_0 - 1)}{h_3} & \dfrac{\beta_A h_4}{\mathcal{R}_0} - h_1 & \dfrac{\beta_I h_4}{\mathcal{R}_0} \\ 0 & \alpha & -h_2 \end{pmatrix},$$

where we have used (2.15-2.17). With the same arguments as in [61, Sec. 2.1], we can conclude that x^* is locally asymptotically stable if $\mathcal{R}_0 > 1$. □

2.5 Global stability of the endemic equilibrium

2.5.1 Global stability of the endemic equilibrium in the SAIR model.

In this section, we focus on the global asymptotic stability of the endemic equilibrium of the SAIR model, i.e., system (2.3) with $\gamma = 0$, representing a disease which confers permanent immunity. Here, we answer directly to the open problem left in [66]. Let us note that in our model we have in addition, with respect to the model proposed in [66], the possibility of vaccination.
The dynamic of an SAIR model of this type is described by the following system of equations:

$$\begin{aligned}
\frac{dS(t)}{dt} &= \mu - \Big(\beta_A A(t) + \beta_I I(t)\Big) S(t) - (\mu+\nu)S(t), \qquad (2.18)\\
\frac{dA(t)}{dt} &= \Big(\beta_A A(t) + \beta_I I(t)\Big) S(t) - (\alpha+\delta_A+\mu)A(t),\\
\frac{dI(t)}{dt} &= \alpha A(t) - (\delta_I+\mu)I(t),
\end{aligned}$$

The basic reproduction number is

$$\mathcal{R}_0 = \left(\beta_A + \frac{\alpha\beta_I}{\delta_I+\mu}\right)\frac{\mu}{(\alpha+\delta_A+\mu)(\nu+\mu)}.$$

The endemic equilibrium $x^* = (S^*, A^*, I^*)$ satisfies the equation

$$\mu = \Big(\beta_A A^* + \beta_I I^*\Big) S^* + (\mu+\nu)S^*, \qquad (2.19)$$

$$(\alpha+\delta_A+\mu)A^* = \Big(\beta_A A^* + \beta_I(r) I^*\Big) S^*, \qquad (2.20)$$

$$\alpha A^* = (\delta_I+\mu)I^*. \qquad (2.21)$$

Theorem 2.5.1. *The endemic equilibrium $x^* = (S^*, A^*, I^*)$ of (2.18) is globally asymptotically stable in $\mathring{\Gamma}$ if $\mathcal{R}_0 > 1$.*

Proof. For ease of notation, we will omit the dependence on t. Let us consider $c_1, c_2 > 0$ and the function

$$V = c_1 V_1 + c_2 V_2 + V_3,$$

where

$$V_1 = S^* \cdot g\left(\frac{S}{S^*}\right), \qquad V_2 = A^* \cdot g\left(\frac{A}{A^*}\right), \qquad V_3 = I^* \cdot g\left(\frac{I}{I^*}\right),$$

and $g(x) = x - 1 - \ln x \geq g(1) = 0$, for any $x > 0$. Let us introduce the notation

$$u = \frac{S}{S^*}, \qquad y = \frac{A}{A^*}, \qquad z = \frac{I}{I^*}.$$

Differentiating V along the solutions of (2.18), and using (2.19), (2.20), (2.21), we have

$$\begin{aligned}
c_1\frac{dV_1}{dt} =& c_1\left(1 - \frac{S^*}{S}\right)\Big[\mu - (\beta_A A + \beta_I I)S - (\mu+\nu)S\Big]\\
&= c_1\left(1 - \frac{S^*}{S}\right)\Big[- (\mu+\nu)(S - S^*) - \beta_A(AS - A^*S^*) - \beta_I(IS - I^*S^*)\Big]\\
&= c_1\left(1 - \frac{1}{u}\right)\Big[- (\mu+\nu)S^*(u-1) - \beta_A A^* S^*(uy - 1) - \beta_I I^* S^*(uz - 1)\Big], \qquad (2.22)
\end{aligned}$$

$$
\begin{aligned}
c_2\frac{dV_2}{dt} =& c_2\left(1-\frac{A^*}{A}\right)\left[(\beta_A A+\beta_I I)S-(\alpha+\delta_A+\mu)A\right]\\
&= c_2\left(1-\frac{1}{y}\right)\left[\beta_A A^*S^*uy+\beta_I I^*S^*uz-(\beta_A A^*+\beta_I I^*)S^*y\right]\\
&= c_2\left(1-\frac{1}{y}\right)\left[\beta_A A^*S^*(uy-y)+\beta_I I^*S^*(uz-y)\right],
\end{aligned}
\tag{2.23}
$$

$$
\begin{aligned}
\frac{dV_3}{dt} =& \left(1-\frac{I^*}{I}\right)\left[\alpha A-(\delta_I+\mu)I\right]=\left(1-\frac{I^*}{I}\right)\left(\alpha A-\frac{\alpha I A^*}{I^*}\right)\\
&= \alpha A^*\left(1+\frac{A}{A^*}-\frac{I}{I^*}-\frac{AI^*}{A^*I}\right)\\
&\le \alpha A^*\left(-\ln y+y-z+\ln z\right)\\
&= \alpha A^*(g(y)-g(z)),
\end{aligned}
\tag{2.24}
$$

where we have used the inequality $1-y/z\le-\ln(y/z)$. Thus, from (2.22),(2.23), and (2.24),

$$
\begin{aligned}
\frac{dV}{dt} =& -c_1\left(1-\frac{1}{u}\right)(\mu+\nu)S^*(u-1)+c_1\beta_A A^*S^*\left[\left(1-\frac{1}{u}\right)(1-uy)+\frac{c_2}{c_1}\left(1-\frac{1}{y}\right)(uy-y)\right]\\
&+c_1\beta_I I^*S^*\left[\left(1-\frac{1}{u}\right)(1-uz)+\frac{c_2}{c_1}\left(1-\frac{1}{y}\right)(uz-y)\right]+\alpha A^*(g(y)-g(z)).
\end{aligned}
\tag{2.25}
$$

Now, for the second and third term in (2.25), we have

$$
\begin{aligned}
&\left(1-\frac{1}{u}\right)(1-uy)+\frac{c_2}{c_1}\left(1-\frac{1}{y}\right)(uy-y)\\
&=\left(1+\frac{c_2}{c_1}\right)-\frac{1}{u}-uy\left(1-\frac{c_2}{c_1}\right)+y\left(1-\frac{c_2}{c_1}\right)-\frac{c_2}{c_1}u\\
&=-g\left(\frac{1}{u}\right)-g\left(uy\right)\left(1-\frac{c_2}{c_1}\right)+\left(g(y)\left(1-\frac{c_2}{c_1}\right)-g(u)\right),
\end{aligned}
\tag{2.26}
$$

and

$$
\begin{aligned}
&\left(1-\frac{1}{u}\right)(1-uz)+\frac{c_2}{c_1}\left(1-\frac{1}{y}\right)(uz-y)\\
&=\left(1+\frac{c_2}{c_1}\right)-\frac{1}{u}+z-uz\left(1-\frac{c_2}{c_1}\right)-\frac{c_2}{c_1}y-\frac{c_2}{c_1}\frac{uz}{y}\\
&=-g\left(\frac{1}{u}\right)-\frac{c_2}{c_1}g\left(\frac{uz}{y}\right)+\left(g(z)-\frac{c_2}{c_1}g(y)\right)-uz\left(1-\frac{c_2}{c_1}\right).
\end{aligned}
\tag{2.27}
$$

Thus, substituting (2.26) and (2.27) in (2.25), we obtain

$$\begin{aligned}\frac{dV}{dt} =& -c_1\left(1-\frac{1}{u}\right)(\mu+\nu)S^*(u-1)\\ &-c_1\beta_A A^*S^*\left[g\left(\frac{1}{u}\right)+g(uy)\left(1-\frac{c_2}{c_1}\right)\right]+c_1\beta_A A^*S^*\left[g(y)\left(1-\frac{c_2}{c_1}\right)-g(u)\right]\\ &-c_1\beta_I I^*S^*\left[g\left(\frac{1}{u}\right)+\frac{c_2}{c_1}g\left(\frac{uz}{y}\right)\right]+c_1\beta_I I^*S^*\left[g(z)-\frac{c_2}{c_1}g(y)-uz\left(1-\frac{c_2}{c_1}\right)\right]\\ &+\alpha A^*(g(y)-g(z)).\end{aligned}$$

Now, by taking $c_1 = c_2 = \dfrac{\alpha A^*}{\beta_I I^* S^*}$, we have

$$\begin{aligned}\frac{dV}{dt} =& -c_1\frac{(u-1)^2}{u}(\mu+\nu)S^* - c_1\beta_A A^*S^*\left(g\left(\frac{1}{u}\right)+g(u)\right)\\ &-c_1\beta_I I^*S^*\left(g\left(\frac{1}{u}\right)+g\left(\frac{uz}{y}\right)\right).\end{aligned}$$

Hence, $\dfrac{dV}{dt}\leq 0$. Moreover, the set where $\dfrac{dV}{dt}=0$ is $Z=\{(S,A,I): S=S^*, I=\dfrac{AI^*}{A^*}\}$, and the only compact invariant subset of Z is the singleton $\{x^*\}$. The claim follows by LaSalle's Invariance Principle [78]. □

2.5.2 Global stability of the SAIRS model with equal transmission rates and recovery rates

In this section, we conduct a global stability analysis in the case $\beta_A = \beta_I := \beta$ and $\delta_A = \delta_I := \delta$. In [66], the authors study a SAIR model (without vaccination) in this specific case, i.e. when the disease transmission and the recovery rates are the same for asymptomatic and symptomatic individuals. Here, we extend their analysis to the SAIRS model with vaccination.

In this case, from (2.5), the expression of the basic reproduction number becomes

$$\mathcal{R}_0 = \frac{\beta(\gamma+\mu)}{(\delta+\mu)(\nu+\gamma+\mu)}.$$

Theorem 2.5.2. *Let us assume that $\beta_A = \beta_I =: \beta$ and $\delta_A = \delta_I =: \delta$. The endemic equilibrium $x^* = (S^*, A^*, I^*)$ is globally asymptotically stable in $\mathring{\Gamma}$ for system (2.3) if $\mathcal{R}_0 > 1$.*

Proof. Let us define $M(t) := A(t) + I(t)$, for all $t \geq 0$. Then, we can rewrite (2.3) as

$$\begin{aligned}\frac{dS(t)}{dt} &= \mu - \beta M(t)S(t) - (\mu+\nu+\gamma)S(t) + \gamma(1-M(t)),\\ \frac{dM(t)}{dt} &= \beta M(t)S(t) - (\delta+\mu)M(t).\end{aligned}$$

At the equilibrium it holds that

$$\mu + \gamma = \beta M^* S^* + (\mu + \nu + \gamma) S^* + \gamma M^*, \tag{2.28}$$
$$\delta + \mu = \beta S^*, \tag{2.29}$$

where $M^* = A^* + I^*$. In the following, for ease of notation, we will omit the dependence on t. Consider the following positively definite function

$$V = \frac{1}{2}(S - S^*)^2 + w\left(M - M^* - M^* \ln\left(\frac{M}{M^*}\right)\right),$$

where w is a non negative constant.

Differentiating along (2.3) and using the equilibrium conditions (2.28-2.29) we obtain

$$\begin{aligned}
\frac{dV}{dt} =& (S - S^*)\left(\beta(M^* S^* - MS) - (\mu + \nu + \gamma)(S - S^*) + \right. \\
&\left. + \gamma(M^* - M)\right) + w\left(1 - \frac{M^*}{M}\right)\beta M(S - S^*) \\
=& \beta(S - S^*)(M^* S^* - MS^* + MS^* - MS) - (\mu + \nu + \gamma)(S - S^*)^2 + \\
&+ \gamma(M^* - M)(S - S^*) + w\beta(M - M^*)(S - S^*) \\
=& \beta S^*(S - S^*)(M^* - M) - (\beta M + \mu + \nu + \gamma)(S - S^*)^2 + \\
&+ \gamma(M^* - M)(S - S^*) + w\beta(M - M^*)(S - S^*) \\
\leq& \left(\beta S^* + \gamma - w\beta\right)(S - S^*)(M - M^*).
\end{aligned}$$

Choosing $w := \dfrac{\beta S^* + \gamma}{\beta} > 0$, it follows that $\dfrac{dV}{dt} \leq 0$. The claim follows from the same argument used in [66, Thm 7]. □

2.5.3 Global stability of the SAIRS model: a geometric approach

In this section, we use a geometric approach for the global stability of equilibria of nonlinear autonomous differential equations proposed in [69], that is a generalisation of the approach developed by Li and Muldowney [17, 18]. We briefly report the salient concepts in Appendix 2.A.

Theorem 2.5.3. *Under the assumptions (H1)-(H4), the unique endemic equilibrium x^* of* (2.35) *is globally asymptotically stable in $D \subset \Omega$.*

For our system (2.1), we have that the invariant manifold (2.36) is the set $\bar{\Gamma}$ in (2.2), so $n = 4$, $m = 1$, and $N(x) = -\mu$. It is easy to see that (H1) holds, and that for $\mathcal{R}_0 > 1$, by Theorem 2.4.2 and Lemma 2.4.3, (H2)-(H3) follows.

Theorem 2.5.4. *Assume that $\mathcal{R}_0 > 1$ and $\beta_A < \delta_I$. Then, the endemic equilibrium x^* is globally asymptotically stable in $\overset{\circ}{\bar{\Gamma}}$ for system* (2.1).

Proof. Let us recall that from (2.11), there exists $T > 0$ such that for $t > T$,

$$\varepsilon \leq S(t), A(t), I(t), R(t) \leq 1 - \varepsilon. \tag{2.30}$$

The Jacobian matrix of (2.1) may be written as

$$J = -\mu I_{4\times 4} + \Phi,$$

where $I_{4\times 4}$ is the 4×4 identity matrix and

$$\Phi = \begin{pmatrix} -(\beta_A A + \beta_I I + \nu) & -\beta_A S & -\beta_I S & \gamma \\ \beta_A A + \beta_I I & \beta_A S - (\delta_A + \alpha) & \beta_I S & 0 \\ 0 & \alpha & -\delta_I & 0 \\ \nu & \delta_A & \delta_I & -\gamma \end{pmatrix}.$$

From the definition of the third additive compound matrix (see, e.g., [19, Appendix]), we have

$$J^{[3]} = \Phi^{[3]} - 3\mu I_{4\times 4},$$

with

$$\Phi^{[3]} = \left(\phi_1^{[3]}, \phi_2^{[3]}, \phi_3^{[3]}, \phi_4^{[3]}\right)^T,$$

where

$$\begin{aligned}
\phi_1^{[3]} &= \left(-(\beta_A A + \beta_I I + \nu) + \beta_A S - (\delta_A + \alpha) - \delta_I,\ 0,\ 0,\ \gamma\right)^T, \\
\phi_2^{[3]} &= \left(\delta_I,\ -(\beta_A A + \beta_I I + \nu) + \beta_A S - (\delta_A + \alpha) - \gamma,\ \beta_I S,\ \beta_I S\right)^T, \\
\phi_3^{[3]} &= \left(-\delta_A,\ \alpha,\ -(\beta_A A + \beta_I I + \nu) - \delta_I - \gamma,\ -\beta_A S\right)^T, \\
\phi_4^{[3]} &= \left(\nu,\ 0,\ \beta_A A + \beta_I I,\ \beta_A S - (\delta_A + \alpha + \delta_I + \gamma)\right)^T.
\end{aligned}$$

Let $P(x)$ be such that

$$P(x) = \operatorname{diag}(R, cI, A, S),$$

where c is a constant such that $\dfrac{\delta_I + \mu}{\beta_I \varepsilon + \nu + \delta_I + \mu} < c < 1$, then from (2.37) by direct computation we have

$$B(t) = P_f P^{-1} + P J^{[3]} P^{-1} + \mu I_{4\times 4} = \operatorname{diag}\left(\frac{R'}{R}, \frac{I'}{I}, \frac{A'}{A}, \frac{S'}{S}\right) + P\Phi^{[3]}P^{-1} - 2\mu I_{4\times 4},$$

where

$$P\Phi^{[3]}P^{-1} = \left(\zeta_1^{[3]}, \zeta_2^{[3]}, \zeta_3^{[3]}, \zeta_4^{[3]}\right)^T,$$

and

$$\zeta_1^{[3]} = \left(-(\beta_A A + \beta_I I + \nu) + \beta_A S - (\delta_A + \alpha) - \delta_I,\ 0,\ 0,\ \gamma\frac{R}{S}\right)^T,$$

$$\zeta_2^{[3]} = \left(c\frac{\delta_I I}{R},\ -(\beta_A A + \beta_I I + \nu) + \beta_A S - (\delta_A + \alpha) - \gamma,\ c\frac{\beta_I IS}{A},\ c\beta_I I \right)^T,$$

$$\zeta_3^{[3]} = \left(-\frac{\delta_A A}{R},\ \frac{\alpha A}{cI},\ -(\beta_A A + \beta_I I + \nu) - \delta_I - \gamma,\ -\beta_A A \right)^T,$$

$$\zeta_4^{[3]} = \left(\frac{\nu S}{R},\ 0,\ (\beta_A A + \beta_I I)\frac{S}{A},\ \beta_A S - (\delta_A + \alpha + \delta_I + \gamma) \right)^T.$$

From the system of equations (2.1), we obtain

$$\frac{\gamma R}{S} = \mu\left(1 - \frac{1}{S}\right) + (\beta_A A + \beta_I I) + \nu + \frac{S'}{S}, \qquad \frac{\beta_I IS}{A} = \alpha + \delta_A + \mu - \beta_A S + \frac{A'}{A}, \tag{2.31}$$

$$\frac{\alpha A}{I} = \delta_I + \mu + \frac{I'}{I}, \qquad \frac{\delta_I I}{R} = \gamma + \mu - \frac{\delta_I I}{R} - \frac{\nu S}{R} + \frac{R'}{R}. \tag{2.32}$$

Consequently, by using (2.30) and (2.31)-(2.32), we have

$$\begin{aligned} h_1(t) &= b_{11}(t) + \sum_{j\neq 1} |b_{1j}(t)| \\ &= -(\beta_A A + \beta_I I + \nu) + \beta_A S - (\delta_A + \alpha) - \delta_I - 2\mu + \frac{R'}{R} + \frac{\gamma R}{S} \\ &= \beta_A S - \delta_A - \alpha - \delta_I - \frac{\mu}{S} + \frac{R'}{R} + \frac{S'}{S} \\ &\leq \beta_A - \delta_A - \alpha - \delta_I + \frac{R'}{R} + \frac{S'}{S} =: \bar{h}_1(t), \end{aligned}$$

$$\begin{aligned} h_2(t) &= b_{22}(t) + \sum_{j\neq 2} |b_{2j}(t)| \\ &= -(\beta_A A + \beta_I I + \nu) + \beta_A S - (\delta_A + \alpha) - \gamma - 2\mu + \frac{I'}{I} + c\frac{\delta_I I}{R} + c\frac{\beta_I SI}{A} + c\beta_I I \\ &\leq -\varepsilon\beta_A - \nu - \gamma - \mu + c(\gamma + \mu) + c\frac{I'}{I} + c\frac{R'}{R} + \frac{A'}{A} =: \bar{h}_2(t), \end{aligned}$$

$$
\begin{aligned}
h_3(t) &= b_{33}(t) + \sum_{j\neq 3} |b_{3j}(t)| \\
&= -(\beta_A A + \beta_I I + \nu) - \delta_I - \gamma - 2\mu + \frac{A'}{A} + \frac{\delta_A A}{R} + \frac{\alpha A}{cI} + \beta_A A \\
&\leq -\varepsilon\beta_I - \nu - \delta_I - \mu + \frac{\delta_I + \mu}{c} + \frac{A'}{A} + \frac{R'}{R} + \frac{I'}{cI} =: \bar{h}_3(t),
\end{aligned}
$$

$$
\begin{aligned}
h_4(t) &= b_{44}(t) + \sum_{j\neq 4} |b_{4j}(t)| \\
&= \beta_A S - (\delta_A + \alpha) - \delta_I - \gamma - 2\mu + \frac{S'}{S} + \frac{\nu S}{R} + \beta_A S + \frac{\beta_I S I}{A} \\
&\leq -\delta_I + \beta_A + \frac{S'}{S} + \frac{R'}{R} + \frac{A'}{A} =: \bar{h}_4(t).
\end{aligned}
$$

Then, we can take the matrix C in condition (H4) as

$$
C(t) = \operatorname{diag}\left(\bar{h}_1(t), \bar{h}_2(t), \bar{h}_3(t), \bar{h}_4(t)\right),
$$

based on (2.30) and by the assumption $\beta_A < \delta_I$, we can assert that

$$
\lim_{t\to\infty} \frac{1}{t} \int_0^t \bar{h}_i(s)ds = \bar{H}_i < 0, \qquad i = 1, \ldots, 4,
$$

where

$$
\begin{aligned}
\bar{H}_1 &= \beta_A - \delta_A - \alpha - \delta_I, \qquad \bar{H}_2 = -\varepsilon\beta_A - \nu - \gamma - \mu + c(\gamma + \mu), \\
\bar{H}_3 &= -\varepsilon\beta_I - \nu - \delta_I - \mu + \frac{\delta_I + \mu}{c}, \qquad \bar{H}_4 = -\delta_I + \beta_A.
\end{aligned}
$$

Indeed, if $\beta_A < \delta_I$ holds, both $\bar{H}_1$ and $\bar{H}_4$ are less than zero; moreover, $\bar{H}_2$ and $\bar{H}_3$ are less than zero by the choice of c. The claim then follows from Theorem 2.5.3. □

We proved the global asymptotic stability of the endemic equilibrium for the SAIRS model with a condition on the parameters, that is $\beta_A < \delta_I$. However, supported also by numerical simulations in Sec. 2.7, we are led to think that this assumption could be relaxed. Thus, we state the following conjecture.

Conjecture 2.5.5. *The endemic equilibrium x^* is globally asymptotically stable in $\mathring{\bar{\Gamma}}$ for system* (2.1) *if $R_0 > 1$.*

2.6 SAIRS without vaccination

Let us note that in the SAIRS-type models proposed so far, we have obtained results for the global stability of the DFE equilibrium when $\mathcal{R}_0 < 1$ and for the global stability of the endemic equilibrium when $\mathcal{R}_0 > 1$ (with further conditions), but we are not able to

study the stability of our system in the case $\mathcal{R}_0 = 1$. However, if we consider the SAIRS model without vaccination, i.e. the model (2.3) with $\nu = 0$, we are able to study also the case $\mathcal{R}_0 = 1$. From (2.5), in the case $\nu = 0$, we have

$$\mathcal{R}_0 = \left(\beta_A + \frac{\alpha\beta_I}{\delta_I + \mu}\right) \frac{1}{(\alpha + \delta_A + \mu)}, \tag{2.33}$$

the DFE is $x_0 = (1, 0, 0)$, and we obtain the following result.

Theorem 2.6.1. *The disease-free equilibrium x_0 is global asymptotically stable in Γ if $\mathcal{R}_0 \leq 1$.*

Proof. We follow the idea in [28, Prop. 3.1]. Let

$$C = \begin{pmatrix} \alpha + \delta_A + \mu & 0 \\ -\alpha & \delta_I + \mu \end{pmatrix},$$

and

$$Y = (A, I)^T.$$

Thus, we have

$$\frac{dY}{dt} = (C(M(S) - I_{2\times 2}))\, Y,$$

where

$$M(S) = \begin{pmatrix} \dfrac{\beta_A S}{\alpha + \delta_A + \mu} & \dfrac{\beta_I S}{\alpha + \delta_A + \mu} \\ \dfrac{\alpha\beta_A S}{(\delta_I + \mu)(\alpha + \delta_A + \mu)} & \dfrac{\alpha\beta_I S}{(\delta_I + \mu)(\alpha + \delta_A + \mu)} \end{pmatrix}.$$

Since, in this case, $S_0 = 1$, we have that $0 \leq S \leq S_0$, and $0 \leq M(S) \leq M(S_0)$, meaning that each element of $M(S)$ is less than or equal to the corresponding element of $M(S_0)$.
At this point, let us consider the positive-definite function

$$V(Y) = w\, C^{-1} Y,$$

where w is the left-eigenvector of $M(S_0)$ corresponding to $\rho(S_0)$; since $M(S_0)$ is a positive matrix, by Perron's theorem, $w > 0$. It is easy to see that $\rho(M(S_0)) = \mathcal{R}_0$ in (2.33), thus if $\mathcal{R}_0 \leq 1$, we have

$$\begin{aligned} \frac{dV}{dt} &= w\, C^{-1} \frac{dY}{dt} = w\,(M(S) - I_{2\times 2})\, Y \\ &\leq w\,(M(S_0) - I_{2\times 2})\, Y = (\rho(M(S_0)) - 1) wY \leq 0. \end{aligned}$$

If $\mathcal{R}_0 < 1$, then $\dfrac{dV}{dt} = 0 \iff Y = 0$. If $\mathcal{R}_0 = 1$, then

$$wM(S)Y = wY. \tag{2.34}$$

Now, if $S \neq S_0$, $wM(S) < wM(S_0) = \rho(M(S_0))w = w$: Thus, (2.34) holds if and only if $Y = 0$. If $S = S_0$, $wM(S) = wM(S_0) = w$, and $\dfrac{dV}{dt} = 0$ if $S = S_0$ and $Y = 0$. It can be seen that the maximal compact invariant set where $\dfrac{dV}{dt} = 0$ is the singleton $\{x_0\}$. Thus, by the LaSalle invariance principle the DFE x_0 is globally asymptotically stable if $\mathcal{R}_0 \leq 1$. □

Remark 1. *Note that the expression of $\mathcal{R}_0$ in (2.33), i.e. for the SAIRS model with $\nu = 0$, does not depend on the parameter γ. Thus, when $\nu = 0$, the SAIR ($\gamma = 0$) and SAIRS ($\gamma > 0$) models have the same $\mathcal{R}_0$. On the contrary, when we consider the vaccination, the expression of $\mathcal{R}_0$ depends both by γ and ν, as in (2.5).*

By denoting the expression in (2.5) as $\mathcal{R}_0^{\text{vacc}}$ and that in (2.33) as $\mathcal{R}_0^{\text{no-vacc}}$, we have

$$\mathcal{R}_0^{\text{vacc}} = \mathcal{R}_0^{\text{no-vacc}} \frac{\mu + \gamma}{\mu + \gamma + \nu}.$$

Hence, we can find the minimum vaccination proportion of susceptible individuals that will eradicate the disease in the long-run, namely

$$\nu_{\text{crit}} = (\mu + \gamma)\left(\mathcal{R}_0^{\text{no-vacc}} - 1\right).$$

An increase of γ, meaning a shorter immunity time-window, corresponds to an increase in the minimum vaccination effort necessary to keep R_0 below 1.

2.7 Numerical analysis

In this section, we provide numerous realizations of system (2.1). In particular, to back the claim we made in Conjecture 2.5.5, in all the figures we chose $\beta_A > \delta_I$, with the exception of Figure 2.7, still obtaining numerical convergence towards the endemic equilibrium when $\mathcal{R}_0 > 1$.
Considering all the other parameters to be fixed, $\mathcal{R}_0$ becomes a linear function of β_A and β_I; in particular, the line $\mathcal{R}_0(\beta_A, \beta_I) = 1$ is clearly visible in all the subfigures of Figure 2.2, in which we visualize the equilibrium values of S, A, I, R as functions of β_A and β_I. When $R_0 < 1$, the values of β_A and β_I do not influence the value of the equilibrium point (2.4), and the value of the fraction of individuals in each compartment remains constant. For values of $R_0 > 1$, we can see the influence of the infection parameters on each components of the endemic equilibrium (see (2.12), (2.13), (2.14)).

Figures 2.3a, 2.3b, 2.3c and 2.3d confirm our analytical results on the asymptotic values of the fraction of individuals in each compartment. In particular, the endemic equilibrium value of S (2.13) does not depend on γ, the loss of immunity rate, as shown by the time series corresponding to $\gamma = 0.01$, 0.02 and 0.05, whereas the disease free equilibrium value of S (2.4), corresponding to the $\gamma = 0.001$ plot, does. Increasing the value of γ, which corresponds to decreasing the average duration $1/\gamma$ of the immunity

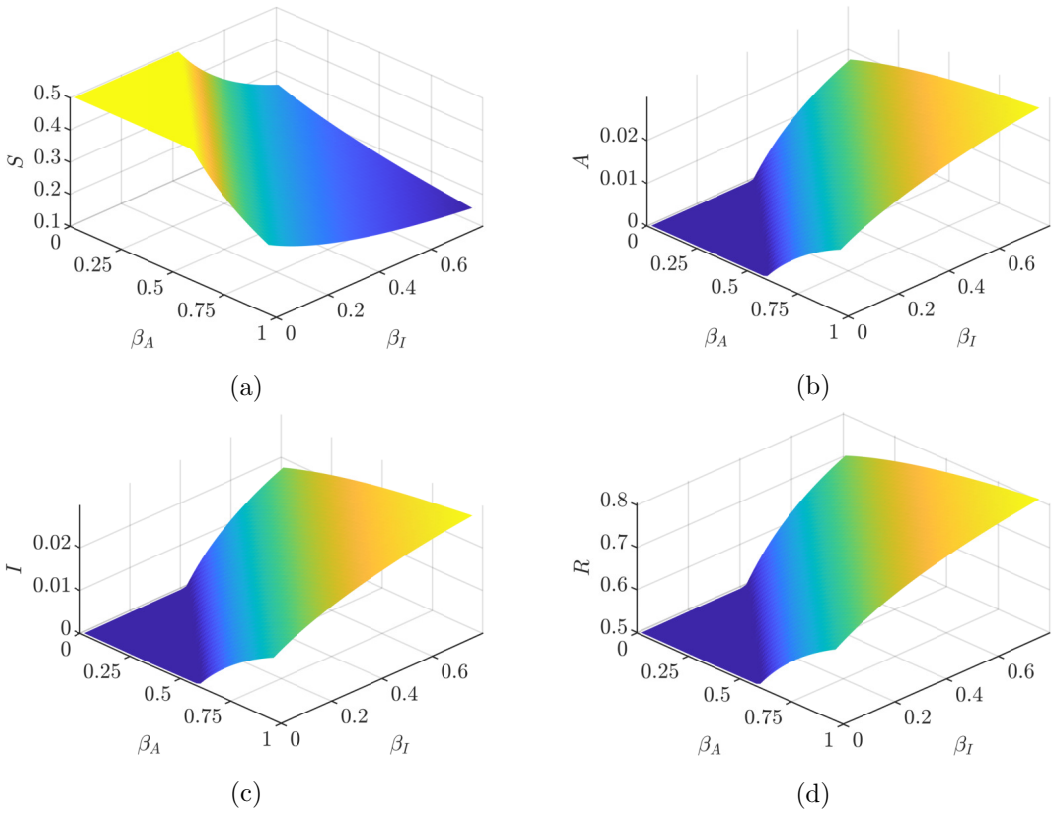

Figure 2.2: Asymptotic values of S, A, I, and R as a function of β_A and β_I. Values of the parameters: $\mu = 1/(70 \cdot 365)$, meaning an average lifespan of 70 years; $\beta_A \in [0.01, 0.8]$ $\beta_I \in [0.01, 0.95]$, $\nu = 0.01$, $\gamma = 1/100$, meaning the immunity lasts on average 100 days; $\alpha = 0.15$, $\delta_A = 0.1$, $\delta_I = 0.15$.

time-window, results in bigger asymptotic values for the asymptomatic and symptomatic infected population A and I, and in a smaller asymptotic value for the recovered population R. This trend is quite intuitive: indeed, by keeping the other parameters fixed, if the average immune period decreases (i.e., γ increases), a removed individual quickly returns to the susceptible state, hence the Behaviour of the SAIRS model approaches that of a SAIS model.

Next, we explore the effect of changing α, the rate of symptoms onset, in three scenarios: equally infectious asymptomatic and symptomatic individuals ($\beta_A = \beta_I$), in Figure 2.4; asymptomatic individuals more infectious than symptomatic individuals ($\beta_A > \beta_I$: this case can be of interest if we consider that asymptomatic individuals can, in principle, move and spread the infection more than symptomatic ones) in Figure 2.5; and vice-versa ($\beta_A < \beta_I$), in Figure 2.6. If $\mathcal{R}_0 > 1$, A^* and I^* are related by $A^* = \dfrac{\delta_I + \mu}{\alpha} I^*$ (2.12). This means that, regardless of the values of β_A and β_I, $A^* > I^*$ if

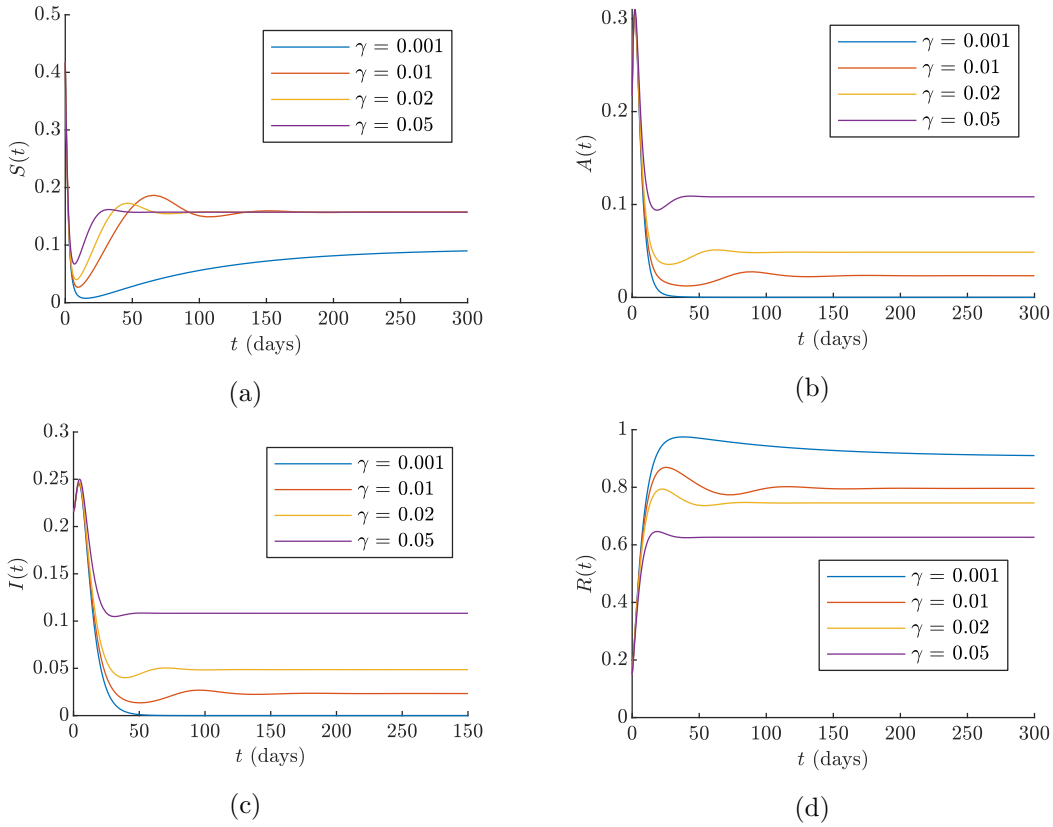

Figure 2.3: Behaviour of system (2.1) as γ, the rate of loss of immunity, varies. Values of the parameters: $\mu = 1/(70 \cdot 365)$, meaning an average lifespan of 70 years; $\beta_A = 0.8$ $\beta_I = 0.95$, $\nu = 0.01$, γ varying as shown; $\alpha = 0.15$, $\delta_A = 0.125$, $\delta_I = 0.15$.

and only if $\dfrac{\delta_I + \mu}{\alpha} > 1$. This is evident in Figures 2.4b, 2.5b and 2.6b, where the smallest value of that ratio, corresponding to $\alpha = 0.9$, is smaller than 1, results in $I^* > A^*$; the biggest value of that ratio, and the only one significantly bigger than 1 is attained for $\alpha = 0.01$, and results in $I^* < A^*$. Increasing α leads to a smaller asymptotic value for A, and a bigger asymptotic value for I. Effectively, by keeping fixed the other parameters and increasing α leads to a decreasing of the average time-period before developing symptoms, thus the Behaviour of the SAIRS model approaches that of the SIRS one, as α increases.

Finally, in Figure 2.7, we compare the effect of varying ν, the vaccination rate, on the epidemic dynamics. In particular, the parameter values chosen satisfy the assumption of Theorem 2.5.4, i.e. $\mathcal{R}_0 > 1$ and simultaneously $\beta_A < \delta_I$. We observe that the asymptotic values of A and I are decreasing in ν, whereas the endemic equilibrium value of S is independent of this parameter, as we expect from (2.13), and the endemic equilibrium value of R is increasing in ν.

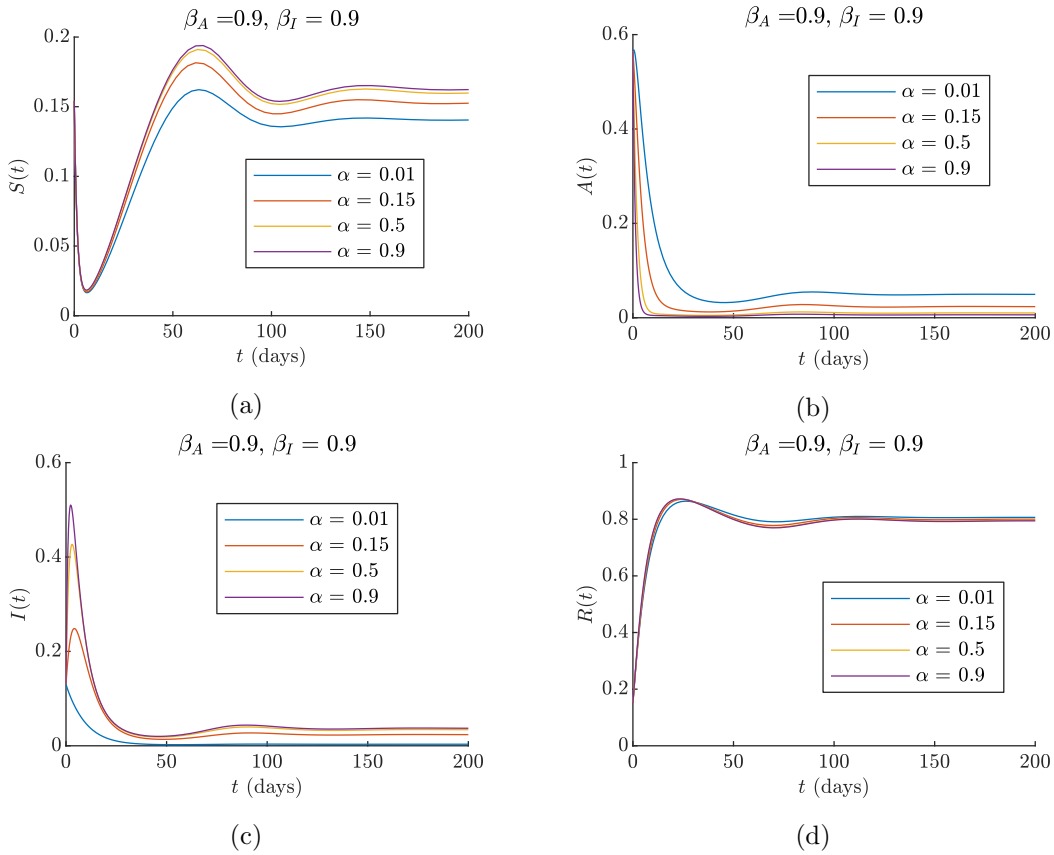

Figure 2.4: Behaviour of system (2.1) as α, the rate of symptoms onset, varies. Values of the parameters: $\mu = 1/(70 \cdot 365)$, meaning an average lifespan of 70 years; $\beta_A = \beta_I = 0.9$, $\nu = 0.01$, $\gamma = 1/100$, meaning the immunity lasts on average 100 days; α varying as shown, $\delta_A = 0.125$, $\delta_I = 0.15$.

2.8 Summary and Outlook

We analysed the behaviour of an SAIRS compartmental model with vaccination. We determined the value of the basic reproduction number $\mathcal{R}_0$; then, we proved that the disease-free equilibrium is globally asymptotically stable, i.e. the disease eventually dies out if $\mathcal{R}_0 < 1$. Moreover, in the SAIRS-type model without vaccination ($\nu = 0$), we were able to generalise the result on the global asymptotic stability of the DFE also in the case $\mathcal{R}_0 = 1$.

Furthermore, we proved the uniform persistence of the disease and the existence of a unique endemic equilibrium if $\mathcal{R}_0 > 1$. Later, we analysed the stability of this endemic equilibrium for some sub-cases of the model.

The first case describes a disease which confers permanent immunity, i.e. $\gamma = 0$: the model reduces to an SAIR. In this framework, we answered the open problem presented in [66], including the additional complexity of vaccination: we proved the global asymptotic

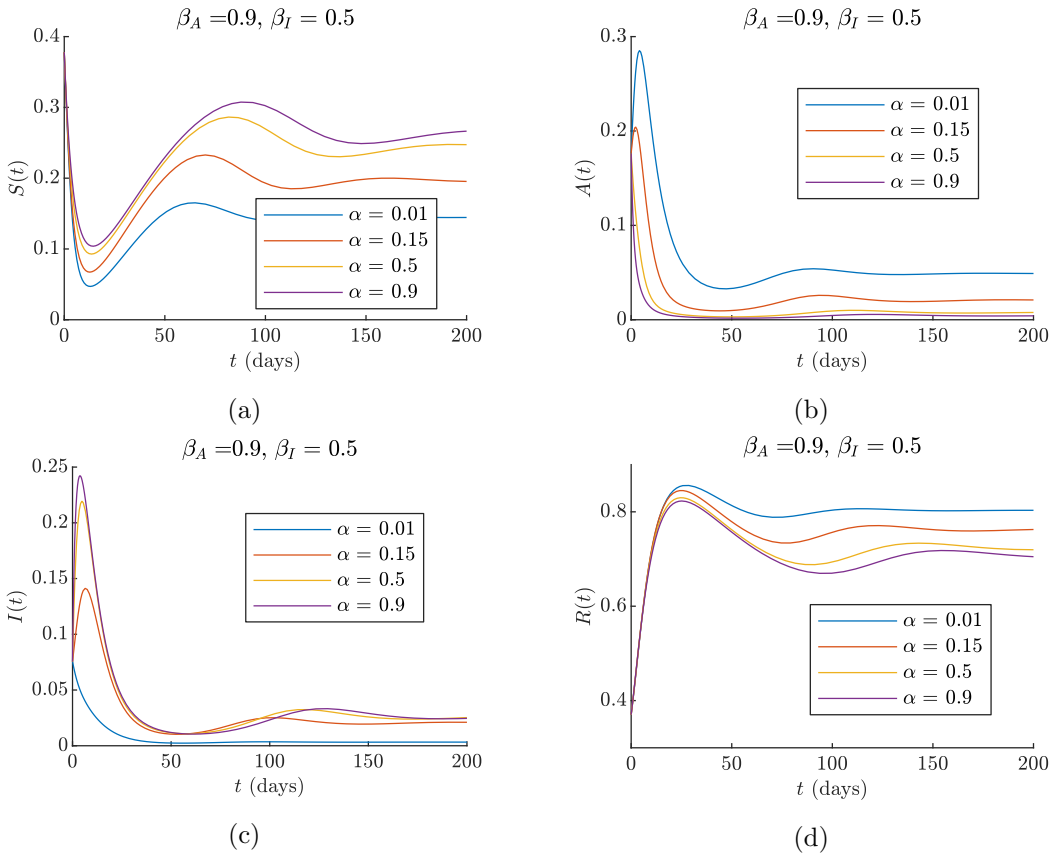

Figure 2.5: Behaviour of system (2.1) as α, the rate of symptoms onset, varies. Values of the parameters: $\mu = 1/(70 \cdot 365)$, meaning an average lifespan of 70 years; $\beta_A = 0.9$ $\beta_I = 0.5$, $\nu = 0.01$, $\gamma = 1/100$, meaning the immunity lasts on average 100 days; α varying as shown, $\delta_A = 0.125$, $\delta_I = 0.15$.

stability of the endemic equilibrium when $\mathcal{R}_0 > 1$.

We then proceeded to extend the results provided in [61] on the local stability analysis for a SAIRS-type model. We first considered the SAIRS model with the assumption that both asymptomatic and symptomatic infectious have the same transmission rate and recovery rate, i.e., $\beta_A = \beta_I$ and $\delta_A = \delta_I$, respectively. We were able to show that the endemic equilibrium is globally asymptotically stable if $\mathcal{R}_0 > 1$. Moreover, we analysed the model without restrictions; we used the geometric approach proposed in [69] to find the conditions under which the endemic equilibrium is globally asymptotically stable. We proved the global stability in the case $\mathcal{R}_0 > 1$ and $\beta_A < \delta_I$.

We leave, as an open problem, the global asymptotic stability of the endemic equilibrium without any restriction on the parameters: we conjecture that the global asymptotic stability for the endemic equilibrium only requires $\mathcal{R}_0 > 1$, as our numerical simulations suggest.

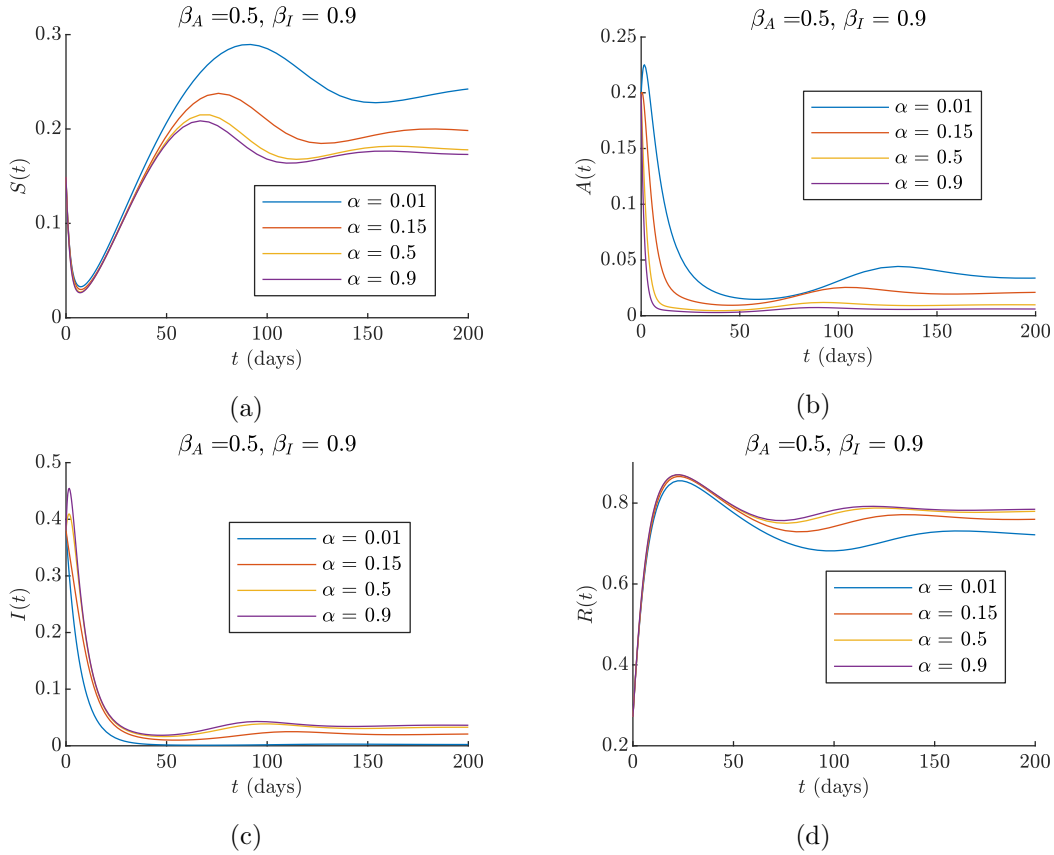

Figure 2.6: Behaviour of system (2.1) as α, the rate of symptoms onset, varies. Values of the parameters: $\mu = 1/(70 \cdot 365)$, meaning an average lifespan of 70 years; $\beta_A = 0.5$ $\beta_I = 0.9$, $\nu = 0.01$, $\gamma = 1/100$, meaning the immunity lasts on average 100 days; α varying as shown, $\delta_A = 0.125$, $\delta_I = 0.15$.

Many generalisations and investigations of our model are possible. For example, we considered the vital dynamics without distinguish between natural death and disease related deaths; an interesting, although complex, generalisation of our model could explore the implications of including disease-induced mortality.

A natural extension of our SAIRS model could take into account different groups of individual among which an epidemic can spread. One modelling approach for this are multi-group compartmental models, which is discussed in Chapter 3. Other more realistic extensions may involve a greater number of compartments, for example the "Exposed" group, or time-dependent parameters which can describe the seasonality of a disease or some response measures from the population, as well as non-pharmaceutical interventions.

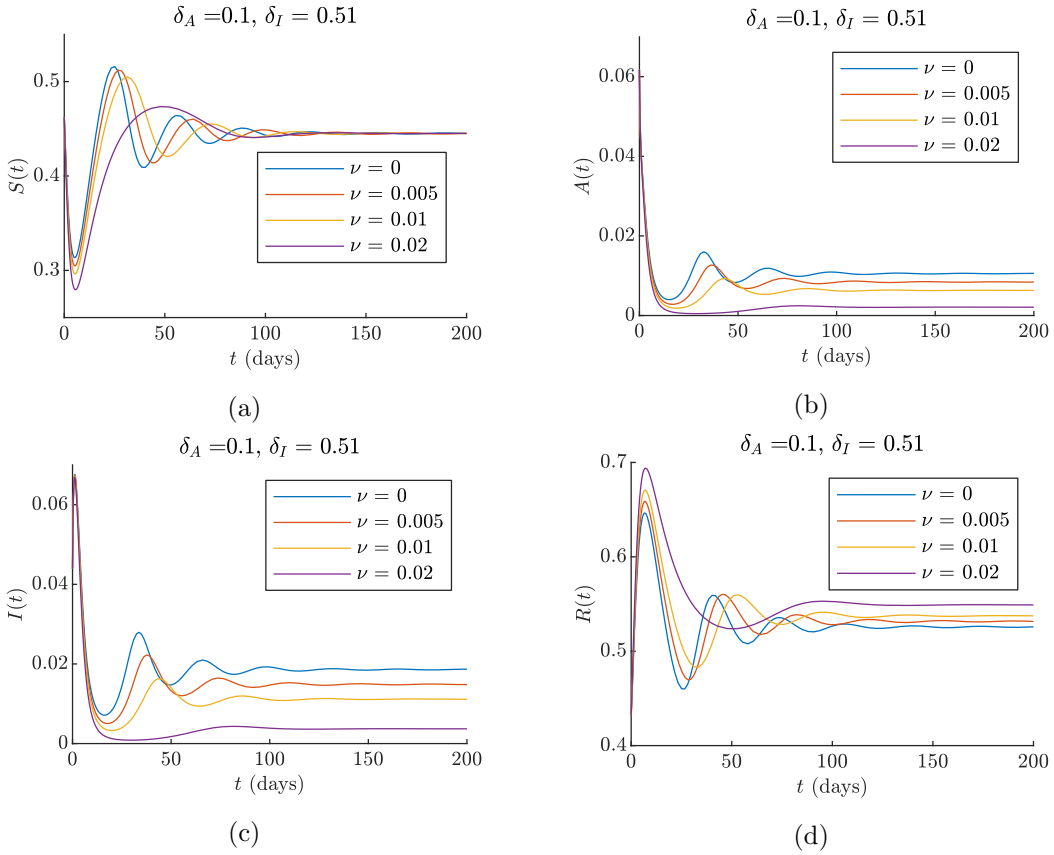

Figure 2.7: Behaviour of system (2.1) as ν, the vaccination rate, varies. Values of the parameters: $\mu = 1/(70 \cdot 365)$, meaning an average lifespan of 70 years; $\beta_A = 0.5$ $\beta_I = 0.9$, ν varying as shown, $\gamma = 1/50$, meaning the immunity lasts on average 50 days; $\alpha = 0.9$, $\delta_A = 0.1$, $\delta_I = 0.51$. The condition $\beta_A < \delta_I$ is satisfied.

Appendix

2.A The geometric approach

We recall the salient concepts of the geometric approach proposed in [69] for the global stability of equilibria of nonlinear autonomous differential equations, that generalises the criteria developed by Li and Muldowney [17, 18].

Consider the following autonomous system

$$x' = f(x), \qquad x \in D \subset \mathbb{R}^n, \tag{2.35}$$

where $f : D \to \mathbb{R}^n$ is a continuous differentiable function on D. Let $x(t, x(0))$ be the solution of system (2.35) with the initial value $x(0, x(0)) = x(0)$. We assume that system (2.35) has an $n - m$ dimensional invariant manifold Ω defined by

$$\Omega = \{x \in \mathbb{R}^n | g(x) = 0\}, \tag{2.36}$$

where $g(x)$ is an $\mathbb{R}^m$-valued twice continuously differentiable function with $\dim(\frac{\partial g}{\partial x}) = m$ when $g(x) = 0$. In [18], Li and Muldowney proved that if Ω is invariant with respect to system (2.35), then there exists a continuous $m \times m$ dimensional matrix-valued function $N(x)$, such that

$$g_f(x) = \frac{\partial g}{\partial x} \cdot f(x) = N(x) \cdot g(x),$$

where $g_f(x)$ is the directional derivative of $g(x)$ in the direction of the vector field f. Moreover, let us define the real valued function $\sigma(x)$ on Ω, by

$$\sigma(x) = tr(N(x)),$$

and make the following assumptions:

(H1) Ω is simply connected;

(H2) There is a compact absorbing set $K \subset D \subset \Omega$;

(H3) x^* is the unique equilibrium of system (2.35) in $D \subset \Omega$ which satisfies $f(x^*) = 0$.

Now, consider the following linear differential equation, associated to system (2.35)

$$z'(t) = \left[P_f P^{-1} + P J^{[m+2]} P^{-1} - \sigma I\right] z(t) =: B(x(t, x(0))z(t), \tag{2.37}$$

where $x \mapsto P(x)$ is a C^1 nonsingular $\binom{n}{m+2} \times \binom{n}{m+2}$ matrix-valued function in Ω such that $||P^{-1}(x)||$ is uniformly bounded for $x \in K$ and P_f is the directional derivative of P in the direction of the vector field f, and $J^{[m+2]}$ is the $m+2$ additive compound matrix of the Jacobian matrix of (2.35). Assume that the following additional condition holds:

(H4) for the coefficient matrix $B(x(t, x(0))$, there exists a matrix $C(t)$, a large enough $T_1 > 0$ and some positive numbers $\alpha_1, \alpha_2, \ldots, \alpha_n$ such that for all $t \geq T_1$ and all $x(0) \in K$ it holds

$$b_{ii}(t) + \sum_{i \neq j} \frac{\alpha_j}{\alpha_i} |b_{ij}(t)| \leq c_{ii}(t) + \sum_{i \neq j} \frac{\alpha_j}{\alpha_i} |c_{ij}(t)|,$$

and

$$\lim_{t \to \infty} \frac{1}{t} \int_0^t c_{ii}(s) + \sum_{i \neq j} \frac{\alpha_j}{\alpha_i} |c_{ij}(s)| \, ds = h_i < 0,$$

where $b_{ij}(t)$ and $c_{ij}(t)$ represent entries of matrices $B(x(t, x(0))$ and $C(t)$, respectively. Basically, condition (H4) is a Bendixson criterion for ruling out non-constant periodic solutions of system (2.35) with invariant manifold Ω. From this, by a similar argument as in Ballyk et al. [79], based on [18, Thm 6.1], the following theorem can be deduced (see [69, Thm 2.6]).

3. Global stability of multi-group SAIRS epidemic models

3.1 Introduction and Outline

One of the most common assumptions in classic population models is the homogeneity of interactions between individuals, which then happen completely at random. While such an assumption significantly simplifies the analysis of the models, it can be beneficial to renounce it and to formulate models with more realistic interactions. Heterogeneity in the interactions among the population can depend on many factors. The most common division regards the geographical distinction and the membership to different communities, cities or countries, in which the same infectious disease can have a different behaviour based on the group under study.

The division in groups can also depend on the specific disease under study. For example, individuals can be divided into age groups to study children's diseases, such as measles, mumps or rubella, or can be differentiated by the number of sexual partners for sexually transmitted infections. Multi-group models can also be useful to study disease transmitted via vectors or multiple hosts, such as Malaria or West-Nile virus.

The concept of equitable partitions has been used to study networks partitioned into local communities with some regularities in their structure, in the case of SIS and SIRS models [80, 81, 82], by means of the N-Intertwined Mean-Field approximation [83]. In the aforementioned works, the macroscopic structure of hierarchical networks is described by a quotient graph and the stability of the endemic equilibrium can be investigated by a lower-dimensional system with respect to the starting one. Several authors proposed multi-group models to describe the transmission behaviour between different communities or cities, see for example [84, 85, 86]

Due to the aforementioned motivations, in this chapter we present a multi-group model, as extension of the SAIRS-type model proposed in Chapter 2. We assume that each individual interacts within a network of relationships, due e.g. to different social or spatial patterns; individuals are hence divided into groups, which are not isolated from one another.

In our model, we denote with S_i, A_i, I_i and R_i, $i = 1, \dots, n$, the fraction of Susceptible, Asymptomatic infected, symptomatic Infected and Recovered individuals, respectively, in the $i-$th group, such that $S_i + A_i + I_i + R_i = 1$. We remark that, from here

on, we will use the terms community and group interchangeably.

The disease can be transmitted by individuals in the classes A_i and I_i, within their group, to the susceptible S_i, with transmission rate β_{ii}^A and β_{ii}^I, respectively, but also between different groups: e.g., individuals A_j and I_j, belonging to the j-th community, may infect susceptible individuals S_i of group i with transmission rate β_{ij}^A and β_{ij}^I, respectively. From the asymptomatic compartment, an individual can either progress to the class of symptomatic infectious or recover without ever developing symptoms. We assume that the average time of the symptoms developing, denoted by $1/\alpha$, and the recovery rates from both the infectious compartments, δ_A and δ_I, do not depend on the community of origin, i.e. these parameters depend only on the disease. Furthermore, the average time to return to the susceptible state, $1/\gamma$, only depends on the specific disease under study, and not on the community to which an individual belongs. The remaining parameters of the model depend on the community's membership. First, the proportion of susceptible individuals who receive the vaccine might be different for each group; we denote with ν_i, $i = 1, \dots, n$, the proportion of susceptible in the $i-$th group who receive a vaccine-induced temporary immunity. Moreover, μ_i, $i = 1, \dots, n$ represent both the birth rates and the natural death rates in community i. Finally, individuals of different communities may have contacts each other, by direct transport, but they never permanently move to another community. Therefore, the total population in each group may only change through births and natural deaths; we do not distinguish between natural deaths and disease-related deaths.

The chapter is organized as follows. In Sec. 3.2, we present the system of equations for the multi-group SAIRS model with vaccination, providing its positive invariant set. In Sec. 3.3, we determine the basic reproduction number $\mathcal{R}_0$ and prove that the disease-free equilibrium (DFE) is globally asymptotically stable (GAS) if $\mathcal{R}_0 < 1$ and unstable if $\mathcal{R}_0 > 1$. Moreover, we prove the GAS of the DFE also in the case $\mathcal{R}_0 = 1$, for the model in which no vaccination is administered to the susceptible individuals. In Sec. 3.4, we prove the existence and uniqueness of an endemic equilibrium (EE) by a fixed point argument, as in [26], since there is no explicit expression for $\mathcal{R}_0$. Later, we provide sufficient conditions for the local asymptotic stability of the EE. In Sec. 3.5, we discuss the uniform persistence of the disease and we investigate the global asymptotic stability of the EE for two variations of the original model under study. Precisely, in Thm. 3.5.2, we study the global stability of the SAIR model (i.e. $\gamma = 0$) and we prove that the EE is GAS if $\mathcal{R}_0 > 1$. In Sec. 3.5.2, we establish sufficient conditions for the GAS of the EE for the SAIRS model (i.e., $\gamma \neq 0$) with vaccination, under the restriction that asymptomatic and symptomatic individuals have the same average recovery period, i.e. $\delta_A = \delta_I$. The problem of the global stability of the endemic equilibrium in the most general case, i.e. $\delta_A \neq \delta_I$, remains open. In Sec. 3.7, we provide some numerical simulations in which we simulate the evolution of the epidemics in four different structures of community networks.

3.2 The multi-group SAIRS model with vaccination

The system of ODEs which describes the evolution of the disease in the i-th community is the following:

$$\begin{aligned}
\frac{dS_i(t)}{dt} &= \mu_i - \sum_{j=1}^{n} \left(\beta_{ij}^A A_j(t) + \beta_{ij}^I I_j(t)\right) S_i(t) - (\mu_i + \nu_i) S_i(t) + \gamma R_i(t), \\
\frac{dA_i(t)}{dt} &= \sum_{j=1}^{n} \left(\beta_{ij}^A A_j(t) + \beta_{ij}^I I_j(t)\right) S_i(t) - (\alpha + \delta_A + \mu_i) A_i(t), \\
\frac{dI_i(t)}{dt} &= \alpha A_i(t) - (\delta_I + \mu_i) I_i(t), \\
\frac{dR_i(t)}{dt} &= \delta_A A_i(t) + \delta_I I_i(t) + \nu_i S_i(t) - (\gamma + \mu_i) R_i(t), \qquad i = 1, \ldots, n,
\end{aligned} \tag{3.1}$$

with initial condition $(S_1(0), A_1(0), I_1(0), R_1(0), \ldots, S_n(0), A_n(0), I_n(0), R_n(0))$ belonging to the set

$$\bar{\Gamma} = \{(S_1, A_1, I_1, R_1, \ldots, S_n, A_n, I_n, R_n) \in \mathbb{R}_+^{4n} | S_i + A_i + I_i + R_i = 1, i = 1, \ldots, n\}, \tag{3.2}$$

where $\mathbb{R}_+^{4n}$ indicates the non-negative orthant of $\mathbb{R}^{4n}$. The flow diagram representing the interaction among two groups of system (3.1), as well as their internal dynamics, is given in Figure 1.

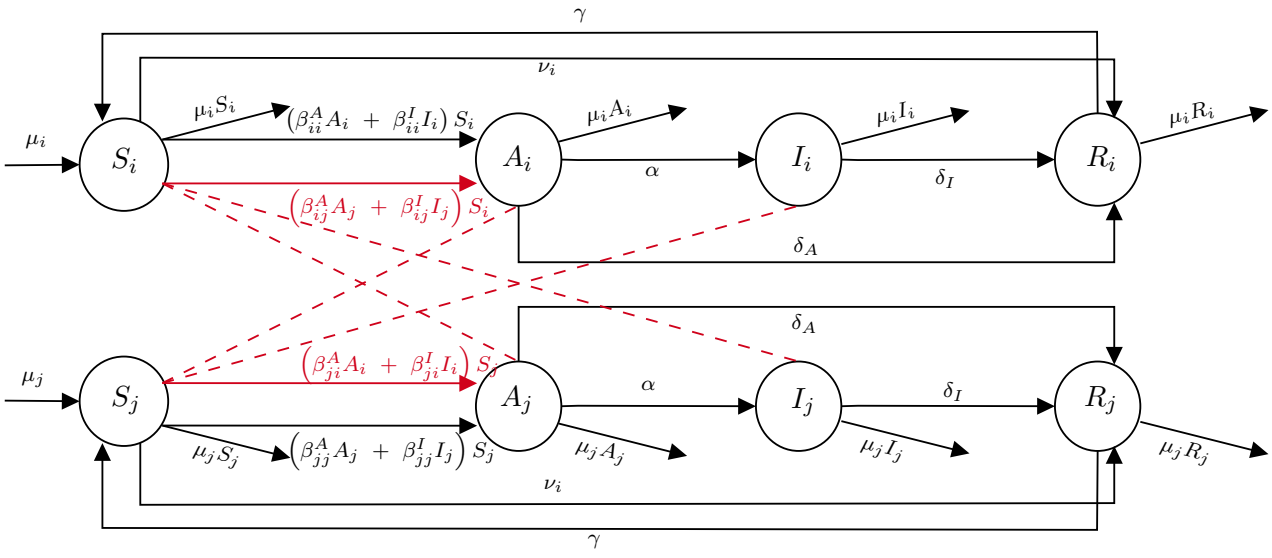

Figure 1: Flow diagram for system (3.1), depicting the interaction between communities i and j, as well as their internal dynamics. The solid lines represent internal dynamics within each group, whereas the dashed lines represent the inter-group influence of infected individuals.

Assuming initial conditions in $\bar{\Gamma}$, $S_i(t) + A_i(t) + I_i(t) + R_i(t) = 1$, for all $t \geq 0$ and $i = 1, \ldots, n$; hence, system (3.1) is equivalent to the following $3n$-dimensional dynamical system:

$$\begin{aligned}
\frac{dS_i(t)}{dt} &= \mu_i - \sum_{j=1}^{n} \left(\beta_{ij}^A A_j(t) + \beta_{ij}^I I_j(t) \right) S_i(t) - (\mu_i + \nu_i + \gamma) S_i(t) + \gamma(1 - A_i(t) - I_i(t)), \\
\frac{dA_i(t)}{dt} &= \sum_{j=1}^{n} \left(\beta_{ij}^A A_j(t) + \beta_{ij}^I I_j(t) \right) S_i(t) - (\alpha + \delta_A + \mu_i) A_i(t), \\
\frac{dI_i(t)}{dt} &= \alpha A_i(t) - (\delta_I + \mu_i) I_i(t), \qquad\qquad i = 1, \ldots, n,
\end{aligned} \tag{3.3}$$

with initial condition $(S_1(0), A_1(0), I_1(0), \ldots, S_n(0), A_n(0), I_n(0))$ belonging to the set

$$\Gamma = \{(S_1, A_1, I_1, \ldots, S_n, A_n, I_n) \in \mathbb{R}_+^{3n} | S_i + A_i + I_i \leq 1, i = 1, \ldots, n\}.$$

System (3.3) can be written in vector notation as

$$\frac{dx(t)}{dt} = f(x(t)), \tag{3.4}$$

where $x(t) = (S_1(t), A_1(t), I_1(t), \ldots, S_n(t), A_n(t), I_n(t))$ and $f(x(t)) = (f_1(x(t)), f_2(x(t)), \ldots, f_{3n}(x(t)))$ is defined according to (3.3).

We make the following assumptions:

Assumption 1.

- *The matrices* $[\beta^A_{ij}]_{i,j=1,\dots,n}$ *and* $[\beta^I_{ij}]_{i,j=1,\dots,n}$ *are irreducible. This means that every pair of communities is connected by a path.*
- $\beta^A_{ii} \neq 0$, $\beta^I_{ii} \neq 0, i = 1, \dots, n$. *This means that infection can spread within each community.*

Theorem 3.2.1. Γ *is positively invariant for system* (3.3)*. That is, for all initial values* $x(0) \in \Gamma$*, the solution* $x(t)$ *of* (3.3) *will remain in* Γ *for all* $t > 0$*.*

Proof. Let us consider the boundary $\partial\Gamma$, as in Theorem 2.2.1. It consists of the following hyperplanes:

$$\begin{aligned}
H_{1,i} &= \{(S_1, A_1, I_1, \dots, S_n, A_n, I_n) \in \Gamma \mid S_i = 0\},\\
H_{2,i} &= \{(S_1, A_1, I_1, \dots, S_n, A_n, I_n) \in \Gamma \mid A_i = 0\},\\
H_{3,i} &= \{(S_1, A_1, I_1, \dots, S_n, A_n, I_n) \in \Gamma \mid I_i = 0\},\\
H_{4,i} &= \{(S_1, A_1, I_1, \dots, S_n, A_n, I_n) \in \Gamma \mid S_i + A_i + I_i = 1\}, \qquad i = 1, \dots, n.
\end{aligned}$$

Let us consider $H_{k,1}$, $k = 1, 2, 3, 4$. The outward normal vectors of $H_{1,1}$, $H_{2,1}$, $H_{3,1}$, and $H_{4,1}$ are, respectively

$$\begin{aligned}
\eta_{1,1} &= (-1, 0, 0, \dots, 0, 0, 0), \qquad & \eta_{2,1} &= (0, -1, 0, \dots, 0, 0, 0),\\
\eta_{3,1} &= (0, 0, -1, \dots, 0, 0, 0), \qquad & \eta_{4,1} &= (1, 1, 1, \dots, 0, 0, 0).
\end{aligned}$$

Let $x \in H_{k,1}$, $k = 1, \dots, 4$, and consider the following cases:

Case 1: $S_1 = 0$. Then, since $A_1 + I_1 \leq 1$,

$$\langle f(x), \eta_{1,1} \rangle = -\mu_1 - \gamma(1 - A_1 - I_1) \leq 0.$$

Case 2: $A_1 = 0$. Then, since $S_1 \geq 0$, $A_i \geq 0$, $I_i \geq 0$, $i = 2, \dots, n$

$$\langle f(x), \eta_{2,1} \rangle = -\underbrace{\left(\sum_{j=2}^{n} \beta^A_{ij} A_j + \sum_{j=1}^{n} \beta^I_{ij} I_j \right)}_{\geq 0} S_1 \leq 0.$$

Case 3: $I_1 = 0$. Then, since $A_1 \geq 0$

$$\langle f(x), \eta_{3,1} \rangle = -\alpha A_1 \leq 0.$$

Case 4: $S_1 + A_1 + I_1 = 1$. Then, since $S_1 \geq 0$, $A_1 \geq 0$, $I_1 \geq 0$

$$\langle f(x), \eta_{4,1} \rangle = -\nu_1 S_1 - \delta_A A_1 - \delta_I I_1 \leq 0.$$

The proof for the hyperplanes $H_{k,i}$, $k = 1, \dots, 4$ and $i = 2, \dots, n$ is analogous. □

3.3 Disease Elimination

System (3.3) always admits a disease-free equilibrium, whose expression is:

$$x_0 = (S_{0,1}, A_{0,1}, I_{0,1}, \ldots, S_{0,n}, A_{0,n}, I_{0,n}),$$

where

$$S_{0,i} = \frac{\gamma + \mu_i}{\gamma + \mu_i + \nu_i}, \qquad A_{0,i} = I_{0,i} = 0, \qquad i = 1, \ldots, n. \tag{3.5}$$

Note that, in general, $S_{0,i} \neq S_{0,j}$ if $i \neq j$.

Lemma 3.3.1. *Consider the matrix*

$$M_1 = \left(\left(\beta_{ij}^A + \frac{\alpha \beta_{ij}^I}{\delta_I + \mu_i} \right) \frac{S_{0,i}}{\alpha + \delta_A + \mu_i} \right)_{i,j=1,\ldots,n}. \tag{3.6}$$

The basic reproduction number $\mathcal{R}_0$ of (3.3) is

$$\mathcal{R}_0 = \rho(M_1) = \rho \left(\left(\left(\beta_{ij}^A + \frac{\alpha \beta_{ij}^I}{(\delta_I + \mu_i)} \right) \frac{\gamma + \mu_i}{(\gamma + \mu_i + \nu_i)(\alpha + \delta_A + \mu_i)} \right)_{i,j=1,\ldots,n} \right), \tag{3.7}$$

where $\rho(M_1)$ is the spectral radius of the matrix M_1.

Proof. We shall use the next generation matrix method [74] to find $\mathcal{R}_0$. System (3.3) has $2n$ disease compartments, namely A_i and I_i, $i = 1, \ldots, n$. Rearranging the order of the equations such that the disease compartments can be written as $x = (A_1, \ldots, A_n, I_1, \ldots, I_n)^T$, we can rewrite the corresponding ODEs as

$$\begin{aligned} \frac{dA_i(t)}{dt} &= \mathcal{F}_{1_i}(S_i(t), A_i(t), I_i(t)) - \mathcal{V}_{1,i}(S_i(t), A_i(t), I_i(t)), \\ \frac{dI_i(t)}{dt} &= \mathcal{F}_{2,i}(S_i(t), A_i(t), I_i(t)) - \mathcal{V}_{2,i}(S_i(t), A_i(t), I_i(t)), \end{aligned}$$

where

$$\begin{aligned} \mathcal{F}_{1,i} &= \sum_{i=1}^{n} \left(\beta_{ij}^A A_j(t) + \beta_{ij}^I I_j(t) \right) S_i(t), & \mathcal{V}_{1,i} &= (\alpha + \delta_A + \mu_i) A_i(t), \\ \mathcal{F}_{2,i} &= 0, & \mathcal{V}_{2,i} &= -\alpha A_i(t) + (\delta_I + \mu_i) I_i(t). \end{aligned}$$

Thus, we obtain

$$F = \begin{pmatrix} \left(\dfrac{\partial \mathcal{F}_{1,i}}{\partial A_j}(x_0)\right)_{i,j=1,\dots,n} & \left(\dfrac{\partial \mathcal{F}_{1,i}}{\partial I_j}(x_0)\right)_{i,j=1,\dots,n} \\ \left(\dfrac{\partial \mathcal{F}_{2,i}}{\partial A_j}(x_0)\right)_{i,j=1,\dots,n} & \left(\dfrac{\partial \mathcal{F}_{2,i}}{\partial I_j}(x_0)\right)_{i,j=1,\dots,n} \end{pmatrix}, \tag{3.8}$$

$$V = \begin{pmatrix} \left(\dfrac{\partial \mathcal{V}_{1,i}}{\partial A_j}(x_0)\right)_{i,j=1,\dots,n} & \left(\dfrac{\partial \mathcal{V}_{1,i}}{\partial I_j}(x_0)\right)_{i,j=1,\dots,n} \\ \left(\dfrac{\partial \mathcal{V}_{2,i}}{\partial A_j}(x_0)\right)_{i,j=1,\dots,n} & \left(\dfrac{\partial \mathcal{V}_{2,i}}{\partial I_j}(x_0)\right)_{i,j=1,\dots,n} \end{pmatrix}, \tag{3.9}$$

which can be written in matrix notation

$$F = \begin{pmatrix} \tilde{B}^A & \tilde{B}^I \\ 0 & 0 \end{pmatrix} \qquad \text{and} \qquad V = \begin{pmatrix} (\alpha+\delta_A)\mathbb{I}+\mu & 0 \\ -\alpha\mathbb{I} & \delta_I\mathbb{I}+\mu \end{pmatrix},$$

where $(\tilde{B}^A)_{ij} = \beta^A_{ij} S_{0,i}$, $(\tilde{B}^I)_{ij} = \beta^I_{ij} S_{0,i}$, $\mu = \operatorname{diag}(\mu_1, \dots, \mu_n)$, and 0 and $\mathbb{I}$ are the zero matrix and the identity matrix of order n, respectively. Since V is a block lower triangular matrix, its inverse is the $2n \times 2n$ block matrix:

$$V^{-1} = \begin{pmatrix} \operatorname{diag}\left(\dfrac{1}{\alpha+\delta_A+\mu_i}\right)_{i=1,\dots,n} & 0 \\ \operatorname{diag}\left(\dfrac{\alpha}{(\alpha+\delta_A+\mu_i)(\delta_I+\mu_i)}\right)_{i=1,\dots,n} & \operatorname{diag}\left(\dfrac{1}{\delta_I+\mu_i}\right)_{i=1,\dots,n} \end{pmatrix}.$$

The next generation matrix is defined as $M := FV^{-1}$. By direct calculation, we obtain

$$M = \begin{pmatrix} \left(\left(\dfrac{\beta^A_{ij}}{\alpha+\delta_A+\mu_i} + \dfrac{\alpha\beta^I_{ij}}{(\alpha+\delta_A+\mu_i)(\delta_I+\mu_i)}\right) S_{0,i}\right)_{i,j=1,\dots,n} & \left(\dfrac{\beta^I_{ij} S_{0,i}}{\delta_I+\mu_i}\right)_{i,j=1,\dots,n} \\ 0 & 0 \end{pmatrix}. \tag{3.10}$$

The basic reproduction number $\mathcal{R}_0$ is defined as the spectral radius of M, denoted by $\rho(M)$, that is $\rho(M) = \max\{\rho(M_1), 0\}$, where

$$M_1 = \left(\left(\beta^A_{ij} + \frac{\alpha\beta^I_{ij}}{\delta_I+\mu_i}\right)\frac{S_{0,i}}{\alpha+\delta_A+\mu_i}\right)_{i,j=1,\dots,n}.$$

As a direct consequence of the Perron Frobenius theorem [87], $\rho(M_1) > 0$. This proves our claim. □

In the following, we present some results to prove the global asymptotic stability of the DFE x_0.

Recall that a matrix M is called *non-negative* if each entry is non-negative; we simply write $M \geq 0$ to indicate this. We use the following results from [73]:

Lemma 3.3.2 ([73, Lemma 2])**.** *If F is non-negative and V is a non-singular M-matrix, then $\mathcal{R}_0 = \rho(FV^{-1}) < 1$ if and only if all eigenvalues of $(F-V)$ have negative real parts.*

Note that the matrices F and V defined in Lemma 3.3.1 satisfy the hypotheses of Lemma 3.3.2, thus the following result holds:

Theorem 3.3.3. *The disease-free equilibrium of* (3.3) *is locally asymptotically stable if $\mathcal{R}_0 < 1$ and unstable if $\mathcal{R}_0 > 1$.*

Proof. See [73, Theorem 1]. □

Theorem 3.3.4. *The disease-free equilibrium x_0 of* (3.3) *is globally asymptotically stable in Γ if $\mathcal{R}_0 < 1$.*

Proof. Let $x(t) = (S_1(t), \ldots, S_n(t), A_1(t), \ldots, A_n(t), I_1(t) \ldots, I_n(t))$ be the solutions of system (3.3) with initial condition $x(0) \in \Gamma$, in which we have rearranged the order of the equations. In view of Theorem 3.3.3, it is sufficient to prove that for all $i = 1, \ldots, n$

$$\lim_{t\to\infty} S_i(t) = S_{0,i}, \qquad \lim_{t\to\infty} A_i(t) = 0, \qquad \text{and} \qquad \lim_{t\to\infty} I_i(t) = 0,$$

with $S_{0,i}$ as in (3.5). From the first n equations of (3.3), it follows that

$$\frac{dS_i(t)}{dt} \leq \mu_i + \gamma - (\mu_i + \nu_i + \gamma)S_i(t), \qquad i = 1, \ldots, n.$$

Thus, $S_{0,i}$ is a global asymptotically stable equilibrium for the comparison equation

$$\frac{dz_i(t)}{dt} = \mu_i + \gamma - (\mu_i + \nu_i + \gamma)z_i(t), \qquad i = 1, \ldots, n.$$

Then, for any $\varepsilon > 0$, there exists $\bar{t}_i > 0$, such that for all $t \geq \bar{t}_i$, it holds

$$S_i(t) \leq S_{0,i} + \varepsilon, \tag{3.11}$$

hence

$$\limsup_{t\to\infty} S_i(t) \leq S_{0,i}, \qquad i = 1, \ldots, n. \tag{3.12}$$

Let $\bar{t} = \max\{t_1, \ldots, t_n\}$, then for all $t \geq \bar{t}$, from (3.11) and the remaining $2n$ equations of (3.3) it follows that

$$\frac{dA_i(t)}{dt} \leq \sum_{j=1}^{n} \left(\beta_{ij}^A A_j(t) + \beta_{ij}^I I_i(t)\right)(S_{0,i} + \varepsilon) - (\alpha + \delta_A + \mu_i)A_i(t), \qquad i = 1, \ldots, n,$$

$$\frac{dI_i(t)}{dt} = \alpha A_i(t) - (\delta_I + \mu_i)I_i(t), \qquad i = 1, \ldots, n.$$

Let us now consider the comparison system

$$\frac{dv_i(t)}{dt} = \sum_{j=1}^{n} \left(\beta_{ij}^A v_j(t) + \beta_{ij}^I u_i(t)\right)(S_{0,i} + \varepsilon) - (\alpha + \delta_A + \mu_i)v_i(t),$$
$$\frac{du_i(t)}{dt} = \alpha v_i(t) - (\delta_I + \mu)u_i(t), \qquad v_i(\bar{t}) = A_i(\bar{t}), \quad u_i(\bar{t}) = I_i(\bar{t}), \quad i = 1, \ldots, n.$$

Let $w = (v_1, \ldots, v_n, u_1, \ldots, u_n)^T$, then one can rewrite this system as

$$\frac{dw(t)}{dt} = (F_\varepsilon - V_\varepsilon)w(t),$$

where F_ε and V_ε are the matrices defined in (3.8) and (3.9), respectively, evaluated in $x_0(\varepsilon)$ whose components are $S_{0,i} + \varepsilon$ for $i = 1, \ldots, n$ and 0 in the remaining $2n$ components.

Notice that we can choose $\varepsilon > 0$ sufficient small such that $\rho(F_\varepsilon V_\varepsilon^{-1}) < 1$ and then, from Lemma 3.3.2, all the eigenvalues of matrix $(F_\varepsilon - V_\varepsilon)$ have negative real parts. It follows that $\lim_{t\to\infty} w_i(t) = 0$ from any initial conditions in Γ, from which

$$\lim_{t\to\infty} A_i(t) = 0 \qquad \text{and} \qquad \lim_{t\to\infty} I_i(t) = 0.$$

Thus, for any $\varepsilon > 0$, there exists $\bar{t}_1 > 0$ such that, for all $t \geq \bar{t}_1$, we have

$$A_i(t) < \varepsilon \quad \text{and} \quad I_i(t) < \varepsilon, \qquad i = 1, \ldots, n.$$

From that and the first n equations of system (3.3), we get that for all $i = 1, \ldots, n$ and for $t \geq \bar{t}_1$

$$\frac{dS_i(t)}{dt} \geq \mu_i - \varepsilon \sum_{j=1}^{n} (\beta_{ij}^A + \beta_{ij}^I)S_i(t) - (\mu_i + \nu_i + \gamma)S_i(t) + \gamma(1 - 2\varepsilon).$$

The comparison system

$$\frac{dz_i(t)}{dt} = \mu_i - \varepsilon \sum_{j=1}^{n} (\beta_{ij}^A + \beta_{ij}^I)z_i(t) - (\mu_i + \nu_i + \gamma)z_i(t) + \gamma(1 - 2\varepsilon), \qquad i = 1, \ldots, n,$$

has a globally asymptotically stable equilibrium

$$z_0 = \left(\frac{\mu_1 + \gamma(1 - 2\varepsilon)}{\varepsilon(\sum_{j=1}^{n} \beta_{1j}^A + \beta_{1j}^I) + (\mu_1 + \nu_1 + \gamma)}, \ldots, \frac{\mu_n + \gamma(1 - 2\varepsilon)}{\varepsilon(\sum_{j=1}^{n} \beta_{nj}^A + \beta_{nj}^I) + (\mu_n + \nu_n + \gamma)} \right).$$

Thus, we get that for any $\zeta > 0$, there exists $\bar{t}_2 > 0$ such that for all $t \geq \bar{t}_2$,

$$S_i(t) \geq \frac{\mu_i + \gamma(1 - 2\varepsilon)}{\varepsilon(\sum_{j=1}^{n} \beta_{ij}^A + \beta_{ij}^I) + (\mu_i + \nu_i + \gamma)} - \zeta, \qquad i = 1, \ldots, n.$$

This implies that for all $\varepsilon > 0$

$$\liminf_{t\to\infty} S_i(t) \geq \frac{\mu_i + \gamma(1-2\varepsilon)}{\varepsilon(\sum_{j=1}^n \beta_{ij}^A + \beta_{ij}^I) + (\mu_i + \nu_i + \gamma)}, \qquad i = 1, \ldots, n.$$

Letting ε go to 0, we have $\liminf_{t\to\infty} S_i(t) \geq S_{0,i}$ for all $i = 1, \ldots, n$, which combined with (3.12) gives us

$$\lim_{t\to\infty} S_i(t) = S_{0,i}, \qquad i = 1, \ldots, n.$$

□

3.4 Existence and uniqueness of endemic equilibrium

To prove the existence and uniqueness of an endemic equilibrium point, we recall the following definition and theorem from [7].

Definition 2. *A function $F(x) : \mathbb{R}_+^n \to \mathbb{R}_+^n$ is called* strictly sublinear *if for fixed $x \in (0,\infty)^n$ and fixed $r \in (0,1)^n$, there exists an $\varepsilon > 0$ such that $F(rx) \geq (1+\varepsilon)rF(x)$, where $\geq$ denotes the pointwise ordering in $\mathbb{R}^n$.*

Theorem 3.4.1 (Thm 2.2 [7])**.** *Let $F(x) : \mathbb{R}_+^n \to \mathbb{R}_+^n$ be a continuous, monotone nondecreasing, strictly sublinear, and bounded function. Let $F(0) = 0$ and $J_F(0)$ exists and be irreducible, where J_F is the Jacobian matrix of F. Then $F(x)$ does not have a nontrivial fixed point on the boundary of $\mathbb{R}_+^n$. Moreover, $F(x)$ has a positive fixed point if and only if $\rho(J_F(0)) > 1$. If there is a positive fixed point, then it is unique.*

By using the above result, we can prove the following theorem.

Theorem 3.4.2. *System (3.3) admits a unique endemic equilibrium $x^* := (S_1^*, A_1^*, I_1^*, \ldots, S_n^*, A_n^*, I_n^*)$ in $\mathring{\Gamma}$ if and only if $\mathcal{R}_0 > 1$.*

Proof. An equilibrium point is a solution of the non linear equations obtained by setting the right-hand side of equations (3.3) equal to zero. Then, the following must hold:

$$\mu_i - \sum_{j=1}^n \left(\beta_{ij}^A A_j^* + \beta_{ij}^I I_j^*\right) S_i^* - (\mu_i + \nu_i + \gamma) S_i^* + \gamma(1 - A_i^* - I_i^*) = 0, \tag{3.13}$$

$$\sum_{j=1}^n \left(\beta_{ij}^A A_j^* + \beta_{ij}^I I_j^*\right) S_i^* - (\alpha + \delta_A + \mu_i) A_i^* = 0, \tag{3.14}$$

$$\alpha A_i^* - (\delta_I + \mu_i) I_i^* = 0, \tag{3.15}$$

for $i = 1, 2, \ldots, n$. By excluding as solution the DFE (3.5), we assume $A_i^* > 0$, for some $1 \leq i \leq n$. From (3.15), we immediately obtain

$$I_i^* = \frac{\alpha}{\delta_I + \mu_i} A_i^* =: K_i A_i^*, \tag{3.16}$$

for all $i = 1, 2, \ldots, n$. Substituting (3.16) in (3.14), we obtain

$$S_i^* = \frac{(\alpha + \delta_A + \mu_i)A_i^*}{\sum_{j=1}^n (\beta_{ij}^A + \beta_{ij}^I K_j) A_j^*}. \tag{3.17}$$

By our assumption on x^*, the denominator of (3.17) is strictly positive. Lastly, substituting (3.16) and (3.17) into (3.13), we obtain

$$\mu_i - (\alpha + \delta_A + \mu_i)A_i^* - (\mu_i + \nu_i + \gamma)\frac{(\alpha + \delta_A + \mu_i)A_i^*}{\sum_{j=1}^n (\beta_{ij}^A + \beta_{ij}^I K_j) A_j^*} + \gamma(1 - (1 + K_i)A_i^*) = 0,$$

which can be rearranged to give

$$A_i^* = \frac{(\mu_i + \gamma)\sum_{j=1}^n (\beta_{ij}^A + \beta_{ij}^I K_j) A_j^*}{(\mu_i + \nu_i + \gamma)(\alpha + \delta_A + \mu_i) + (\alpha + \delta_A + \mu_i + \gamma + \gamma K_i)\sum_{j=1}^n (\beta_{ij}^A + \beta_{ij}^I K_j) A_j^*}.$$

We can collect $(\mu_i + \nu_i + \gamma)(\alpha + \delta_A + \mu_i)$ and $(\mu_i + \gamma)$ in both the numerator and denominator, to obtain

$$A_i^* = \frac{\sum_{j=1}^n (M_1)_{i,j} A_j^*}{1 + (\mu_i + \gamma)^{-1}(\alpha + \delta_A + \mu_i + \gamma + \gamma K_i)\sum_{j=1}^n (M_1)_{i,j} A_j^*}, \tag{3.18}$$

with M_1 as in (3.7).

Define a function $H = (h_1, \ldots, h_n) : \mathbb{R}_+^n \to \mathbb{R}_+^n$, in the following way:

$$h_i(y) = \frac{\sum_{j=1}^n (M_1)_{i,j} y_j}{1 + (\mu_i + \gamma)^{-1}(\alpha + \delta_A + \mu_i + \gamma + \gamma K_i)\sum_{j=1}^n (M_1)_{i,j} y_j}, \qquad i = 1, 2, \ldots, n.$$

Then, since

$$\frac{\partial h_j}{\partial y_i} > 0,$$

for all $i, j = 1, 2, \ldots, n$, H is monotonically increasing in all its components. Moreover, $J_H(0) = M_1$ that is a non-negative and irreducible matrix and the function $H(x)$ is bounded and strictly sublinear with

$$\varepsilon = \min_i \frac{(1 - r)\xi_i \sum_{j=1}^n (M_1)_{i,j} y_j}{1 + r\xi_i \sum_{j=1}^n (M_1)_{i,j} y_j},$$

where

$$\xi_i = (\mu_i + \gamma)^{-1}(\alpha + \delta_A + \mu_i + \gamma + \gamma K_i).$$

Thus, by Theorem 3.4.1, we have that system (3.3) has an unique endemic equilibrium in $\mathring{\Gamma}$. □

Remark 2. *From Eq.* (3.16) *we can note that since* $I_i^* < 1$, *we have that* $A_i^* < \dfrac{\delta_I + \mu_i}{\alpha}$.

Now, we investigate the local asymptotic stability of the endemic equilibrium.

Theorem 3.4.3. *Assume $\mathcal{R}_0 > 1$ and that for any fixed j, $\beta_{ij}^I = h_j \beta_{ij}^A$ for all $i = 1, \dots, n$,. Moreover, let us assume that*

$$\delta_A > \nu_i, \quad \delta_I > \nu_i, \quad \text{and} \quad (\delta_I - \nu_i)\alpha \leq 2(\mu_i + 2\nu_i + \gamma + \delta_I)\sqrt{((\mu_i + \nu_i + \gamma)(\delta_I + \nu_i))} + (\mu_i + 2\nu_i + \gamma + \delta_I)^2,$$

for $i = 1, \dots, n$. Then, the endemic equilibrium $x^* := (S_1^*, A_1^*, I_1^*, \dots, S_n^*, A_n^*, I_n^*)$ is local asymptotically stable.

Proof. Usually, the asymptotic local stability of the endemic equilibrium point is studied by linearizing system (3.4) around that point. However, it is known that the endemic equilibrium is asymptotically stable if the linearized system $\dfrac{dy}{dt} = J_f(x^*)y$ has no solution of the form $y(t) = Ye^{zt}$ with

$$Y = (U_1, \dots, U_n, V_1, \dots, V_n, W_1, \dots, W_n) \in \mathbb{C}^{3n},$$

$z \in \mathbb{C}$, $\Re z \geq 0$, i.e., it means that $zY = J_f(x^*)Y$ with $Y \in \mathbb{C}^n \setminus \{0\}, z \in \mathbb{C}$ implies $\Re z < 0$ [7, 26]. To prove our statement with this strategy, we consider the following system, equivalent to (3.4):

$$\frac{dx}{dt} = f(x(t)),$$

where $x(t) = (A_1(t), I_1(t), R_1(t), \dots, A_n(t), I_n(t), R_n(t))$ and $f(x(t)) = (f_1(x(t)), f_2(x(t)), \dots, f_{3n}(x(t)))$, with

$$\begin{aligned}
f(x_1(t)) &= \sum_{j=1}^{n} (\beta_{ij}^A A_j(t) + \beta_{ij}^I I_j(t))(1 - A_i(t) - I_i(t) - R_i(t)) - (\alpha + \mu_i + \delta_A)A_i(t), \\
f(x_2(t)) &= \alpha A_i(t) - (\mu_i + \delta_I)I_i(t), \\
f(x_3(t)) &= \delta_A A_i(t) + \delta_I I_i(t) + \nu_i(1 - A_i(t) - I_i(t) - R_i(t)) - (\mu_i + \gamma)R_i(t).
\end{aligned}$$

Now, to prove the asymptotic local stability of x^*, we consider the following equations:

$$\begin{aligned}
zU_i &= (1 - A_i^* - I_i^* - R_i^*) \sum_{j=1}^{n} (\beta_{ij}^A U_j + \beta_{ij}^I V_j) - \sum_{j=1}^{n} (\beta_{ij}^A A_j^* + \beta_{ij}^I I_j^*)(U_i + V_i + W_i) - (\alpha + \mu_i + \delta_A)U_i, \\
zV_i &= \alpha U_i - (\delta_I + \mu_i)V_i, \\
zW_i &= (\delta_A - \nu_i)U_i + (\delta_I - \nu_i)V_i - (\mu_i + \nu_i + \gamma)W_i, \qquad i = 1, \dots, n,
\end{aligned} \tag{3.19}$$

with $U_i, V_i, W_i, z \in \mathbb{C}$. We proceed by assuming that $\Re z \geq 0$ and showing that this assumption leads to a contradiction.

From the second and third equation of (3.19), we have respectively

$$V_i = \frac{\alpha}{z + \delta_I + \mu_i} U_i := K_i^1(z)U_i, \tag{3.20}$$

and

$$W_i = \left[\frac{1}{z + \mu_i + \nu_i + \gamma} \left((\delta_A - \nu_i) + \frac{(\delta_I - \nu_i)\alpha}{z + \delta_I + \nu_i} \right) \right] U_i := K_i^2(z)U_i. \tag{3.21}$$

Now, considering the assumption that fixed j, $\beta_{ij}^I = h_j\beta_{ij}^A$ for all $i = 1, \ldots, n$, and replacing (3.20) and (3.21) in the first equation of (3.19), we obtain

$$zU_i = S_i^* \sum_{j=1}^{n} \beta_{ij}^A (1+h_j K_j^1(z))U_j - \left[\sum_{j=1}^{n} \beta_{ij}^A (A_j^* + h_j I_j^*)(1 + K_i^1(z) + K_i^2(z)) + (\alpha + \mu_i + \delta_A) \right] U_i,$$

from which

$$\left[1 + \frac{1}{\alpha + \mu_i + \delta_A} \left(z + \sum_{j=1}^{n} \beta_{ij}^A (A_j^* + h_j I_j^*)(1 + K_i^1(z) + K_i^2(z)) \right) \right] U_i = \frac{S_i^*}{\alpha + \mu_i + \delta_A} \sum_{j=1}^{n} \beta_{ij}^A (1+h_j K_j^1(z))U_j. \tag{3.22}$$

Now, let

$$\eta_i(z) = \frac{1}{\alpha + \mu_i + \delta_A} \left(z + \sum_{j=1}^{n} \beta_{ij}^A (A_j^* + h_j I_j^*)(1 + K_i^1(z) + K_i^2(z)) \right),$$

and consider the following transformation:

$$U_j = \left(1 + \frac{h_j \alpha}{z + \delta_I + \mu_j} \right)^{-1} \left(1 + \frac{h_j \alpha}{\delta_I + \mu_j} \right) \tilde{U}_j.$$

Then, we get

$$(1 + \eta_i(z)) \left(1 + \frac{h_i \alpha}{z + \delta_I + \mu_i} \right)^{-1} \left(1 + \frac{h_i \alpha}{\delta_I + \mu_i} \right) \tilde{U}_i = \frac{S_i^*}{\alpha + \mu_i + \delta_A} \sum_{j=1}^{n} \beta_{ij}^A \left(1 + \frac{h_j \alpha}{\delta_I + \mu_j} \right) \tilde{U}_j. \tag{3.23}$$

Now, let us note that if $\Re z \geq 0$, then

$$\Re \left(\left(1 + \frac{h_i \alpha}{z + \delta_I + \mu_i} \right)^{-1} \left(1 + \frac{h_i \alpha}{\delta_I + \mu_i} \right) \right) \geq 1. \tag{3.24}$$

Hence, we can rewrite (3.23) in the following form:

$$(1 + \eta_i(z)) \, (1 + \tilde{\eta}_i(z)) \tilde{U}_i = (C\tilde{U})_i. \tag{3.25}$$

where $C = (c_{ij})$ with

$$c_{ij} = \frac{S_i^*}{\alpha + \mu_i + \delta_A} \sum_{j=1}^{n} \beta_{ij}^A \left(1 + \frac{h_j \alpha}{\delta_I + \mu_j} \right), \qquad i, j = 1, \ldots, n.$$

From (3.24), we have that $\Re\tilde{\eta}_i(z) \geq 0$. Moreover, the following claim, whose proof is given in Appendix 3.A, holds:

Claim 3.4.4. *If $\Re z \geq 0$, then $\Re\eta_i(z) > 0$.*

Now, let us note that C is a non-negative matrix and that $A^* = CA^*$, where $A^* = (A_1^*, \ldots, A_n^*)$. Let

$$\eta(z) = \inf\{\Re\eta_i(z), i = 1, \ldots, n\}, \qquad \text{and} \qquad |\tilde{U}| = (|\tilde{U}_1|, \ldots, |\tilde{U}_n|),$$

and taking the absolute values in (3.25), we get

$$(1 + \eta(z))|\tilde{U}| \leq C|\tilde{U}|. \tag{3.26}$$

It is easy to verify that if $\Re z \geq 0$, then $\Re\eta_i(z) > 0$ for all i, hence $\eta(z) > 0$. Now, we define ϵ to be the minimum value for which $|\tilde{U}| \leq \epsilon A^*$. Since the components of A^* belong to $(0, 1)$, $\epsilon < \infty$. Hence, by (3.26), $(1 + \eta(z))|\tilde{U}| \leq C|\tilde{U}| \leq \epsilon CA^* = \epsilon A^*$. This inequality contradicts the minimality of ϵ because $\eta(z) > 0$ if $\Re z \geq 0$, thus we can conclude that $\Re z < 0$ and the equilibrium is stable. □

As in Sec. 2.5.3, we conjecture that some, if not all, these technical assumptions could be relaxed, as our numerical simulations suggest. However, the techniques we use in this chapter require such assumptions on the parameters in order to reach a result, and multigroup models often require cumbersome hypotheses [88, 89, 90].

3.5 Global stability of the endemic equilibrium

In this section, we first discuss the persistence of the disease, then we investigate the global stability property of the endemic equilibrium for some variations of the original model (3.1).

Definition 3. *System* (3.3) *is said to be* uniformly persistent *if there exists a constant* $0 < \varepsilon < 1$ *such that any solution* $x(t)$ *with* $x(0) \in \mathring{\Gamma}$ *satisfies*

$$\min\{\liminf_{t\to\infty} S_i(t), \quad \liminf_{t\to\infty} A_i(t), \quad \liminf_{t\to\infty} I_i(t)\} \geq \varepsilon, \qquad i = 1, \ldots, n. \tag{3.27}$$

Theorem 3.5.1. *If* $\mathcal{R}_0 > 1$*, system* (3.3) *is uniformly persistent.*

Proof. From Theorem 3.4.2 we know that DFE x_0 is the unique equilibrium of (3.3) on $\partial\Gamma$, i.e., the largest invariant set on $\partial\Gamma$ is the singleton $\{x_0\}$, which is isolated. If $\mathcal{R}_0 > 1$, we know from Theorem 3.3.3 that x_0 is unstable. Then, by using [76, Thm 4.3], and similar arguments in [19, Prop. 3.3], we can assert that the instability of x_0 implies the uniform persistence of (3.3). □

3.5.1 Global stability of the endemic equilibrium in the SAIR model

In this section, we study the global asymptotic stability of the endemic equilibrium of the SAIR model, which describes the dynamic of a disease which confers permanent

immunity (i.e. $\gamma = 0$). The dynamic of an SAIR model of this type is described by the following system of equations:

$$\begin{aligned}
\frac{dS_i(t)}{dt} &= \mu_i - \sum_{j=1}^{n} \left(\beta_{ij}^A A_j(t) + \beta_{ij}^I I_j(t) \right) S_i(t) - (\mu_i + \nu_i) S_i(t), \\
\frac{dA_i(t)}{dt} &= \sum_{j=1}^{n} \left(\beta_{ij}^A A_j(t) + \beta_{ij}^I I_j(t) \right) S_i(t) - (\alpha + \delta_A + \mu_i) A_i(t), \\
\frac{dI_i(t)}{dt} &= \alpha A_i(t) - (\delta_I + \mu_i) I_i(t), \qquad\qquad i = 1, \ldots, n.
\end{aligned} \tag{3.28}$$

The basic reproduction number is derived by substituting γ with 0 in (3.7):

$$\mathcal{R}_0 = \rho \left(\left(\left(\beta_{ij}^A + \frac{\alpha \beta_{ij}^I}{(\delta_I + \mu_i)} \right) \frac{\mu_i}{(\mu_i + \nu_i)(\alpha + \delta_A + \mu_i)} \right)_{i,j=1,\ldots,n} \right).$$

If $\mathcal{R}_0 > 1$, system (3.28) has a unique equilibrium in $\mathring{\Gamma}$, which satisfies

$$\mu_i = \sum_{j=1}^{n} \left(\beta_{ij}^A A_j^* + \beta_{ij}^I I_j^* \right) S_i^* + (\mu_i + \nu_i) S_i^*, \tag{3.29}$$

$$(\alpha + \delta_A + \mu_i) A_i^* = \sum_{j=1}^{n} \left(\beta_{ij}^A A_j^* + \beta_{ij}^I I_j^* \right) S_i^*, \tag{3.30}$$

$$\alpha A_i^* = (\delta_I + \mu_i) I_i^*. \tag{3.31}$$

Theorem 3.5.2. *The endemic equilibrium x^* is globally asymptotically stable in $\mathring{\Gamma}$ if $\mathcal{R}_0 > 1$.*

Proof. In order to prove the statement, we use a graph-theoretic approach as in [12] to establish the existence of a Lyapunov function. Let us define

$$\tilde{s}_i = \frac{S_i}{S_i^*}, \qquad \tilde{a}_i = \frac{A_i}{A_i^*}, \qquad \tilde{i}_i = \frac{I_i}{I_i^*},$$

and $g(x) := x - 1 - \ln(x) \geq 0$ for all $x > 0$. Let $V_i = V_{i,1} + V_{i,2}$, where $V_{i,1} = S_i^* \cdot g(\tilde{s}_i)$, $V_{i,2} = A_i^* \cdot g(\tilde{a}_i)$, and $V_{n+i} = I_i^* \cdot g(\tilde{i}_i)$, for $i = 1, \ldots, n$.

Define $h(x) := -g(x) - 1 = -x + \ln(x)$ and note that

$$\left(1 - \frac{1}{x}\right)(x-1) = -2 + x + \frac{1}{x} = -1 + x - \ln x - 1 + \frac{1}{x} - \ln \frac{1}{x} = g(x) + g\left(\frac{1}{x}\right). \tag{3.32}$$

Substituting (3.29), (3.30), and (3.31) in (3.28), we obtain

$$\begin{aligned}
\frac{dS_i(t)}{dt} &= -S_i^*(\mu_i+\nu_i)(\tilde{s}_i-1)+\sum_{j=1}^{n}\left(\beta_{ij}^A\left(A_j^*S_i^*-A_jS_i\right)+\beta_{ij}^I\left(I_j^*S_i^*-I_jS_i\right)\right),\\
\frac{dA_i(t)}{dt} &= \sum_{j=1}^{n}\left(\left(\beta_{ij}^AA_j+\beta_{ij}^II_j\right)S_i-\left(\beta_{ij}^AA_j^*+\beta_{ij}^II_j^*\right)S_i^*\frac{A_i}{A_i^*}\right),\\
\frac{dI_i(t)}{dt} &= \alpha\left(A_i-A_i^*\frac{I_i}{I_i^*}\right), \qquad\qquad i=1,\ldots,n.
\end{aligned}$$

For $i=1,\ldots,n$, differentiating V_i along the solutions of (3.28) and using (3.32), we have

$$\begin{aligned}
\frac{dV_{i,1}}{dt} &= \left(1-\frac{1}{\tilde{s}_i}\right)\frac{dS_i(t)}{dt}\\
&= \left(1-\frac{1}{\tilde{s}_i}\right)\left[-S_i^*(\mu_i+\nu_i)(\tilde{s}_i-1)+\sum_{j=1}^{n}\left(\beta_{ij}^A\left(A_j^*S_i^*-A_jS_i\right)+\beta_{ij}^I\left(I_j^*S_i^*-I_jS_i\right)\right)\right]\\
&= \left(1-\frac{1}{\tilde{s}_i}\right)\left[-S_i^*(\mu_i+\nu_i)(\tilde{s}_i-1)+\sum_{j=1}^{n}\left(\beta_{ij}^AA_j^*S_i^*\left(1-\tilde{a}_j\tilde{s}_i\right)+\beta_{ij}^II_j^*S_i^*\left(1-\tilde{i}_j\tilde{s}_i\right)\right)\right]\\
&= -S_i^*(\mu_i+\nu_i)\frac{(\tilde{s}_i-1)^2}{S_i}+\sum_{j=1}^{n}\left(\beta_{ij}^AA_j^*S_i^*\left(1-\tilde{a}_j\tilde{s}_i-\frac{1}{\tilde{s}_i}+\tilde{a}_j\right)\right.\\
&\quad\left.+\beta_{ij}^II_j^*S_i^*\left(1-\tilde{i}_j\tilde{s}_i-\frac{1}{\tilde{s}_i}+\tilde{i}_j\right)\right),
\end{aligned}\tag{3.33}$$

$$\begin{aligned}
\frac{dV_{i,2}}{dt} &= \left(1-\frac{1}{\tilde{a}_i}\right)\frac{dA_i(t)}{dt}\\
&= \left(1-\frac{1}{\tilde{a}_i}\right)\left[\sum_{j=1}^{n}\left(\left(\beta_{ij}^AA_j+\beta_{ij}^II_j\right)S_i-\left(\beta_{ij}^AA_j^*+\beta_{ij}^II_j^*\right)S_i^*\frac{A_i}{A_i^*}\right)\right]\\
&= \left(1-\frac{1}{\tilde{a}_i}\right)\left[\sum_{j=1}^{n}\left(\beta_{ij}^AA_j^*S_i^*\left(\tilde{a}_j\tilde{s}_i-\tilde{a}_i\right)+\beta_{ij}^II_j^*S_i^*\left(\tilde{i}_j\tilde{s}_i-\tilde{a}_i\right)\right)\right]\\
&= \sum_{j=1}^{n}\left(\beta_{ij}^AA_j^*S_i^*\left(\tilde{a}_j\tilde{s}_i-\tilde{a}_i-\frac{\tilde{a}_j\tilde{s}_i}{\tilde{a}_i}+1\right)+\beta_{ij}^II_j^*S_i^*\left(\tilde{i}_j\tilde{s}_i-\tilde{a}_i-\frac{\tilde{i}_j\tilde{s}_i}{\tilde{a}_i}+1\right)\right),
\end{aligned}\tag{3.34}$$

Thus, from (3.33) and (3.34), we obtain

$$\frac{dV_i}{dt}\leq\sum_{j=1}^{n}\left(\beta_{ij}^AA_j^*S_i^*\left(2-\frac{1}{\tilde{s}_i}+\tilde{a}_j-\tilde{a}_i-\frac{\tilde{a}_j\tilde{s}_i}{\tilde{a}_i}\right)+\beta_{ij}^II_j^*S_i^*\left(2-\frac{1}{\tilde{s}_i}+\tilde{i}_j-\tilde{a}_i-\frac{\tilde{i}_j\tilde{s}_i}{\tilde{a}_i}\right)\right)\tag{3.35}$$

Using the fact that $1 - x \leq -\ln(x)$, we can write

$$2 - \frac{1}{\tilde{s}_i} + \tilde{a}_j - \tilde{a}_i - \frac{\tilde{a}_j \tilde{s}_i}{\tilde{a}_i} \leq \tilde{a}_j - \tilde{a}_i - \ln\left(\frac{1}{\tilde{s}_i}\right) - \ln\left(\frac{\tilde{a}_j \tilde{s}_i}{\tilde{a}_i}\right) = h(\tilde{a}_i) - h(\tilde{a}_j),$$
$$2 - \frac{1}{\tilde{s}_i} + \tilde{i}_j - \tilde{a}_i - \frac{\tilde{i}_j \tilde{s}_i}{\tilde{a}_i} \leq \tilde{i}_j - \tilde{a}_i - \ln\left(\frac{1}{\tilde{s}_i}\right) - \ln\left(\frac{\tilde{i}_j \tilde{s}_i}{\tilde{a}_i}\right) = h(\tilde{a}_i) - h(\tilde{i}_j),$$

Thus, we obtain

$$\frac{dV_i}{dt} \leq \sum_{j=1}^{n} \left(\beta_{ij}^A A_j^* S_i^* (h(\tilde{a}_i) - h(\tilde{a}_j)) + \beta_{ij}^I I_j^* S_i^* (h(\tilde{a}_i) - h(\tilde{i_j}))\right) =: \sum_{j=1}^{2n} \tilde{\beta}_{ij} G_{i,j},$$

where

$$\tilde{\beta}_{ij} = \begin{cases} \beta_{ij}^A A_j^* S_i^*, & 1 \leq j \leq n, \\ \beta_{ij-n}^I I_{j-n}^* S_i^*, & n+1 \leq j \leq 2n, \end{cases} \quad \text{and} \quad G_{i,j} = \begin{cases} h(\tilde{a}_i) - h(\tilde{a}_j), & 1 \leq j \leq n, \\ h(\tilde{a}_i) - h(\tilde{i}_{j-n}), & n+1 \leq j \leq 2n. \end{cases}$$

Moreover, for all $i = 1, \ldots, n$

$$\begin{aligned} \frac{dV_{n+i}}{dt} &= \left(1 - \frac{1}{\tilde{i}_i}\right) \frac{dI_i}{dt} = \alpha \left(1 - \frac{1}{\tilde{i}_i}\right) \left[A_i - A_i^* \frac{I_i}{I_i^*}\right] \\ &= \alpha A_i^* \left(1 - \frac{1}{\tilde{i}_i}\right) (\tilde{a}_i - \tilde{i}_i) = \alpha A_i^* \left(\tilde{a}_i - \tilde{i}_i - \frac{\tilde{a}_i}{\tilde{i}_i} + 1\right), \end{aligned} \tag{3.36}$$

and again, using the fact that $1 - x \leq -\ln(x)$, we have

$$1 + \tilde{a}_i - \tilde{i}_i - \frac{\tilde{a}_i}{\tilde{i}_i} \leq \tilde{a}_i - \tilde{i}_i - \ln\left(\frac{\tilde{a}_i}{\tilde{i}_i}\right) = h(\tilde{i}_i) - h(\tilde{a}_i).$$

Thus,

$$\frac{dV_{n+i}}{dt} \leq \alpha A_i^* (h(\tilde{i}_i) - h(\tilde{a}_i)) =: \tilde{\beta}_{n+i,i} G_{n+i,i}. \tag{3.37}$$

We can construct a weighted digraph $\mathcal{G}$, associated with the weight matrix $\tilde{B} = (\tilde{\beta}_{ij})_{i,j=1,\ldots,2n}$, with $\tilde{\beta}_{ij} > 0$ as defined above and zero otherwise; see Figure 2. Let us note that, from Assumption 1, the digraph $(\mathcal{G}, \tilde{B})$ is strongly connected. Since $G_{i,n+j} + G_{n+j,j} = -\tilde{a}_i + \ln(\tilde{a}_i) + \tilde{a}_j - \ln(\tilde{a}_j) = G_{i,j}$, $i, j = 1, \ldots, n$, it can be verified that each directed cycle $\mathcal{C}$ of $(\mathcal{G}, \tilde{B})$ has $\sum_{(s,r)\in\mathcal{E}(\mathcal{C})} G_{rs} = 0$, where $\mathcal{E}(\mathcal{C})$ denotes the arc set of the directed cycle $\mathcal{C}$. Thus, the assumptions of [12, Theorem 3.5] hold, hence the function

$$V = \sum_{i=1}^{n} \left(c_i V_i + c_{n+i} V_{n+i}\right),$$

for constants $c_i > 0$ defined as in [12, Prop. 3.1], satisfies $\dfrac{dV}{dt} \leq 0$, meaning that V is a Lyapunov function for system (3.28). It can be verified that the largest compact invariant set in which $\dfrac{dV}{dt} = 0$ is the singleton $\{x^*\}$. Hence, our claim follows by LaSalle's Invariance Principle [78]. □

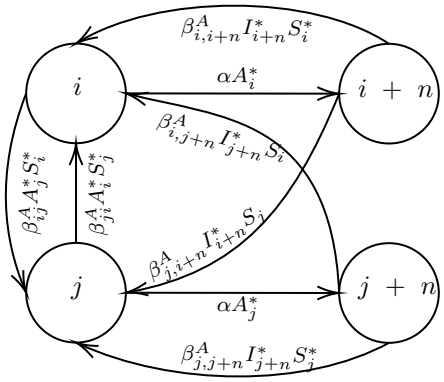

Figure 2: The weighted digraph $(G, \tilde{B})$ constructed for system (3.28).

Remark 3. *We observe that the proof of Theorem 3.5.2 also holds for the case $\delta_A = 0$ in system (3.3). That is to say, for a model with two stages of infection I_1 and I_2, in which from the first class of infection one passes to the second at the rate α and one cannot directly pass into the compartment of recovered individuals. Then, from the second stage of infection, one can recover at the rate δ_{I_2}. It is known that, if $\alpha = \delta_{I_2}$, the length of the infectious period follows a gamma distribution; otherwise, the resulting distribution is not a standard one. Moreover, we remark that Theorem 3.5.2 only requires $\mathcal{R}_0 > 1$, and no additional conditions on the parameters, despite the complexity of the model under study. Models with multiple infected compartments have been studied, e.g., in [91, 92, 93]* .

3.5.2 Global stability of the SAIRS model with equal recovery rates

In the $\delta_A = \delta_I =: \delta$ case, from (3.7) we have

$$\mathcal{R}_0 = \rho\left(\left(\left(\beta^A_{ij} + \frac{\alpha\beta^I_{ij}}{(\delta+\mu_i)}\right)\frac{\gamma+\mu_i}{(\gamma+\mu_i+\nu_i)(\alpha+\delta+\mu_i)}\right)_{i,j=1,\dots,n}\right).$$

If $\mathcal{R}_0 > 1$, system (3.1) with $\delta_A = \delta_I =: \delta$ has a unique equilibrium in $\mathring{\Gamma}$, which satisfies

$$\begin{aligned}
\mu_i &= \sum_{j=1}^{n}\left(\beta^A_{ij}A^*_j + \beta^I_{ij}I^*_j\right)S^*_i + (\mu_i+\nu_i)S^*_i - \gamma R^*_i,\\
(\alpha+\delta+\mu_i)A^*_i &= \sum_{j=1}^{n}\left(\beta^A_{ij}A^*_j + \beta^I_{ij}I^*_j\right)S^*_i,\\
\alpha A^*_i &= (\delta+\mu_i)I^*_i,\\
\nu_i S^*_i &= -\delta(A^*_i + I^*_i) + (\gamma+\mu_i)R^*_i.
\end{aligned} \tag{3.38}$$

Theorem 3.5.3. *Assume that $(\mu_i+\nu_i)S^*_i \geq \gamma R^*_i$ and $\delta > \nu_i$, for each $i = 1,\dots,n$. Then, the endemic equilibrium x^* is globally asymptotically stable in $\mathring{\Gamma}$ if $\mathcal{R}_0 > 1$.*

Proof. Let $\tilde{s}_i, \tilde{a}_i, \tilde{i}_i$, V_i, and V_{n+i} as in Theorem 3.5.2. Let us define $\tilde{r}_i = \dfrac{R_i}{R_i^*}$ and

$$W_i = \frac{\gamma}{S_i^*(\delta - \nu_i)} \frac{(R_i - R_i^*)^2}{2}, \qquad i = 1, \dots, n.$$

By using equations (3.38), and differentiating along the solution of (3.1) with $\delta_A = \delta_I =: \delta$, we obtain

$$\begin{aligned}
\frac{dV_{i,1}}{dt} &= \left(1 - \frac{1}{\tilde{s}_i}\right) \frac{dS_i(t)}{dt} \\
&= \left(1 - \frac{1}{\tilde{s}_i}\right) \left[-S_i^*(\mu_i + \nu_i)(\tilde{s}_i - 1) + \gamma R_i^*(\tilde{r}_i - 1) + \sum_{j=1}^{n} \left(\beta_{ij}^A A_j^* S_i^* \left(1 - \tilde{a}_j \tilde{s}_i\right) + \beta_{ij}^I I_j^* S_i^* \left(1 - \tilde{i}_j \tilde{s}_i\right) \right) \right] \\
&= - S_i^*(\mu_i + \nu_i) \left(1 - \frac{1}{\tilde{s}_i}\right) (\tilde{s}_i - 1) + \gamma R_i^* \left(1 - \frac{1}{\tilde{s}_i}\right) (\tilde{r}_i - 1) + \sum_{j=1}^{n} \left(\beta_{ij}^A A_j^* S_i^* \left(1 - \tilde{a}_j \tilde{s}_i - \frac{1}{\tilde{s}_i} + \tilde{a}_j \right) \right. \\
&\quad \left. + \beta_{ij}^I I_j^* S_i^* \left(1 - \tilde{i}_j \tilde{s}_i - \frac{1}{\tilde{s}_i} + \tilde{i}_j \right) \right),
\end{aligned} \tag{3.39}$$

and the derivatives $\dfrac{dV_{i,2}}{dt}$ and $\dfrac{dV_{n+i}}{dt}$ as in (3.34) and (3.36), respectively. Moreover,

$$\begin{aligned}
\frac{dW_i}{dt} &= \frac{\gamma}{S_i^*(\delta - \nu_i)} (R_i - R_i^*) \frac{dR_i}{dt} \\
&= \frac{\gamma}{S_i^*(\delta - \nu_i)} (R_i - R_i^*) \left[\delta(A_i - A_i^* + I_i - I_i^*) + \nu_i(S_i - S_i^*) - (\gamma + \mu_i)(R_i - R_i^*) \right] \\
&= \frac{\gamma}{S_i^*(\delta - \nu_i)} (R_i - R_i^*) \left[\delta(S_i^* - S_i + R_i^* - R_i) + \nu_i(S_i - S_i^*) - (\gamma + \mu_i)(R_i - R_i^*) \right] \\
&= \frac{\gamma}{S_i^*(\delta - \nu_i)} R_i^* S_i^* (\nu_i - \delta)(\tilde{s}_i - 1)(\tilde{r}_i - 1) - (\gamma + \mu_i + \delta) R_i^* (\tilde{r}_i - 1)^2,
\end{aligned} \tag{3.40}$$

by assumption $\delta > \nu_i$, thus

$$\frac{dW_i}{dt} \leq -\gamma R_i^* (\tilde{s}_i - 1)(\tilde{r}_i - 1). \tag{3.41}$$

Let us consider the weighted digraph $\mathcal{G}$, the weight matrix $\tilde{B}$, and the functions $G_{i,j}$, for $i, j = 1, \dots, 2n$ defined as in Theorem 3.5.2. Consider the following function:

$$V = \sum_{i=1}^{n} (c_i V_i + c_{n+1} V_{n+i}) + \sum_{i=1}^{n} c_i W_i,$$

where the constant $c_i > 0$ are defined as in [12, Prop. 3.1]. Then, by following similar steps as in Theorem 3.5.2 and from (3.41), we obtain

$$\frac{dV}{dt} \leq \sum_{i=1}^{2n}\sum_{j=1}^{2n} c_i\tilde{\beta}_{ij}G_{i,j} - \sum_{i=1}^{n} c_i(\mu_i+\nu_i)S_i^*\left(1-\frac{1}{\tilde{s}}\right)(\tilde{s}_i-1) + \sum_{i=1}^{n} c_i\gamma R_i^*(\tilde{r}_i-1)\left[\left(1-\frac{1}{\tilde{s}_i}\right)-(\tilde{s}_i-1)\right] \tag{3.42}$$

$$= \sum_{i=1}^{2n}\sum_{j=1}^{2n} c_i\tilde{\beta}_{ij}G_{i,j} - \sum_{i=1}^{n} c_i(\mu_i+\nu_i)S_i^*\left(1-\frac{1}{\tilde{s}}\right)(\tilde{s}_i-1) + \sum_{i=1}^{n} c_i\gamma R_i^*(\tilde{r}_i-1)\left(1-\frac{1}{\tilde{s}_i}\right)(1-\tilde{s}_i)$$

$$= \sum_{i=1}^{2n}\sum_{j=1}^{2n} c_i\tilde{\beta}_{ij}G_{i,j} - \sum_{i=1}^{n} c_i\left[(\mu_i+\nu_i)S_i^*+\gamma R_i^*(\tilde{r}_i-1)\right]\left(1-\frac{1}{\tilde{s}}\right)(\tilde{s}_i-1).$$

Now, since it can be verified that over each directed cycle $\mathcal{C}$ of $(\mathcal{G},\tilde{B})$, $\sum_{(s,r)\in\mathcal{E}(\mathcal{C})} G_{rs} = 0$, by following the same arguments in the proof of [12, Thm 3.5], we have that $\sum_{i=1}^{2n}\sum_{j=1}^{2n} c_i\tilde{\beta}_{ij}G_{i,j} = 0$. Moreover, by assumption $(\mu_i+\nu_i)S_i^* \geq \gamma R_i^*$, for each $i = 1,\dots,n$, hence

$$(\mu_i+\nu_i)S_i^*+\gamma R_i^*(r_i-1) \geq (\mu_i+\nu_i)S_i^*-\gamma R_i^* \geq 0, \qquad i=1,\dots,n.$$

Thus, we have $\dfrac{dV}{dt} \leq 0$. Since the largest compact invariant set in which $\dfrac{dV}{dt} = 0$ is the singleton $\{x^*\}$, by LaSalle invariance principle our claim follows. □

Remark 4. *Note that if $\nu_i = 0$ for all i, we obtain the same sufficient conditions for the GAS of the EE found for the SIRS model in [31].*

3.6 SAIRS without vaccination

Let us consider the SAIRS model without vaccination, that is (3.3) with $\nu_i = 0$, $i = 1,\dots,n$. From (3.7), the expression of the basic-reproduction number is

$$\mathcal{R}_0 = \rho\left(\left(\left(\beta_{ij}^A + \frac{\alpha\beta_{ij}^I}{\delta_I+\mu_i}\right)\frac{1}{\alpha+\delta_A+\mu_i}\right)_{i,j=1,\dots,n}\right), \tag{3.43}$$

and the components of the DFE (3.5) become $S_{0,i} = 1$, $A_{0,i} = I_{0,i} = 0$, for all $i = 1,\dots,n$.

In Theorem 3.3.3 and 3.3.4 we proved that the DFE is globally asymptotically stable if $R_0 < 1$ and unstable if $R_0 > 1$. In the following theorem, which describe the case when we do not have any vaccination, we are able to prove that the DFE is globally asymptotically stable also when $R_0 = 1$.

Theorem 3.6.1. *The disease-free equilibrium x_0 is globally asymptotically stable in Γ for (3.3) if $\mathcal{R}_0 \leq 1$.*

Proof. To prove the statement, we use the method presented in [12].

Rearranging the order of the equations such that the disease compartments can be written as $x = (A_1, \ldots, A_n, I_1, \ldots, I_n)$, system (3.3), restricted to these compartments, can be rewritten as:

$$x' = (F - V)x - f(x, S),$$

where

$$f(x,S) = \left(\sum_{j=1}^{n} \left(\beta_{1j}^{A} A_j + \beta_{1j}^{I} I_j\right)(S_{0,1} - S_1), \ldots, \sum_{j=1}^{n} \left(\beta_{nj}^{A} A_j + \beta_{nj}^{I} I_j\right)(S_{0,n} - S_n), 0, \ldots, 0 \right) \geq 0,$$

and $f(x, S)$ is a vector with non-negative elements for all $(x, S) \in \Gamma$ and $f(x, S_0) = 0$, for all $(x, S_0) \in \Gamma$.

Let ω^T be the left eigenvector of M corresponding to the eigenvalue $\mathcal{R}_0$. Note that in our case the irreducibility assumption for M in [12, Thm 2.2] fails. However, we can show that $\omega > 0$. Indeed, let $\omega^T = (\omega_1, \omega_2)$, where ω_1 and ω_2 are both vectors with n components. It is easy to see that ω_1 is the left-eigenvector of the non-negative matrix M_1 (3.6) corresponding to its spectral radius $\rho(M_1) = \mathcal{R}_0$. Since M_1 is irreducible and non-negative, it follows by the Perron-Frobenius theorem that $\omega_1 > 0$. Moreover, from (3.10), let

$$M_2 = \left(\frac{\beta_{ij}^{I} S_{0,i}}{\delta_I + \mu_i} \right)_{i,j=1,\ldots,n},$$

then, we have $\omega_1 M_2 = \mathcal{R}_0 \omega_2$; since $\omega_1 M_2 > 0$ it follows that $\omega_2 > 0$. Hence, $\omega > 0$. Now, consider the following Lyapunov function

$$Q = \omega^T V^{-1} x.$$

By differentiating Q along the solution of (3.3), we obtain

$$\begin{aligned} Q' &= \omega^T V^{-1} x' \\ &= \omega^T V^{-1} (F - V)\, x - \omega^T V^{-1} f(x, S) \\ &= (\mathcal{R}_0 - 1)\omega^T x - \omega^T V^{-1} f(x, S). \end{aligned}$$

Since $\omega^T > 0$, $V^{-1} \geq 0$ and $f(x, S) \geq 0$, it follows that $Q' \leq (\mathcal{R}_0 - 1)\omega^T x$, Hence, $Q' \leq 0$ provided $\mathcal{R}_0 \leq 1$. Moreover, $Q' = 0$ if $x = 0$ or $S_i = S_{0,i}$, for all $i = 1, \ldots, n$, but this last case still implies $x = 0$. It can be verified that the only invariant set where $x = 0$ is the singleton $\{x_0\}$. Hence, by LaSalle's invariance principle, the DFE x_0 is globally asymptotically stable if $\mathcal{R}_0 \leq 1$. □

3.7 Numerical analysis

In this section, we explore the role of the network structures in the evolution of the epidemics. The primary criterion for parameter selection is the clarity of the resulting

plot. Hence, the simulations were carried out with a set of parameters considered in Sec. 2.7. These parameters, summarized in Table 1, ensure that $\mathcal{R}_0 > 1$ in all the networks we consider, whose shapes are represented in Figure 3.

β_{ii}^A	β_{ij}^A	β_{ii}^I	β_{ij}^I	μ_i	ν_i	γ	δ_A	δ_I	α
0.8	0.4	0.95	0.475	$1/(70 \cdot 365)$	0.01	0.02	0.1	0.51	0.8

Table 1: Values of the parameters used in the simulations: $\beta_{ii}^A = 0.8$, which we reduced to $\beta_{ij}^A = 0.4$ if $i \neq j$, to model a lower inter-community spreading; $\beta_{ii}^I = 0.95$ and $\beta_{ij}^I = 0.475$ if $i \neq j$; $\mu_i = 1/(70 \cdot 365)$, meaning an average lifespan of 70 years for all i; $\nu_i = 0.01$, meaning 1% of the susceptible population is vaccinated every day for all i; $\gamma = 0.02$, meaning an average immunity of 50 days; $\delta_A = 0.1$, $\delta_I = 0.51$, $\alpha = 0.8$.

In particular, we remark on how sensitive $\mathcal{R}_0$ is on the topology of the network, which is reflected in its adjacency matrix. Indeed, let us consider the matrix M_1 defined in (3.6) as follow

$$M_1 = \left(\left(\beta_{ij}^A + \frac{\alpha \beta_{ij}^I}{\delta_I + \mu_i} \right) \frac{S_{0,i}}{\alpha + \delta_A + \mu_i} \right)_{i,j=1,\dots,n},$$

and let

$$\beta_1 = \min_{i,j} (M_1)_{i,j}, \qquad \text{and} \qquad \beta_2 = \max_{i,j} (M_1)_{i,j}.$$

Let us define $\bar{\mathcal{A}} = \mathcal{A} + I_n$, where $\mathcal{A}$ is the adjacency matrix and n the number of nodes of the network we are considering, respectively. Then, as a consequence of the Perron-Frobenius theorem, the following lower and upper bounds for $\mathcal{R}_0$ hold:

$$\beta_1 \rho(\bar{\mathcal{A}}) \leq \mathcal{R}_0 \leq \beta_2 \rho(\bar{\mathcal{A}}) \tag{3.44}$$

In the case of the cycle-tree network in Figure 3(a), we have $\rho(\mathcal{A}) = 3.2877$, for the star network in Figure 3(b), $\rho(\mathcal{A}) = 3.8284$, in the case of the ring network in Figure 3(c), $\rho(\mathcal{A}) = 3$, and for the line network in Figure 3(d) we have $\rho(\mathcal{A}) = 2.9021$. Consequently, in the star network, we found the largest $\mathcal{R}_0 = 4.91$, for the cycle-tree network we have $\mathcal{R}_0 = 4.37$. In the other two networks, i.e. the ring and the line, we find $\mathcal{R}_0 = 4.07$ and $\mathcal{R}_0 = 3.97$, respectively; we can see that the presence of one additional link in the ring increases the spectral radius of the transmission matrices and thus facilitates the spread of the disease.

We provide numerical simulations of the evolution of an epidemics for the different 9-communities networks considered, see Figures 4, 5, 6 and 7. In each simulations, the epidemics starts in community 1, with a small asymptomatic fraction of the population, and no symptomatic individuals. We obtain a delay in the start of the epidemics, directly proportional to the path distance of any community from community 1: this is particularly visible in Figure 7. We observe a delay in the time of the peak, as well, although this is often less pronounced; this is clear in in Figure 6, in which communities

with the same distance (path length) from Community 1 reach the peak at the same time. We can see that in the star network the peak of the non-central communities happens exactly at the same time and has the same magnitude, as one would expect, see Figure 5.

For ease of interpretation, we plot the total number of Asymptomatic infected individuals and symptomatic Infected individuals in all four cases, see Figure 8. The qualitative behaviour of all simulations is the same: after a first spike, the dynamics converges towards the endemic equilibrium, through quickly damping oscillations. In all our simulations, the endemic equilibrium values of I are greater than the ones of A, as we expected from (3.16) and our choice of the parameters involved in the formula.

Notice the significantly lower peaks in Figure 8d, when compared to 8c, even though the corresponding networks only differ for one edge, connecting Community 9 to Community 1, in which the epidemics start.

3.8 Summary and Outlook

We analysed a multi-group SAIRS-type epidemic model with vaccination. In this model, susceptible individuals can be infected by both asymptomatic and symptomatic infectious individuals, belonging to their communities as well as to other adjacent communities.

We derived the expression of the basic reproduction number $\mathcal{R}_0$, which depends on the matrices which encode the transmission rates between and within communities. We showed that if $\mathcal{R}_0 < 1$, the disease-free equilibrium is globally asymptotically stable, i.e. the disease will be eliminated in the long-run, whereas if $\mathcal{R}_0 > 1$ it is unstable. Moreover, in the SAIRS model without vaccination ($\nu_i = 0$, for all $i = 1, \dots, n$), we were able to generalize the result on the global asymptotic stability of the disease-free equilibrium also in the case $\mathcal{R}_0 = 1$. We proved the existence of a unique endemic equilibrium if $\mathcal{R}_0 > 1$. We gave sufficient conditions for the local asymptotic stability of the endemic equilibrium; then, we investigated the global asymptotic stability of the endemic equilibrium in two cases. The first one regards the SAIR model (i.e. $\gamma = 0$), and does not requires any further conditions on the parameters besides $\mathcal{R}_0 > 1$.

The second is the case of the SAIRS model, with the restriction that asymptomatic and symptomatic individuals have the same mean recovery period, i.e. $\delta_A = \delta_I$. In this case, we provided sufficient conditions for the GAS of the endemic equilibrium.

We leave as open problem the study of the global asymptotic stability of the endemic equilibrium for the SAIRS model with vaccination, in the case $\beta_A \neq \beta_I$ and $\delta_A \neq \delta_I$. Lastly, we conjecture that the conditions we derived to prove the asymptotic behaviour of the model are sufficient but not necessary conditions, as our numerical exploration of various settings seems to indicate.

In this chapter, we focused on a generalisation of the SAIRS compartmental model proposed in 2; however, many others elements could be included in further generalisations to increase realism. For example, we may consider a greater number of compartments, e.g. including the "Exposed" group, or consider a nonlinear incidence rate; one could

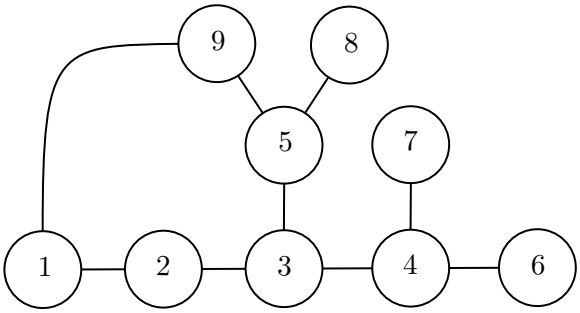

(a) Cycle-tree network, i.e. a tree graph in which we add a cycle linking the first and the last community.

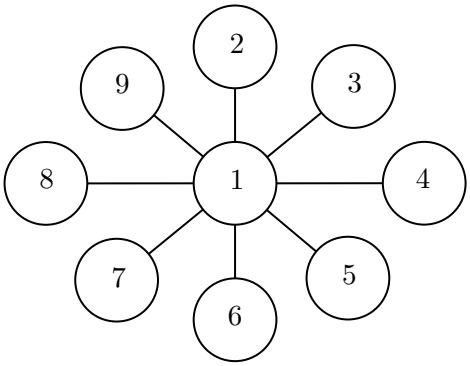

(b) Star network, in which a central community is linked to all the others, and no other connections are present.

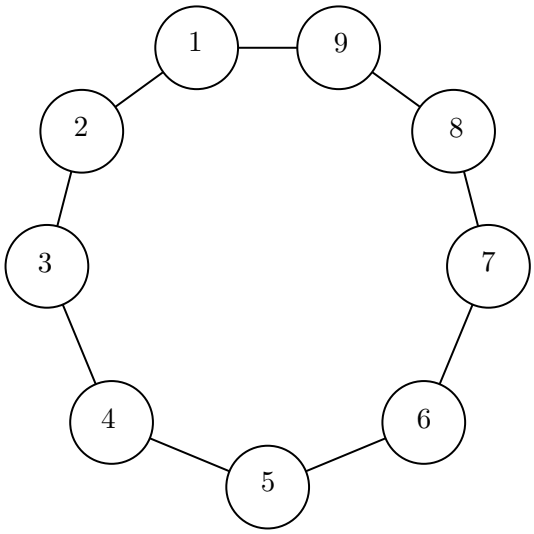

(c) Ring network, in which each community is linked with the previous and next.

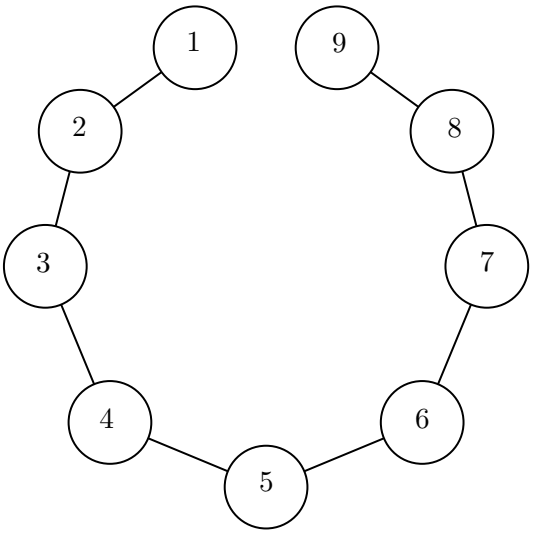

(d) Line network, i.e. the ring network in which we remove the link between the communities 1 and 9.

Figure 3: The four different network structures we consider in our numerical simulations. Circles represent the communities, numbered from 1 to 9, corresponding to C1 to C9 in Figures 4, 5, 6 and 7. Lines represent the links between the various communities. We use lines instead of arrows, since all networks are considered as undirected.

also introduce an additional disease-induced mortality, or an imperfect vaccination. We leave these as future research outlook.

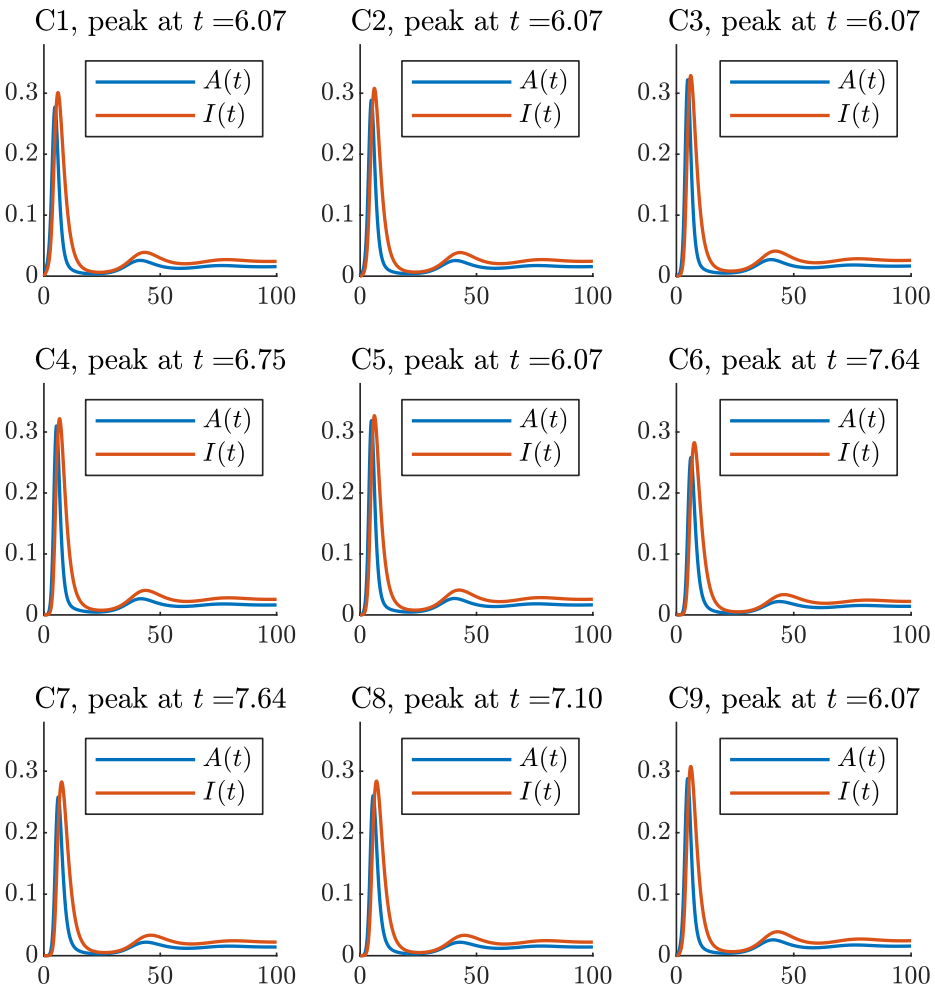

Figure 4: Evolution of the epidemic in each community of the cycle-tree network, see Figure 3a. The title of each subplot indicates the community it represents, as well as the peak time of infected individuals. In this setting, from (3.7) we obtain $\mathcal{R}_0 = 4.37$. Refer to Table 1 for the values of the parameters.

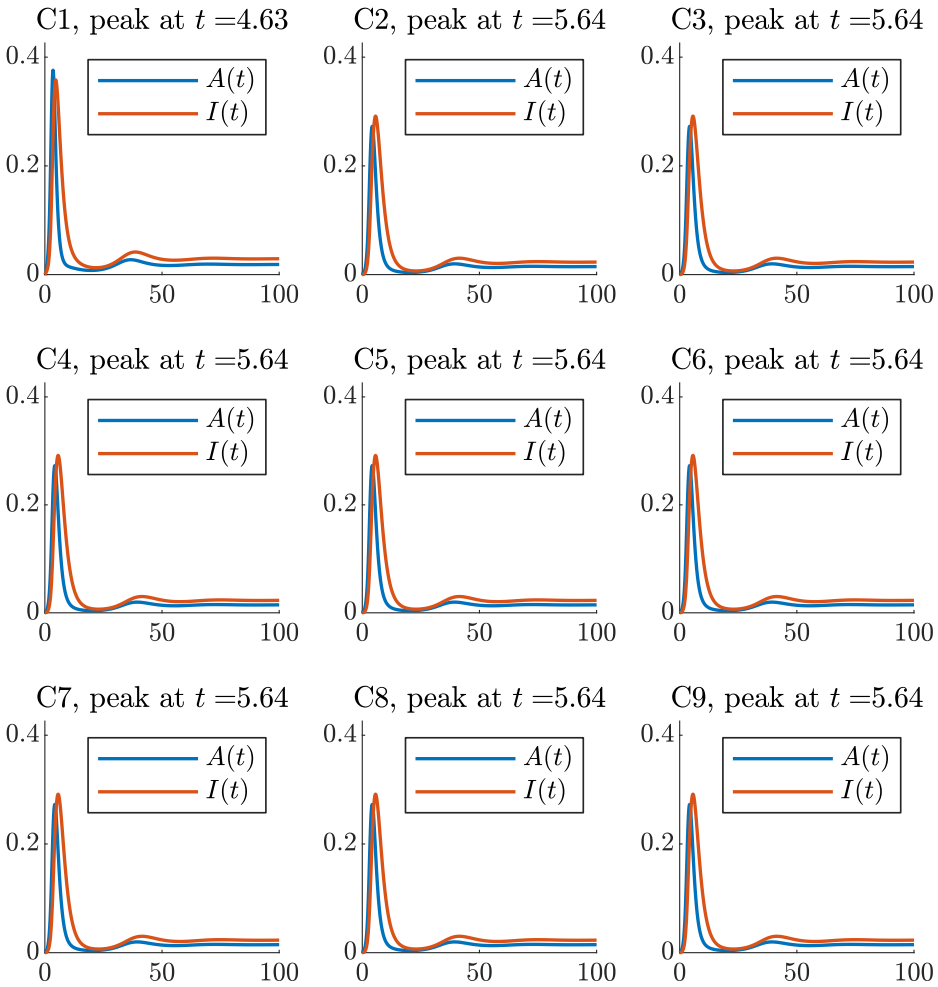

Figure 5: Evolution of the epidemic in each community of the star network, see Figure 3b. The title of each subplot indicates the community it represents, as well as the peak time of infected individuals. In this setting, from (3.7) we obtain $\mathcal{R}_0 = 4.91$. Refer to Table 1 for the values of the parameters.

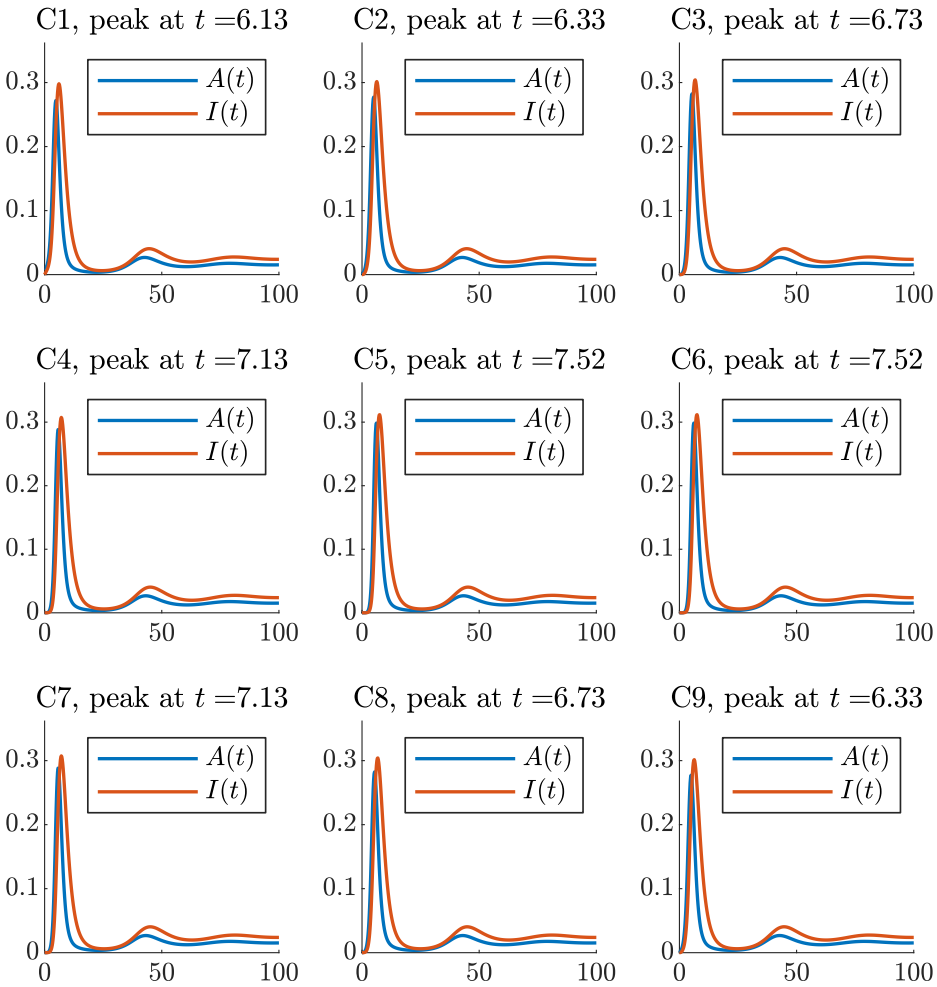

Figure 6: Evolution of the epidemic in each community of the ring network, see Figure 3c. The title of each subplot indicates the community it represents, as well as the peak time of infected individuals. In this setting, from (3.7) we obtain $\mathcal{R}_0 = 4.07$. Refer to Table 1 for the values of the parameters.

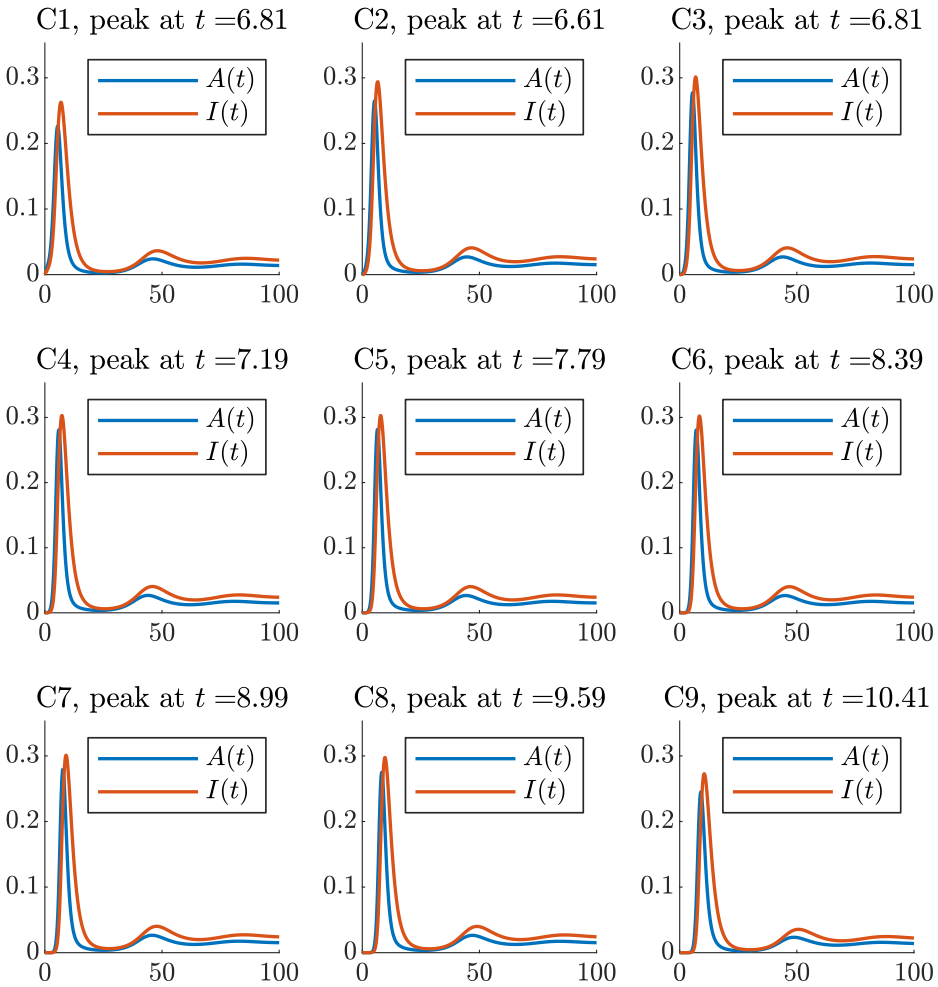

Figure 7: Evolution of the epidemic in each community of the line network, see Figure 3d. The title of each subplot indicates the community it represents, as well as the peak time of infected individuals. In this setting, from (3.7) we obtain $\mathcal{R}_0 = 3.97$. Refer to Table 1 for the values of the parameters.

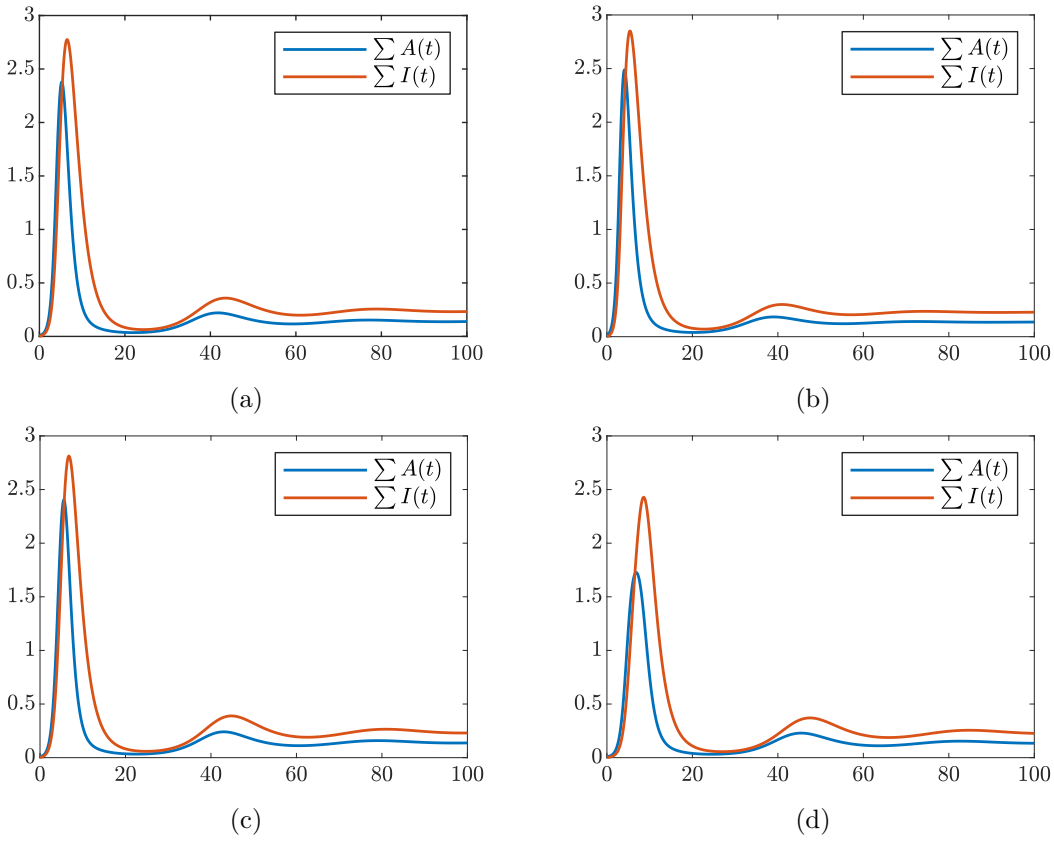

Figure 8: Total amount of Asymptomatic infected ($\sum A(t)$) and symptomatic Infected ($\sum I(t)$) in the four networks we simulate. Respectively: (a) cycle-tree network, see Figure 3a; (b) star network, see Figure 3b; (c) ring network, see Figure 3c; and (d) line network, see Figure 3d. The qualitative behaviour is the same, i.e. convergence towards the endemic equilibrium through damped oscillations. Refer to Table 1 for the values of the parameters.

Appendix

3.A Proof of Claim 3.4.4

We recall that

$$\eta_i(z) = \frac{1}{\alpha + \mu_i + \delta_A} \left(z + \sum_{j=1}^{n} \beta_{ij}^A (A_j^* + h_j I_j^*)(1 + K_i^1(z) + K_i^2(z)) \right).$$

It is easy to see that if $\Re(z) \geq 0$, then $\Re(K_i^1(z)) > 0$. Now, we show that if $\Re(z) \geq 0$, then

$$\Re(1 + K_i^2(z)) = \Re\left(1 + \frac{1}{z + \mu_i + \nu_i + \gamma} \left((\delta_A - \nu_i) + \frac{(\delta_I - \nu_i)\alpha}{z + \delta_I + \nu_i} \right) \right) \geq 0. \tag{3.45}$$

For ease of notation, we define:

$$\varepsilon = (\delta_I - \nu_i)\alpha, \qquad h_1 = \mu_i + \nu_i + \gamma, \qquad h_2 = \delta_I + \nu_i,$$

and let $z = a + ib$ in (3.45). If $\delta_A \geq \nu_i$, again it is easy to see that, if $\Re(z) \geq 0$, then

$$\Re\left(\frac{1}{z + h_1} (\delta_A - \nu_i) \right) \geq 0.$$

Now, let us show that

$$\Re\left(1 + \frac{\varepsilon}{(z + h_1)(z + h_2)}\right) \geq 0. \tag{3.46}$$

We have that

$$\begin{aligned}
\Re\left(\frac{\varepsilon}{(z + h_1)(z + h_2)} \right) &= \Re\left(\frac{\varepsilon}{(a + h_1)(a + h_2) - b^2 + ib(2a + h_1 + h_2)} \right) \\
&= \Re\left(\varepsilon \frac{(a + h_1)(a + h_2) - b^2 - ib(2a + h_1 + h_2)}{((a + h_1)(a + h_2) - b^2)^2 + b^2(2a + h_1 + h_2)} \right) \\
&= \varepsilon \frac{(a + h_1)(a + h_2) - b^2}{((a + h_1)(a + h_2) - b^2)^2 + b^2(2a + h_1 + h_2)} \\
&= \varepsilon \frac{(P - b^2)}{(P - b^2)^2 + b^2 S^2} = g(b),
\end{aligned} \tag{3.47}$$

where we have introduced the notation

$$P = (a + h_1)(a + h_2) \qquad \text{and} \qquad S = (2a + h_1 + h_2).$$

Since we assume $\delta_I \geq \nu_i$, we can see that the minimum of $g(b)$ is equal to

$$\frac{-\varepsilon}{2S\sqrt{P} + S^2},$$

and that

$$\begin{aligned}
\frac{-\varepsilon}{2S\sqrt{P} + S^2} &\geq \frac{-(\delta_I - \nu_i)\alpha}{2(2a + \mu_i + 2\nu_i + \gamma + \delta_I)\sqrt{((a + \mu_i + \nu_i + \gamma)(a + \delta_I + \nu_i))} + (2a + \mu_i + 2\nu_i + \gamma + \delta_I)^2} \\
&\geq \frac{-(\delta_I - \nu_i)\alpha}{2(\mu_i + 2\nu_i + \gamma + \delta_I)\sqrt{((\mu_i + \nu_i + \gamma)(\delta_I + \nu_i))} + (\mu_i + 2\nu_i + \gamma + \delta_I)^2} \\
&\geq -1.
\end{aligned}$$

The last inequality holds since by hypothesis

$$(\delta_I - \nu_i)\alpha \leq 2(\mu_i + 2\nu_i + \gamma + \delta_I)\sqrt{(\mu_i + \nu_i + \gamma)(\delta_I + \nu_i)} + (\mu_i + 2\nu_i + \gamma + \delta_I)^2,$$

thus (3.46) holds and the claim is proved.

4. How network properties and epidemic parameters influence stochastic SIR dynamics on scale-free random networks

4.1 Introduction and Outline

Real systems of interactions between humans are commonly studied as interaction networks. In this setting, an edge in a network represents a possible interaction between the connected nodes. The mechanism of disease transmission upon contact provides a strong case for the use of these networks in modelling epidemic. Spreading processes of infectious diseases take place over these networks, thus their structures can be essential for understanding disease transmission. In particular, knowledge on the interplay between network structure and transmission parameters can improve predictions as well as prevention and control strategies.

A key factor in an epidemic spread is the population network structure where a disease may spread. However, a complete picture, in principle, may require the knowledge of every individual in a population and its relationships, for example, as in contact tracing [94]. Networks used in different fields have some common geometric characteristics regarding the distribution of the nodes and edges, for example, a few nodes that may act as hubs and the vast majority of nodes with a few neighbours [95]. A classification in this context is given by network generation models, used as generators of synthetic networks, with controlled topological properties.

Several types of networks have been proposed over time [96, 97]. [98] proposed a simple model where nodes are connected according to a uniform probability without any preference. However, some structural properties observed in real-world networks cannot be reproduced by this model as empirically verified by [99]. It has been observed in real networks that the degree distribution of individuals is far from homogeneous; on the contrary, only a few individuals have several connections and the majority have a few [100, 101]. Barabási and Albert proposed a model to generate *scale-free networks* [102] with a connection mechanism that mimics the natural formation of social contacts. Recent results highlight criticisms in the use of their approach to model the realistic

spread of an epidemic. In [103], the authors remark about an unexpected, recently discovered assortative behaviour of Barabási-Albert networks. In [104], the authors show a correlation between assortativity and epidemic spread, which might result in misleading simulations. Moreover, the algorithm proposed by [102] cannot control the value of the exponent of the power-law distribution [96]. In [105], assortativity is taken into account and discussed in greater detail in the context of epidemics and vaccinations.

However, [106] state that the *configuration model* can overcome these issues, generating a network with a given degree sequence. The configuration model is used, for example, in social dynamics, as it captures connectivity features of this class of networks [107]. The study of how epidemics evolve on networks has been addressed using various approaches, theoretical and computational. Theoretical results on this topic can be found, for example, in the monographs [108, 109] or in [110]. In [111], the author derives results on a small heterogeneous population before validating them via numerical simulations. In [44], the authors explore the interplay between network properties and disease characteristics on the spread. Many other articles are devoted to the study of the impact of the network structure on the evolution of an epidemic (*e.g.* household structure [112], the influence of network topology on epidemic spread [113, 114, 115], or community structure [116]). In particular, researchers have been interested in identifying the nodes which, if infected, would cause the largest epidemic, the so-called *influential spreaders* [117, 118, 119]. Another interesting feature, studied in [53], is the implementation of dynamic contacts, meaning a network in which nodes may delete and create edges in time. Other studies have been devoted to the extinction time for epidemics on networks [120, 121, 122] and epidemics thresholds [123, 124, 125]. Bounds and estimates on the final size of the epidemics have been investigated assuming both homogeneity and heterogeneity of viral transmission [126, 127]. These estimates have played a major role in quantifying the consequences of different restrictions on the Covid-19 pandemic [128, 49, 129].

In [130] and [131] the authors study the effect of *seeding* on the evolution of the epidemic to consider various realistic scenarios for its beginning. Different scenarios, in this regard, can be integrated into the model. Examples to these scenarios include multiple infected individuals arriving in a country almost simultaneously in different airports, or a localised initial cluster which is then spread by the individuals from the same starting area. In particular, the former scenario is included in our analysis, in Section 4.4.1, in the 'random case' with multiple initially infected individuals.

In this chapter, we investigate how the interplay between the connectivity of different configuration model networks and the contagiousness of the disease affect the magnitude of the epidemic. Observations on empirical data show that standard epidemiological metrics often fail to predict the evolution of an epidemic due to their lack of integrating various aspects of the population that influence the spread dynamics. In this respect, the capability to perform stochastic simulations on graphs indicates a more empirical approach in studying the spread and behaviour of epidemics while maintaining a theoretical grip. To this end, the present work lays the foundation for such refinements to study SIR (Susceptible-Infected-Removed) compartmental models stochastically on graphs to

assess the factors that are otherwise difficult or even impossible. To achieve this, we verify our approach for theoretical rigour by showing an agreement with theoretical results. With the integration of stochastic elements, in the generation of the configuration model and the simulations, we introduce an empirical component that captures the variability in real-world epidemics. This step, in return, provides new capabilities to perform *in silico* experiments by simulations, possibly by introducing additional components that model various epidemic influences.

In the following, after a summary of the relevant mathematical background, we derive a lower bound and a closed formula for the probability of having a minor epidemic of the disease in a network. In other words, we model the contacts in a community as a scale-free network and study how an epidemic spreads over these contacts. For this, we use the derivation of the probability of extinction for a branching process as a function of all the parameters involved and the degree of the initially infected node. A similar analysis of the extinction probability was carried out in [132] where the author considers a more general case for the distribution of the infectious period and proceeds with the so-called *cavity method* and in [133] where the authors obtain a result similar to ours through the *message passing method*. In this work, we provide a different exact result on the probability of a minor epidemic, however, in a form that only allows for numerical exploration. We consequently deduce from it a lower bound for the probability of a minor epidemic, given the parameters of the epidemics and the degree of the initially infected node.

Following the theoretical groundwork, we introduce a stochastic model on scale-free random networks, which we use to run simulations on different instances of the model. The simulations, carried out via a specialised modification of the Gillespie algorithm, validate our theoretical results regarding the probability of a minor epidemic of the disease. Consequently, we provide a thorough analysis via simulations that highlights the influence of network connectivity (which decreases in α, the exponent of the power law) and infectiousness (the parameter β of our SIR model) on three key epidemic indices: the peak of infected individuals, the total number of eventually infected individuals, and the duration of the epidemic. In particular, we focus on the role of the position of the nodes from which the disease starts spreading as well as the number of initially infected nodes, exploring simulations for different instances of the model parameters. We compare the evolution of the epidemic, measured by the aforementioned indices, in four different cases for the initially infected nodes, categorised by their position in the respective network: hub (degree in the tail of the distribution), mean degree, peripheral (low degree), and randomly chosen. The stochastic simulations with our model are in good agreement with the analytical lower bound for the probability of extinction we derived. The comparison between our analytical and numerical results provides a quantification of the role of model parameters in the spread of the epidemic on scale-free networks.

Overall, our results illustrate how theoretical methods in epidemiology can be coupled with discrete stochastic simulations in a rigorous manner. In this regard, our theoretical results set a baseline for discrete simulations for comparison and validation. Our implementation, available through a Github repository, optimises Gillespie's stochastic

simulation algorithm ([134]) by exploiting the network structure for increased efficiency, which is otherwise a bottleneck for simulating networks. Our implementation may thus be used, by us or other researchers, to study broader questions while maintaining the baseline given by our theoretical results.

4.2 Power-law networks

In this section, we describe scale-free networks, which can be used to mathematically evaluate a given model or describe a real network structure, mimicking social contacts between individuals. We then describe the classic algorithm used to generate networks with a certain degree distribution, that is, *configuration model* (CM).

4.2.1 Scale-free networks

Many real-world graphs follow power-law degree distributions [135, 136, 137] (however their actual frequency is debated [138, 139]), that is, degree distributions with the probability of a node to have k direct neighbours given by $p_k \sim k^{-\alpha}$. These kinds of networks are also called *scale-free random graphs*. The preferential attachment model of [102] produces a degree distribution with $\alpha = 3$. However, there are many examples in which $\alpha \in (2, 3]$ (see e.g. [140, Sec. 1.4]). To explain the scale-free property, Barabási defined the power-law distribution both with a discrete and a continuum formalism; we refer to [141] for a more in-depth introduction to this topic and recall here the definitions and results we need for our analysis.

In a scale-free network, the probability of having k neighbours is $p_k = Ck^{-\alpha}$ where C is a normalisation constant. The main difference between an E-R graph and a scale-free network comes in the tail of the degree distribution, representing the high-k region of p_k: high-degree nodes, called *hubs*, are naturally present in scale-free networks, contrary to random networks. Since all real networks are finite, we may expect that nodes assume a maximum degree, $k_{\max}$, called the *natural cut-off of the degree distribution* p_k (see [142]). This quantity represents the expected size of the largest hub in a network and it is determined by

$$k_{\max} = \lfloor k_{\min} N^{\frac{1}{\alpha-1}} \rfloor, \tag{4.1}$$

where $k_{\min}$ is the smallest degree we allow a node to have. Hence, the highest attainable degree is directly proportional to a power of N between $\frac{1}{2}$ (corresponding to $\alpha = 3$) and 1 ($\alpha = 2$).

4.2.2 Configuration model

In the case of large networks, the adjacency matrix may not be immediately available [109]. However, in the case of real networks of which we know the degree sequence, we can generate a graph with precisely the same degrees. Given the number of nodes N and the sequence of degrees $\{k_i\}_{1 \le i \le N}$ of length N (we omit the subscript from now on, for

ease of notation), the aim is to construct an undirected graph with N nodes, in which the i-th node has precisely degree k_i. We denote such graphs with $\mathcal{G}(N, \{k_i\})$. Given a degree distribution obtained from observing a stochastic network, the algorithm used to fit this distribution is called the *configuration model*. To construct the network, we start by assigning to each node i in the set of nodes a random degree k_i, drawn from the chosen probability distribution p_k. Clearly, $k_{\max} \leq N - 1$ since no node can have a degree larger than $N - 1$. The degrees of the nodes are represented as half-links or stubs, thus we impose $\sum_{i=1}^{N} k_i = 2m$, where m is the total number of edges.

First, two stubs are connected to form an edge. After that, another pair of stubs are chosen from the remaining $2m - 2$ stubs and connected, respecting the preassigned degrees. The network is completed by repeating this procedure until the stubs run out. The result of this construction is a random network whose degrees are distributed according to p_k [143]. If L denotes the numbers of degrees assumed in the network and $N_1, N_2, \ldots, N_L$ the number of nodes of each degree, the average degree in the network is given by [109]

$$\langle k \rangle = \frac{1}{N} \sum_{i=1}^{L} N_i k_i.$$

This formula is equivalent to $\langle k \rangle = \sum_i k_i p_{k_i}$ for this specific realisation. Note that this linkage procedure does *not* exclude self-loops or multiple edges, but their expected number is bounded (see e.g. [144, Prop. 7.1]). When the size of the graph $N \to +\infty$ with a fixed degree distribution, self-loops and multiple edges become less and less apparent in the global dynamics (see e.g [140, Th. 3.1.2]).

4.3 Lower bound for the probability of a minor epidemic

We work on an SIR epidemiological dynamics model on a network built with the CM algorithm, described in Section 4.2.2. In this network, we introduce infected individuals in an otherwise fully susceptible population; the exact number of infected individuals is specified each time it changes. Later, in Section 4.4, we study how the introduction of a different number of initially infected individuals affects the evolution of the epidemic. In this section, we consider an epidemic that starts with only one infected individual. We then derive an analytical formula for the *probability of a minor epidemic*, that is, the probability that one infected individual in the network does not cause a major epidemic. In other words, an epidemic in which a large number of individuals are infected simultaneously, a large number of infections occur in total and the disease remains in the population for an extended period [145]. We use this probability as a benchmark to compare with our simulations. As usual, we assume that an individual remains infected for a duration drawn from an exponential distribution with rate parameter γ. During its infectious period, an individual infects each of its neighbours (independently of the others) according to a Poisson process with rate parameter β. Note that modellers often assume that β does not depend on the number of contacts; however, in most epidemic

models (and data that are collected), the infection probability decreases with the number of contacts [146, Chap. 2]. Under the assumptions above, the *basic reproduction number* R_0 is given in [147] as

$$R_0 = \frac{\beta}{\gamma}\langle k\rangle(1 + CV^2),$$

where CV is the coefficient of variation, defined as $CV = \frac{\langle k^2\rangle}{\langle k\rangle}$. Using this definition, the expression of R_0 can be written also as

$$R_0 = \frac{\beta}{\gamma}\frac{\langle k^2\rangle}{\langle k\rangle}. \tag{4.2}$$

We focus on this slightly unrealistic but analytically tractable assumption; we refer to [148, App. 1] for a similar construction, applied however to a power law distribution without cut-off. We approximate the initial phase of an epidemic by a branching process where all contacted individuals are susceptible. This is a property of the configuration model as N goes to infinity; thus, cliques and triangles are neglected, and the population is assumed to be large enough. First, we compute the probability that an infected node i with k_i neighbours infects j of them; for ease of reading, we denote the degree of a node with k. We start by considering one of them, conditioning on the length of the infectious period:

$$\mathbb{P}(\text{a contact is not infected}) = \gamma\int_0^\infty e^{-\beta t}e^{-\gamma t}\,\mathrm{d}t = \frac{\gamma}{\beta+\gamma} = \frac{1}{R+1},$$

where $R := \beta/\gamma$.

We can not use the binomial distribution to obtain the probability of having n infected individuals, because infections of different contacts are not independent, but correlated by the length of the infectious period, whereas an important assumption which would allow us to use the binomial distribution is independence between infections [149]. This is due to the fact that if the infectious period is short, it is likely that no neighbour will be infected, while if it is long, most of them will. Indeed, if Q is the number of infected neighbours,

$$\mathbb{P}(Q = 0) = \gamma\int_0^\infty (e^{-\beta t})^k e^{-\gamma t}\,\mathrm{d}t = \frac{\gamma}{\beta k+\gamma} = \frac{1}{kR+1}.$$

The other expressions are more complicated:

$$\mathbb{P}(Q = j) = \gamma\int_0^\infty \binom{k}{j}(1 - e^{-\beta t})^j(e^{-\beta t})^{k-j}e^{-\gamma t}\,\mathrm{d}t. \tag{4.3}$$

We can verify that $\sum_{j=0}^{k} \mathbb{P}(Q=j) = 1$ as follows

$$\begin{aligned}\sum_{j=0}^{k} \mathbb{P}(Q=j) =& \sum_{j=0}^{k} \gamma \int_0^\infty \binom{k}{j} (1-e^{-\beta t})^j (e^{-\beta t})^{k-j} e^{-\gamma t} \mathrm{d}t \\ =& \gamma \int_0^\infty e^{-\gamma t} \left(\sum_{j=0}^{k} \binom{k}{j} (1-e^{-\beta t})^j (e^{-\beta t})^{k-j} \right) \mathrm{d}t.\end{aligned}$$

Note that $\sum_{j=0}^{k} \binom{k}{j} (1-e^{-\beta t})^j (e^{-\beta t})^{k-j} = (1-e^{-\beta t}+e^{-\beta t})^k = 1$, thus we obtain

$$\sum_{j=0}^{k} \mathbb{P}(Q=j) = \gamma \int_0^\infty e^{-\gamma t} \mathrm{d}t = 1.$$

We can clarify the expression in (4.3) as

$$\begin{aligned}\mathbb{P}(Q=j) =& \gamma \int_0^\infty \binom{k}{j} (1-e^{-\beta t})^j (e^{-\beta t})^{k-j} e^{-\gamma t} \, \mathrm{d}t = \text{(integr. by parts)} \\ =& \int_0^\infty \frac{\gamma\beta}{\gamma + \beta(k-j)} \frac{k!}{(k-j)!(j-1)!} (1-e^{-\beta t})^{j-1} (e^{-\beta t})^{k-j+1} e^{-\gamma t} \, \mathrm{d}t \\ =& \frac{\beta(k-j+1)}{\gamma + \beta(k-j)} \mathbb{P}(Q=j-1).\end{aligned}$$

Then, by induction, we obtain

$$\mathbb{P}(Q=j) = \frac{R^j \prod_{l=1}^{j} (k-l+1)}{\prod_{l=0}^{j} (1+R(k-l))}. \tag{4.4}$$

Although the infections of different contacts are not independent, the expected number of infected contacts can be obtained as

$$\begin{aligned}\mathbb{E}(Q) &= \sum_{j=0}^{k} j \mathbb{P}(Q=j) \\ &= \sum_{j=0}^{k} j\gamma \int_0^\infty \binom{k}{j} (1-e^{-\beta t})^j (e^{-\beta t})^{k-j} e^{-\gamma t} \mathrm{d}t \\ &= \gamma \int_0^\infty e^{-\gamma t} \left(\sum_{j=0}^{k} j \binom{k}{j} (1-e^{-\beta t})^j (e^{-\beta t})^{k-j} \right) \mathrm{d}t,\end{aligned}$$

since the expected value of a finite sum is the sum of the expected values, assuming they are all finite as in our case.

Clearly, $\sum_{j=0}^{k} j\binom{k}{j}(1-e^{-\beta t})^j(e^{-\beta t})^{k-j} = k(1-e^{-\beta t})$ since this sum represents the first moment of a binomial variable of parameters $(k, e^{-\beta t})$. It follows that

$$\begin{aligned}\mathbb{E}(Q) &= \gamma k \int_0^\infty e^{-\gamma t}(1-e^{-\beta t})\mathrm{d}t \\ &= k\gamma \frac{\beta}{\gamma(\beta+\gamma)} \\ &= \frac{kR}{1+R}.\end{aligned}$$

We need these computations to estimate the probability of extinction of the branching process. We define a *minor epidemic* as an epidemic in which we observe such an extinction. For the derivation of the following formulae, we refer to [150, Chap. 2] and [151, Chap. 5]. Indeed, we consider a multi-type branching process, where *types* are the number of different neighbours of each node. Thus, the i-th node has k_1 neighbours of type 1, k_2 neighbours of type 2, and so on until k_L of type L. Note that, $k_1+k_2+\cdots+k_L = k$, where k is the total degree of the chosen node and, if the $i-$th node does not have a neighbour with degree j, then $k_j = 0$.

In the following, we denote a vector with L components with the bold symbol $\boldsymbol{x} = (x_1, \ldots, x_L)$.

The probability of extinction of this branching process is given by the smallest positive solution[1] of $\boldsymbol{s} = \boldsymbol{f}(\boldsymbol{s})$, where $\boldsymbol{s} = (s_1, \ldots, s_L)$ and the components of $\boldsymbol{f}$ are given by

$$f_k(\boldsymbol{s}) = \sum_{\boldsymbol{k}=(k_1,\ldots,k_L)} p_k(\boldsymbol{k}) s_1^{k_1} \cdots s_L^{k_L},$$

with

$$p_k(\boldsymbol{k}) = \mathbb{P}(\text{an infected node of type } k \text{ infects } k_1 \text{ of type } 1, \ldots, \ k_L \text{ of type } L).$$

Once we found the smallest solution $\boldsymbol{s^*}$, $s_k^* = f_k(\boldsymbol{s^*})$ represents the extinction probability starting with one individual of type l. Note that $f_k(1, \ldots, 1) = 1$; hence $\mathbf{1} = (1, \ldots, 1)$ is always a solution of $\boldsymbol{f}(\boldsymbol{s}) = \boldsymbol{s}$. If we find a smaller solution, then the probability of extinction is smaller than 1; otherwise, the probability of extinction is 1. We then need to compute $p_k(\boldsymbol{k})$. An individual with k neighbours will have k_1 neighbours of type 1, ..., k_L of type L with probability

$$\frac{k!}{k_1! \cdots k_L!} q_1^{k_1} \cdots q_L^{k_L},$$

where

$$q_j = \frac{jp_j}{\sum_{l=1}^{L} lp_l} \qquad \text{(size-biased probabilities)}.$$

[1] A positive solution $\boldsymbol{s^*}$ of $\boldsymbol{s} = \boldsymbol{f}(\boldsymbol{s})$ is called the *smallest* if $s_i^* \leq r_i$, for all $i = 1, \ldots, L$, for any other solution $\boldsymbol{r}$.

We could then compute the probability of infecting m_1 out of k_1, m_2 out of k_2, ..., m_L out of k_L, and sum over all possible combinations. We do not need to go through all the components because the probability of infecting one neighbour is independent of its properties, i.e. its degree. Hence, if $j = m_1 + \ldots + m_L$,

$$p_k(\boldsymbol{m}) = \mathbb{P}(Q = j)\frac{j!}{m_1! \cdots m_L!} q_1^{m_1} \cdots q_L^{m_L}.$$

We then compute the probability of infecting $j \leq k$ neighbours; in particular the probability that, among the j infected neighbours, m_1 are of type 1, m_2 of type 2, ..., m_L of type L. We can go a further step in the computation of $f_k(\boldsymbol{s})$; indeed

$$\begin{aligned} f_k(s) &= \sum_{\boldsymbol{m}=(m_1,\ldots,m_L)} \mathbb{P}(Q = j)\frac{j!}{m_1! \cdots m_L!} q_1^{m_1} \cdots q_L^{m_L} s_1^{k_1} \cdots s_L^{k_L} \\ &= \sum_{j=0}^{k} \mathbb{P}(Q = j) \sum_{\boldsymbol{m}:\ m_1+\cdots+m_L=j} \frac{j!}{m_1! \cdots m_L!} (q_1 s_1)^{m_1} \cdots (q_L s_L)^{m_L} \\ &= \sum_{j=0}^{k} \mathbb{P}(Q = j)(q_1 s_1 + \cdots + q_L s_L)^j \\ &= \sum_{j=0}^{k} (R(q_1 s_1 + \cdots + q_L s_L))^j \frac{\prod_{l=1}^{j}(k - l + 1)}{\prod_{l=0}^{j}(1 + R(k - l))}. \end{aligned} \tag{4.5}$$

One could go beyond this, but the formulae would become increasingly cumbersome. In order to compute the relevant solution numerically, one can start with a vector $\boldsymbol{s^0} \leq \boldsymbol{s^*}$ (for instance $\boldsymbol{s^0} = \boldsymbol{0} = (0, \ldots, 0)$) and then compute $\boldsymbol{s^n} = \boldsymbol{f}(\boldsymbol{s^{n-1}})$. Iterating this, we converge to the required fixed point as a consequence of the Dominated Convergence Theorem.

Remark 5. *One may notice the property $s_k^* = f_k(\boldsymbol{s^*}) > f_k(\boldsymbol{0}) = \frac{1}{1+Rk}$. Hence, a lower bound for the probability of extinction is given by*

$$l := \frac{1}{1 + Rk}. \tag{4.6}$$

We recall that $R = \beta/\gamma$ and k is the degree of the initially infected node. For example, if $R = 0.002$ we get $s_k^* > \frac{1}{1.1} \approx 0.91$; thus, we immediately see that the probability of a minor epidemic is very high.

Note that the so called "probability of extinction" of a branching process approximates the probability of having a minor epidemic in the SIR model.

Indeed, since the population is fixed and acquired immunity is permanent, the epidemics always end in finite time, so the epidemics end with extinction of the disease with probability 1*.*

For this reason, in the following we refer to probability of having a minor epidemic as the probability of extinction of a branching process, to avoid misleading in the reading.

Remark 6. *In [132], the author analyses a more general setting, keeping the recovery rate generic in the form of a function $\gamma(\cdot)$ before specialising it for the numerical simulations. Our construction from (4.3) on-wards could be generalised as well to consider infectious periods that follow laws more realistic than the geometric distribution, which we use throughout our analysis in this chapter.*

In order to see if the probability of having a minor epidemic is 1 or lower, we can resort to R_0, the spectral radius of the $N \times N$ matrix M, whose elements m_{jk} are the expected number of infected of type j generated by an infected of type k. This is easy to compute, conditioning on the number of neighbours:

$$\begin{aligned} m_{jk} =& \mathbb{E}\left(\mathbb{E}(\text{infected of type } j \mid k_j \text{ neighbours of type } j)\right) \\ =& \mathbb{E}\left(\frac{k_j R}{R+1}\right) = \frac{k q_j R}{R+1} = \frac{R}{R+1}\frac{k j p_j}{\sum_{l=1}^{L} l p_l}. \end{aligned}$$

Notice that M is a matrix of rank 1; hence, its spectral radius is easy to compute. From $Mv = \rho v$, we obtain

$$\sum_{k=1}^{L} m_{jk} v_k = \frac{R}{R+1}\frac{j p_j}{\sum_{l=1}^{L} l p_l}\sum_{k=1}^{L} k v_k = \rho v_j.$$

Since exists $C > 0$ such that $v_j = C j p_j$, thus

$$C\frac{R}{R+1}\frac{j p_j}{\sum_{l=1}^{L} l p_l}\sum_{k=1}^{L} k^2 p_k = C\rho j p_j,$$

which implies

$$\rho = \frac{R}{R+1}\frac{\sum_{k=1}^{L} k^2 p_k}{\sum_{k=1}^{L} k p_k}.$$

This is exactly the expression in (4.2).

4.4 The stochastic model

We build a network following the CM algorithm[2], choosing $k_{\min} = 1$, and fixing $N = 10000$; $k_{\max}$ then varies with α as described by

$$k_{\max} = \lfloor k_{\min} N^{\frac{1}{\alpha - 1}} \rfloor.$$

[2] All the codes and additional data are available on `https://github.com/SaraSottile/StochasticSIRnetwork`. Animations of sample simulations with different rates are available at `https://www.youtube.com/playlist?list=PLdDHYeVsbaLUY7-9gt9F01JEgIFm8D09m`

We focus on the interval $2 \leq R_0 \leq 3$. The value of R_0 varies with the parameters $\alpha \in [2, 3)$, which is the most commonly used interval for the power-law and $\beta \in [0.002, 0.619]$, following (4.2). First, we consider five couples of values for the parameters α and β, and we compare the behaviour of the epidemics with different numbers of initially infected nodes. Later, we expand the spectrum of parameters taking into account ten values for each. It should be noted that the recovery rate γ has been fixed to $\gamma = 1$, without loss of generality, since this amounts to a rescaling of the chosen time unity by γ. In particular, notice that this implies that all the times in our simulations have been rescaled by that same factor γ. Depending on the disease, it would be necessary to multiply those times by the average recovery period to obtain a result in days.

The simulation algorithm implements a specialised version of the Gillespie algorithm [134], which drastically reduces the simulation times compared to the standard implementation.

In the case of the SIR model, we have two kinds of events. In the standard chemical reaction network notation, these are the following: $S+I \xrightarrow{\beta} I+I$, which is a second-order reaction since it requires two connected individuals, one in the susceptible state and one in the infected state to happen: this results in the infection of the susceptible individual with probability β; and $I \xrightarrow{\gamma} R$, which is a first-order reaction since it happens at a node level. The standard implementation of the algorithm would require $2m + N$ reactions; recall that m is the number of edges in the graph and N is the number of nodes. This computational overhead can be prohibitive for a large scale analysis.

The main difference in our implementation is in the computation of the second-order reaction propensities: on a network, the number of possible infection events is given by the number of edges that connect the susceptible and infected nodes in the network. By exploiting this fact, our algorithm computes the propensity of the second-order reactions as the product of the number of these edges and the reaction rate constant β. This simplification drastically reduces the simulation times in comparison to a direct encoding.

In each simulation, we recorded the *peak of infected* nodes and the number of *eventually infected*, that is, the total number of recovered at the end of the epidemic with $I = 0$ in the SIR model. For each combination of values α and β, we simulated the epidemic 100 times, and we computed the mean of the aforementioned epidemic indices as depicted in Figures 1. With 100 simulations for each pair, the largest coefficient of variation which can be found (namely, the one computed for the eventually infected in the random case) is $CV_{\max} = 8,71$; the mean of the CVs in the random case is $2,273$, while in all the other settings it is close to 1.

4.4.1 Comparison between different numbers of initially infected nodes

We first considered as separate cases epidemics with three different values of initially infected nodes, namely $I(0) = 1$, $I(0) = 5$ and $I(0) = 10$, with four possible initial positions in the network: hub, meaning a node whose degree is in the tail of the distribution; mean degree; peripheral, meaning a node with a low degree; and randomly

chosen. In this section, we illustrate how changing the position of the initially infected node influences the dynamics of the spread of the disease on a network. Indeed, when the first infected nodes are on the periphery, the epidemic is diffusing slowly compared to the case in which the epidemic starts in a node with more contacts, as shown in Figure 1 for the greatest value of the parameter β. The random case is qualitatively intermediate between the peripheral case and the mean-degree case: this follows from the distribution of the degree of nodes in the network since we have few nodes in the tail of the distribution (hub). The resulting numbers of infected nodes do not change significantly between the $I(0) = 5$ and $I(0) = 10$ cases, depicted in Figure 1 by green and blue lines, respectively, suggesting a saturation effect even for a small number of initially infected nodes (compared to the total population). Moreover, in the random, mean-degree and peripheral cases, the numbers of infected nodes (both simultaneously and eventually) increase as the initial number of infected nodes grows.

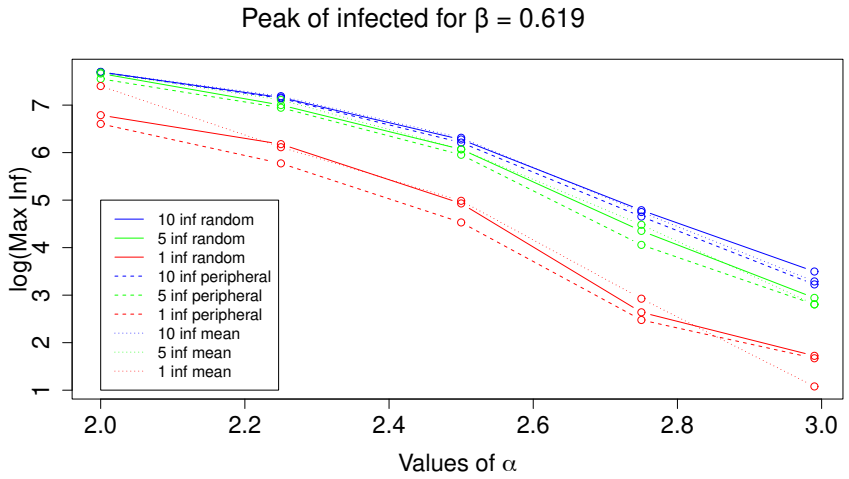

(a) Log-plot of the average of the peak of infected nodes, comparing different numbers of initially infected nodes and their positions.

The hub case, shown in Figure 2, deserves particular attention: as expected, the epidemic spreads more with an increase in β and less with an increase in α; recall that a greater α indicates an overall less connected network. Moreover, the more central the initially infected node is, the more the disease can spread through the network and more so with higher numbers of initially infected nodes. This is because the higher number of initially infected nodes, the smaller the probability of *all of them* being in a hub, disconnected from the giant cluster, except for the greatest value of β. This behaviour can be explained in two distinct ways: firstly, the positions of the initially infected nodes are assigned in a "hierarchical manner". That is, since the hubs live in the tail of the power-law distribution, the second infected node inserted in the network has a degree lower than the first one. Secondly, if two neighbouring nodes are surrounded by several infected ones, they will be infected and they will recover approximately simultaneously.

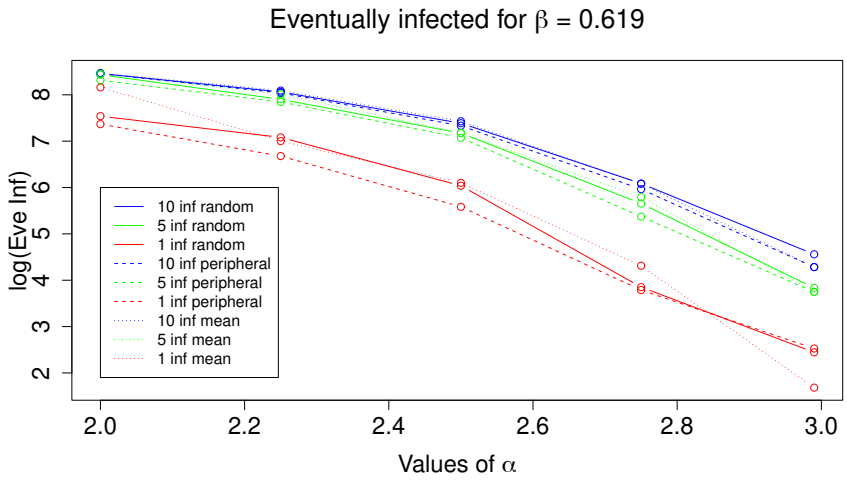

(b) Log-plot of the average of the eventually infected nodes, comparing different numbers of initially infected nodes and their positions.

Figure 1: Comparison of the effect of taking different numbers of initially infected nodes in different positions on the average peak or the average number of eventually infected nodes. The hub case is analysed in greater detail below. Solid line: random case. Dashed lines: peripheral case. Dotted lines: mean case. Blue: 10 initially infected individuals. Green: 5. Black: 1.

This, in return, will create a saturation in the number of available susceptible nodes.

The hub case is a "worst case scenario": the epidemic spreads even if it starts from only one infected node, if it has enough strength in terms of its parameters to do so. Moreover, it is very unlikely that more than one infected node enters a susceptible population *simultaneously*. Hence, in the next section, we analyse the hub scenario with $I(0) = 1$ in greater detail.

Furthermore, we observe a pattern in the final time in Figure 2c, which can be explained as follows: for lower values of β and greater values of α the epidemic does not take off. On the other hand, for greater values of β and lower values of α the epidemic quickly goes to extinction because it starts from a node or nodes with more connections. The noise in the final time, compared to the other quantities, is to be expected since the final part of the epidemic is a subcritical branching process, characterised by variability in its duration [152].

4.4.2 Comparison between different positions of one initially infected node

In this section, we expand the analysis above on Figure 3 to a broader setting. Recalling equation (4.2), the higher values of β correspond to higher values of R_0, thus causing a greater spread of the epidemic for fixed values of α. The opposite is true for α: greater

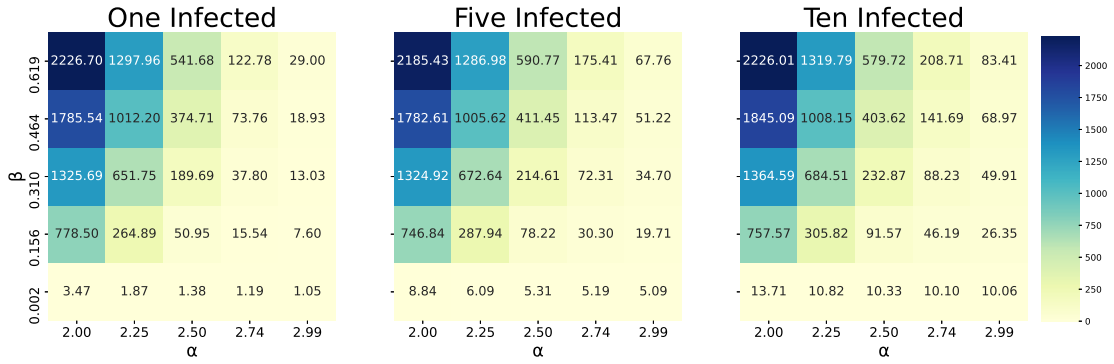

(a) Peak of infected nodes.

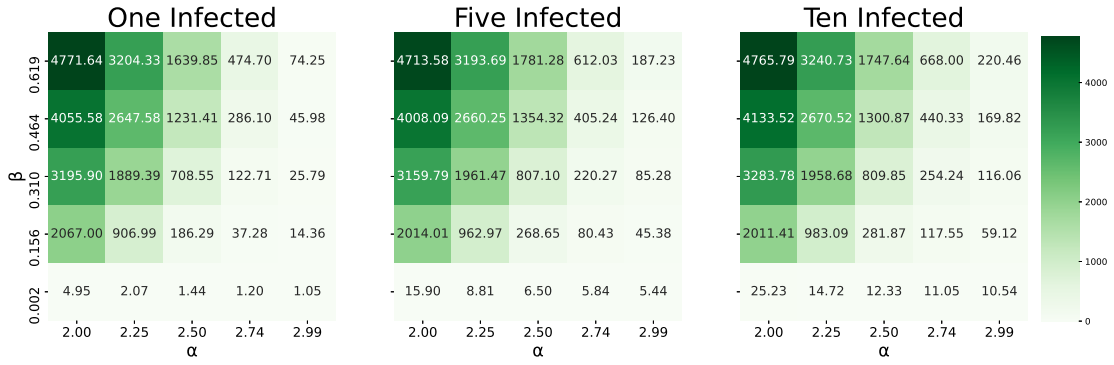

(b) Number of eventually infected nodes.

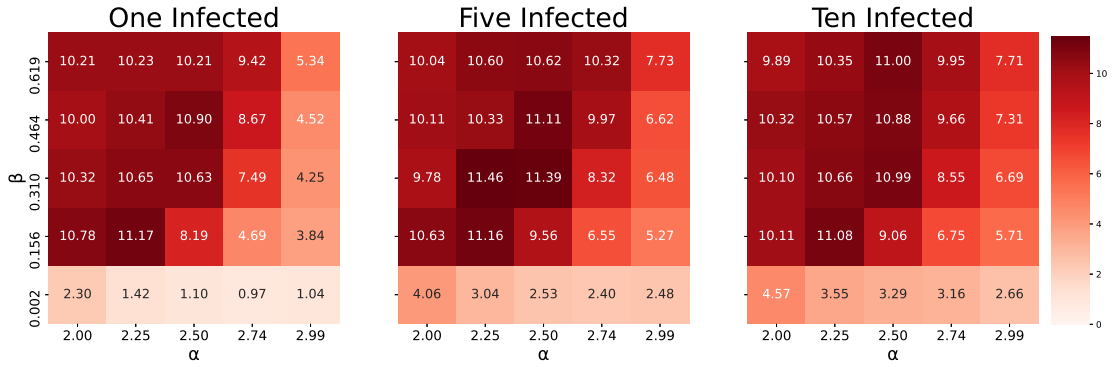

(c) End time for the epidemic.

Figure 2: Comparison between different numbers of initially infected nodes in the hub-degree.

values of α mean a less connected network, which impairs the spread of the disease as it can be noticed in Figure 3. However, it is less evident from equation (4.2) that greater values of α imply smaller values of R_0. In this regard, our simulations confirm

the intuition and what was known in the literature [141].

The more central and connected the initially infected node is, the greater the magnitude of the spread, as the heatmaps labelled "hub", "mean degree" and "peripheral" illustrate; the "random" heatmaps give, qualitatively, an average of the other three. The only quantity which remains noisy is the final time, visualised in Figure 3c. For the "hub node" initial position, the tendency is the same as in Figure 2c. However, in the other cases, the behaviour in the measurements follow a similar trend, i.e. values decreasing with α and increasing with β due to the weakness of the disease together with the effect of the initially infected node positions.

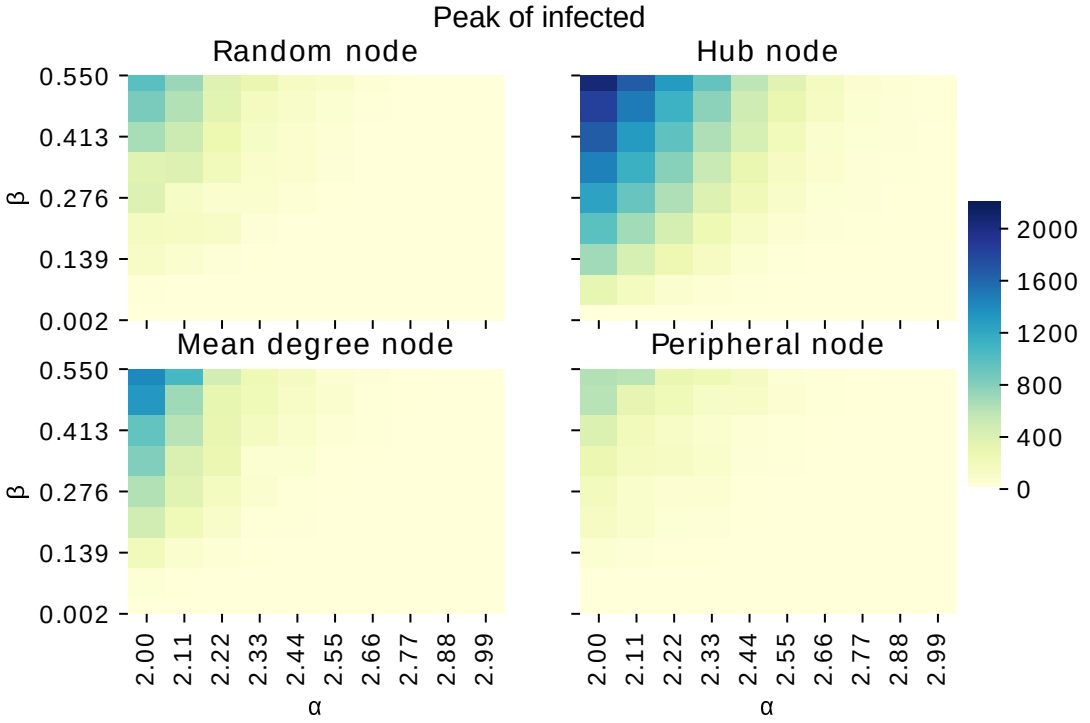

(a) Peak of infected nodes.

4.4.3 Analytical vs. stochastic "hub case"

In this section, we verify our stochastic model with respect to the analytical results in Section 4.3, for the case where the infection starts from a hub of the network. The first infected node is chosen as the node with the maximum degree in the network and the degree is inversely proportional to α: this follows from expression (4.1).

We considered 100 stochastic simulations for each pair of parameters α and β. For each choice of these parameters, we evaluated the probability of a minor epidemic using the analytical derivation in Section 4.3 for a branching process. We denote this with $\mathbb{P}_{\text{ext}}^{\alpha,\beta}$. Note that for the stochastic simulations there is no formal definition of *a minor*

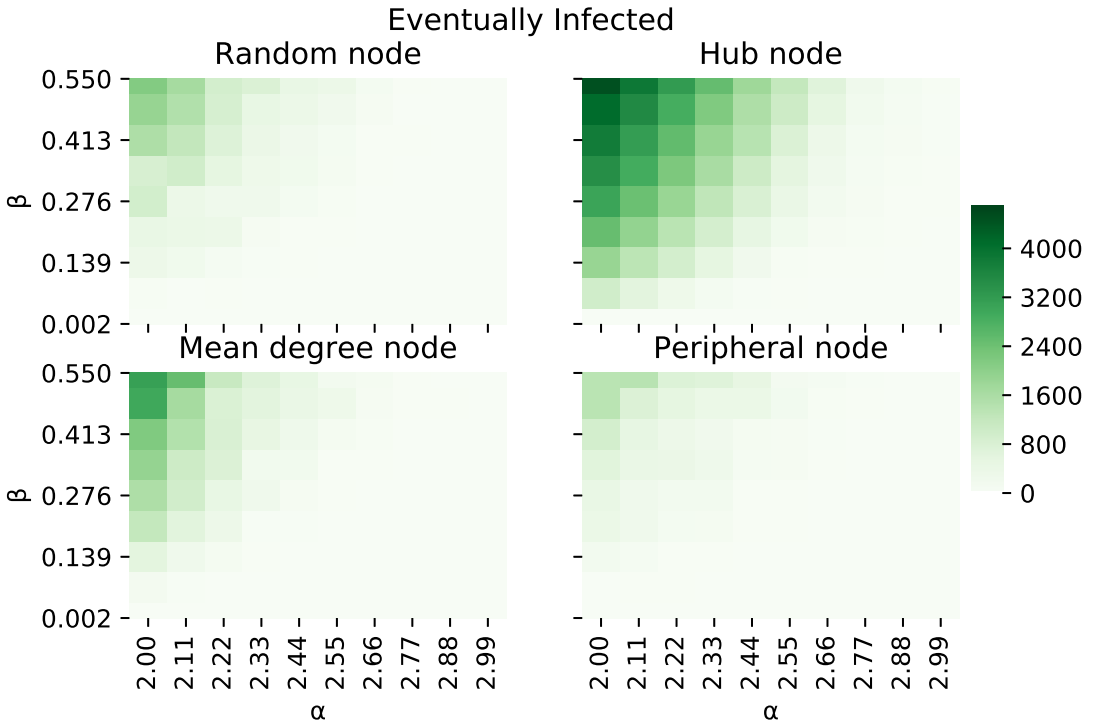

(b) Number of eventually infected nodes.

epidemic. We thus considered different threshold values to have a small number of eventually infected nodes. The thresholds considered in this study are 1, 2, 3 and 4 nodes, which represent epidemics that do not take off.

After collecting the simulation data, we obtained the probability of a minor epidemic for each pair of parameters (α, β) for the four different thresholds. Since we ran 100 simulations, we normalised the results to have a probability measure such that, in the notation $\mathbb{P}_{\text{stoc}}^{\alpha,\beta,T}$, T is the value of the chosen threshold. We then computed the difference between the simulation data (for each threshold) and the analytical probability of a minor epidemic. With $T \in \{1, 2, 3, 4\}$, we compute

$$\text{diff}(\alpha, \beta, T) = \mathbb{P}_{\text{stoc}}^{\alpha,\beta,T} - \mathbb{P}_{\text{ext}}^{\alpha,\beta}.$$

Since we consider 10 different values for each of the parameters α and β, we obtained 100 values of $\text{diff}(\alpha, \beta, T)$ (for each threshold T).

In order to choose the "best threshold value", we computed the mean and the standard deviations for all the datasets $\{\text{diff}(\alpha, \beta, T)\}_{\{\alpha,\beta\}}$. From Table 1, we can observe that the best agreement is with the threshold $T = 3$.

After choosing the threshold to define a minor epidemic, we compared the analytical and simulation results to verify our model. This comparison is depicted in Figure 4. The simulation results are in good agreement with the analytical results, especially for

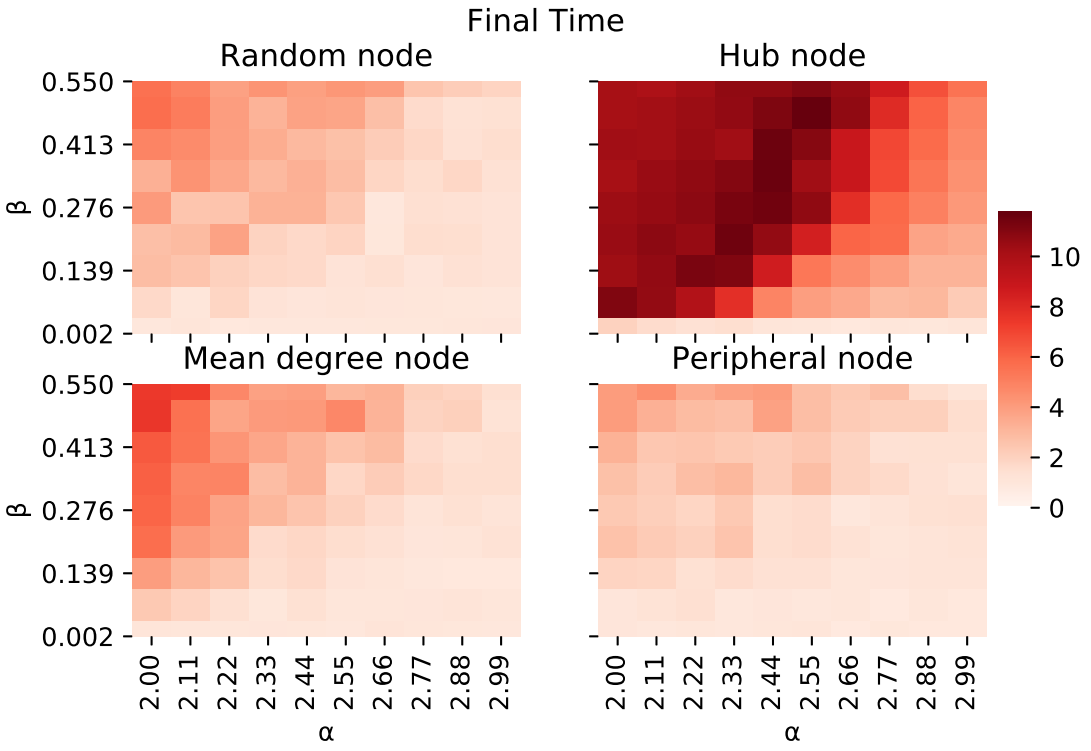

(c) End time for the epidemic.

Figure 3: Comparison between different position of one initially infected node. (a) Peak of infected individuals; (b) eventually infected nodes, the size of the removed compartment at the end of an epidemic that starts with one infected individual in an otherwise susceptible population; (c) end time of the epidemic where we observe more noise.

	Threshold 1	**Threshold 2**	**Threshold 3**	**Threshold 4**
Mean	-0.06	-0.02	0.00	0.02
Sd	0.09	0.05	0.04	0.05

Table 1: Mean and Standard deviation of the difference between the stochastic simulations and analytical results.

the smallest values of the transmission rate β; in the other cases, the results differ no more than the 3%. This behaviour can be explained by the fact that *theoretically* we consider a network with an infinite number of nodes, but *practically* we use a finite network with a large number of nodes. In Figure 4. we compare, for the probability of a minor epidemic, the analytical value (blue) obtained in Section 4.3 with the stochastic realisations (black) by simulations. For each (α, β) pair, we performed 100 simulations.

We observe that for the smallest value of β, probability of a minor epidemic seems to be almost independent of the connectivity of the network. Moreover, when $\beta = 0.002$, even in the cases where the epidemic does not immediately die out, the number of eventually infected individuals in each of the 100 iterations does not exceed 15. However, when the transmission rate increases, the probability of having a minor epidemic increases for greater values of α. This behaviour can be noted also in Fig. 3b ("Hub node").

Remark 7. *The probability of a minor epidemic, even in the analytical case, depends on the degree of the initially infected node chosen as the "hub node". However, even though the value of the maximum degree of each network follows (4.1) (and thus it should decrease with α) when the networks are simulated, the degree k_{max} is rarely reached. Therefore, the degree of the hub node is not monotonic with α, and the blue bars are accordingly sometimes not monotonic.*

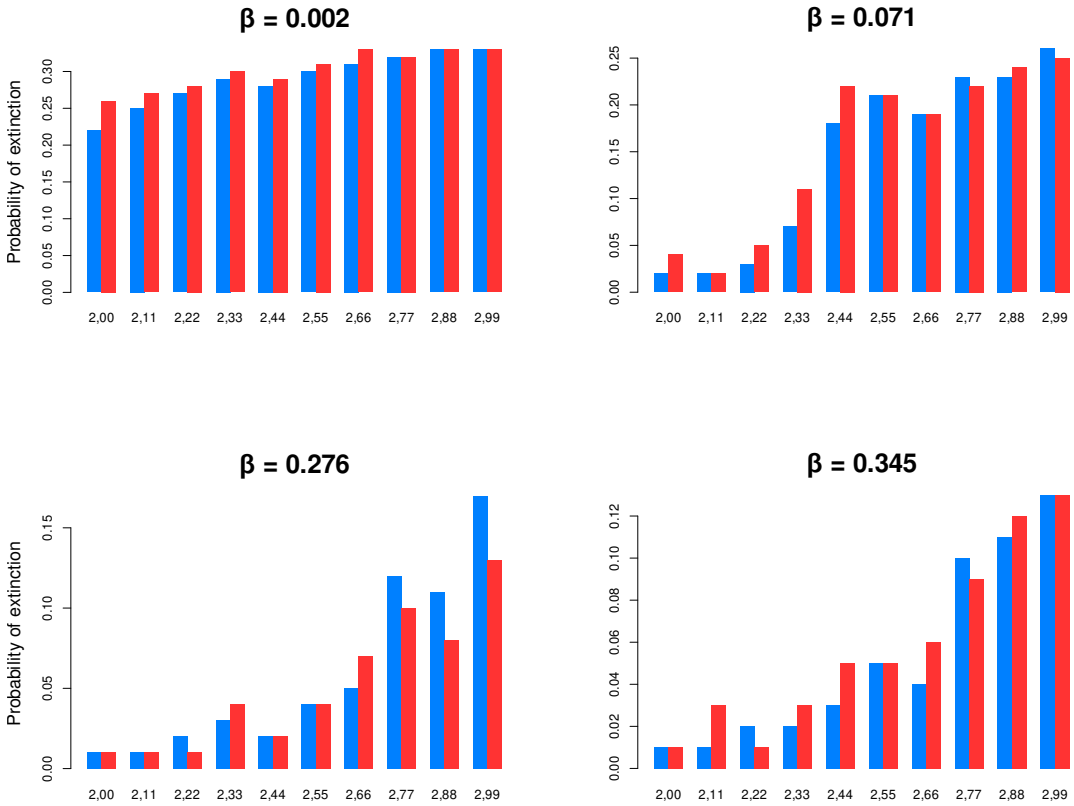

4.5 Summary and Outlook

We have shown how an epidemic affects a synthetic network, following a cut-off power-law distribution for the degree of the nodes through the use of the configuration model.

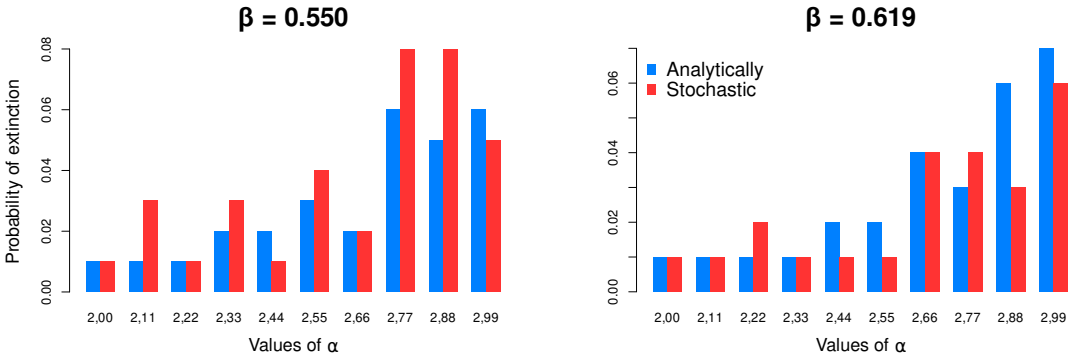

Figure 4: Comparison between stochastic (red bars) and analytical (blue bars) results on the probability of having a minor epidemic of the epidemics, as functions of α and β. The height of each blue bar comes from formula (4.5), whereas the red bars are obtained by counting the number of simulations with less than 3 eventually infected individuals and dividing that number by 100, which is the amount of simulations produced for each couple (α, β) considered.

We provided an analytical result on the probability of minor epidemic of the infectious disease, which is based on the initial condition of the network and the degree of the initially infected node. Our analytical results and stochastic simulation results are in good agreement; the gap in the values stems from the fact that we have considered an infinite network in the analytical framework, and a finite network, yet with a large number of nodes, in the stochastic one.

We have analysed various possible initial conditions for the networks we simulated and compared them with the available analytical insight. In particular, we explored how the positions of the initially infected individuals influence the whole epidemic, measured through three indices: eventually infected individuals, peak of infected individuals and overall duration of the epidemic. Our analysis and numerical exploration confirm that the infectiousness of the disease is directly proportional to the spread of the epidemic; moreover, we conclude that the same disease (i.e., characterised by the same parameters β and γ) infects more individuals in networks generated with a lower exponent power-law, as one would expect intuitively.

We have simulated the epidemic as an SIR model on a network with stochastic dynamics using a specialised and computationally less expensive version of the Gillespie algorithm. Our algorithm is versatile; many different additional features can be implemented, for example, dynamics edges, contact tracing, quarantine. Other generalisations of this work may regard the use of a different model for the epidemic process, e.g. considering a disease in which recovered individuals lose their immunity after a certain period of time (i.e., a SIRS model) or a disease in which there are different types of infected individuals. Moreover, it could be interesting to analyse different structures of the networks, studying how the geometry of the graph may affect the dynamics which occurs

on it.

Other topics which we leave for further investigation include choosing the initially infected nodes based on different centrality measures such as betweenness, percolation centrality [153], eigenvector centrality, random walk centrality, and compare the outcomes in the these settings. A thorough comparison of different centrality measures would highlight the prevalent one in the transmission of infectious diseases in populations modelled by a scale-free network of contacts.

5. Economic evaluation of the introduction of the live attenuated influenza vaccine (Fluenz Tetra®) in the Italian paediatric population (2-6 years)

5.1 Introduction

Many European countries, including Italy, have flu vaccination programs targeting the elderly and people with specific health conditions [154]. These programs aim to offer direct protection to those who are at the highest risk of complications. Some European countries, including the UK and Finland [50, 155], have extended their flu vaccination programs to healthy children. From the 2020/2021 season with the COVID-19 pandemic, the Ministry of Health has recommended influenza vaccination in healthy children aged 6 months - 6 years, also to reduce the circulation of the influenza virus among adults with a risk condition and the elderly [156].

The offer of influenza vaccines in pediatric age (starting from 6 months of age) is currently limited to the use of two vaccines: the quadrivalent vaccine produced on standard dosage eggs (QIVe - *egg-based Quadrivalent Influenza Vaccine*) and the quadrivalent vaccine produced on standard dose cell culture (QIVc - *cell culture-derived Quadrivalent Influenza Vaccine*). In Italy the live attenuated quadrivalent vaccine (LAIVq - *Laive attenuated influenza vaccine quadrivalent*) is also authorised, but until the 2020/2021 season it had never been marketed. The LAIVq vaccine is administered by intranasal spray with one spray per nostril and is authorised for use in Italy in people aged 2 to 18 years. By mimicking natural infection, but without causing disease or subsequent transmission, LAIVq provokes both a humoral and cellular immune response [157].

Considering the current COVID-19 pandemic and the problems related to the supply of flu vaccines, LAIVq was distributed and used in some Italian regions in the 2020/21 season, in order to meet the increased regional demand. It was given to children between 2 and 6 years and, later, also to children and adolescents from 6 to 18 years [158]. Fur-

thermore, in analogy to what is already in place in some countries [159] which considered the protection provided by the first dose of LAIVq vaccine adequate, also in Italy during the 2020/21 season a single dose was administered in children never vaccinated against influenza under 9 years of age [160]. This choice was made considering the studies available in the literature [161, 162] and to allow optimisation of the vaccine offer considering the shortage of influenza vaccines recorded during the 2020/21 season.

In Italy, the data relating to the epidemiology of the different flu seasons tell us that the epidemic curve generally reaches its peak at the beginning of February, affecting mainly the paediatric population (0-4 and 5-14 years), with an incidence that decreases with increasing age [163]. The European Centre for Disease Control (ECDC) estimates that, on average, around 40,000 people die prematurely each year from influenza in the European Union. 90% of deaths occur in subjects over the age of 65, especially among those suffering from chronic clinical conditions and Italy is no exception in this sense [164]. Although in the 2014/15 and 2016/17 seasons, an excess mortality rate attributable to influenza of $1.05/100,000$ and $1.54/100,000$ respectively was observed in children under the age of 5 [165].

Among healthy children, the flu is generally a self-limiting and uncomplicated illness. However, it can be associated with severe morbidity and mortality in healthy children and in certain groups of children and adults who are at increased risk for severe or complicated influenza illness. Influenza causes an appreciable burden of disease (e.g. absence from school and work, increased frequency of outpatient medical visits) and children are important vectors for the spread of the disease.

To assess whether the benefits of the LAIVq vaccine justify the additional costs, economic assessments, such as cost effectiveness analysis (CEA), are essential to support decisions about the allocation of available health care resources.

Evaluations of the cost-effectiveness of health interventions are model-based. Such evaluations play an important role in allocating scarce health resources [166] and the choice of an appropriate model is crucial to arrive at valid cost-effectiveness results [54, 55]. The most used models are decision tree models and Markov models [167, 168, 169]. These models assume that the likelihood of disease exposure is not affected by an intervention against it, and therefore the likelihood of disease exposure does not change over time. This assumed constant probability of exposure is realistic for non-communicable diseases and can be modelled with so-called static models. For communicable infectious diseases, the independence between disease exposure and interventions is not realistic and another class of models is needed. Interventions against communicable diseases not only reduce the likelihood of the individual being treated developing the disease, but also reduce exposure of others to the infection. Models that consider these nonlinear transmission effects over time such as dynamic models are therefore preferable. Nonlinearity arises because the likelihood of infection in susceptible individuals depends on the number of infected individuals. The best known dynamic model for the spread of infection is the SEIR (Susceptible - Exposed - Infectious - Removed) model [170, 171]. For this reason, we performed a cost-effectiveness analysis of paediatric influenza vaccination using a SEIR-type dynamic transmission model to evaluate the cost-effectiveness

of introducing the LAIVq vaccine in Italy in children aged from to 2 and 6 years.

Objective of the study

The general objective is to estimate the economic profile of the introduction in Italy of the LAIVq vaccine in children aged between 2 and 6 years through a cost-effectiveness analysis (CEA - Cost-Effectiveness Analysis) adopting the guidelines for the Economic Evaluation Reporting CHEERS (Consolidated Health Economic Evaluation Reporting Standards Statement) [172].

5.2 Methods

5.2.1 Transmission model

Influenza transmission was simulated using a deterministic SEIR model, already developed for previous cost-effectiveness evaluations [173, 174] to calculate the attack rates of confirmed seasonal influenza infection by age group and viral subtype in the seasons considered.

The total population N is divided into 85 age classes, such that $N = \sum_{a=0}^{85} N_a$. Each class represents one year of life, with the exception of the last one that includes individual with an age of ≥ 85 years old. The population is then partitioned into four compartments, namely S, E, I, R, which represent the fraction of Susceptible, Exposed, Infected and Recovered individuals, respectively, such that $N_a = S_a + A_a + I_a + R_a$, where $a = 0, \ldots, N$.

The infection can be transmitted to a susceptible through a contact with infectious individual, at rate β. Contacts between individuals of different classes are described by a contact matrix, denoted by C. All susceptible individuals, once infected, enter in an exposed state, indicating a pre-symptomatic state of individuals who will become symptomatic. However, unlike other compartmental models, we assume that the susceptibility to the disease depends on the age class, denoted by ρ_a, $a = 0, \ldots, 85$. From the exposed compartment, an individual progress to the class of infectious $I\Pi$, at rate δ. An infected individuals can recover at a rate γ. Since our model has been applied to short period of time, i.e. one influenza season, we assume that the recovered individuals obtain a permanent immunity.

The aforementioned transmission model is described by the following system of ODEs.

$$
\begin{aligned}
\frac{dS_a(t)}{dt} &= -\beta\rho_a S_a(t)\sum_{a'=0}^{85}\frac{C_{aa'}I_{a'}(t)}{N_{a'}(t)},\\
\frac{dE_a(t)}{dt} &= \beta\rho_a S_a(t)\sum_{a'=0}^{85}\frac{C_{aa'}I_{a'}(t)}{N_{a'}(t)} - \delta E_a(t),\\
\frac{dI_a(t)}{dt} &= \delta E_a(t) - \gamma I_a(t),\\
\frac{dR_a(t)}{dt} &= \gamma I_a(t), \qquad\qquad a = 0,\dots,85,
\end{aligned}
\tag{5.1}
$$

with initial conditions take as follow. The model season starts with $I(0) = 10$ infected individuals, choosing randomly in the population. The vaccination campaign is administrated before the epidemic season starts, thus the initial number of recovered people is $R_a(0) = \varepsilon c_a N_a(0)$, for all $a = 0,\dots,85$, where ε denotes the effectiveness of the vaccine and c_a is the age-related coverage. Lastly, $S_a(0) = N_a(0) - I_a(0) - R_a(0)$, for all $a = 0,\dots,85$.

The susceptibility and immunity of the Italian population to infection have been defined with respect to the strains circulating in the last 10 years for the A/H3N2 and B viruses and starting from serum epidemiological investigations carried out before and after the appearance of the A/H1N1pdm09 subtype [175].

The model allows for the development of an influenza epidemic every season and has been calibrated on the data of laboratory-confirmed influenza cases in Italy [176] and on the number of influenza-like syndromes reported to the Sentinel Surveillance System for influenza-like syndromes (INFLUNET) sentinel doctors (general practitioners and paediatricians of free choice) participating in surveillance for 10 seasons (2010/11 – 2019/20, excluding the 2009/2010 pandemic season) [177].

Furthermore, the efficacy of both LAIV and eQIV influenza vaccine have been drawn from the international scientific literature and through the indications coming from [59, Chapter 10].

The dynamic model developed made it possible to simulate an average influenza season based on historical data from ten previous influenza seasons and was used to study the number of infections, clinical outcomes and the cost-effectiveness of the existing vaccination strategy compared to a strategy where in healthy children aged 2-6 years vaccination coverage of 40% is achieved using the live attenuated qLAIV vaccine. We have considered that the programming for the flu vaccination campaign, both at the national and regional level, is carried out annually and therefore we have adopted a time horizon of one flu season.

Simulated infection outcomes (symptomatic and non-symptomatic) were converted into physician visits, hospitalisations and deaths using age-specific probabilities of outcome. Thereafter, the clinical results served as input for the economic analysis which estimates the cost and loss of quality-adjusted life years (QALYs). As recommended by the World Health Organization (WHO) [178] and the Consolidated Health Economic

Evaluation Reporting Standards (CHEERS) guidelines [172] the analysis was conducted from both the "Servizio Sanitario Nazionale (SSN)", i.e. the Italian National Health System, perspective (direct costs) and in the broader perspective of society (direct and indirect costs). Costs and QALYs were discounted to the 2020 season value using a 3% discount rate [179].

The intervention was considered cost-effective for an ICER value $<$ €30,000/QALY [173, 174, 180, 181] in both perspectives considered.

5.2.2 Scenarios assessed

The current flu vaccination program offers free vaccination to all people aged $\geq$ 65 and people aged $<$ 65 with certain health conditions using different types of vaccines [156]. From the 2020/2021 season, with the COVID-19 pandemic, the Ministry of Health has recommended influenza vaccination in healthy children aged 6 months - 6 years, recommending the use of the eQIV vaccine (from 6 months), cQIV (from two years) and LAIVq vaccine (from 2-17 years). The data relating to vaccination coverage by age group in the various seasons under study were taken from the Ministry of Health [182].

In the basic scenario we considered the vaccination of the population with the eQIV vaccine in all age groups, while in the alternative scenario we considered the introduction of the qLAIV vaccine, administered intranasally, in healthy children aged between 2 and 6 years. Vaccination coverage in healthy children between 2 and 6 years in the alternative scenario was assumed to be 40%; whereas such coverage in this age group would be easily achievable at national and regional level.

5.3 Model data

5.3.1 Transmission model

The data used for the dynamic transmission model are available in Table 1 and in [173, 174, 175].

In short, the deterministic transmission model was constructed with demographic data by age group [183] and sex and the social contact structures by age and sex [184] of the Italian population. The model, constructed in this way, on the basis of data from the epidemiological and virological surveillance system of Influenza in Italy (InfluNet) (in the post-pandemic period, from the 2010/11 season to the 2019/20 season) [177] and from studies Italians of serum epidemiology on the A/H1N1pdm09 virus before and after the pandemic season, allows us to estimate the number of cases of influenza confirmed in the laboratory, season by season. The eQIV vaccine field efficacy estimates considered, both by age and by viral subtype, were drawn from data published in recent systematic reviews and meta-analyses [51, 185, 186]. Recent field efficacy studies comparing the efficacy between qLAIV and the eQIV vaccine have found equivocal results [187, 188, 189], while a randomised clinical trial found no differences between LAIV and the community-wide inactivated influenza vaccine [190]. Therefore, we hypothesised a similar efficacy of Q-LAIV and eQIV.

Parameters	Values				Notes
Number of age classes	86				85+ are considered in the same class.
Population	2018				ISTAT 01/01/2019.
Contact Matrix	86x86 matrix				-
Coverage	**Age class**	**Percentage**			In the alternative strategy the coverage in the 2-4y and 5-8y is increased to the 40%.
	6-23m	1,70%			
	2-4y	3,10%			
	5-8y	2,50%			
	9-14y	1,80%			
	15-17y	2,20%			
	18-44y	2,60%			
	45-64y	8,90%			
	65+y	54,60%			
Effectiveness	**Age class**	**H1N1**	**H3N2**	**B**	In the alternative strategy the effectiveness in the 2-6y is increased to the 80% for each strain.
	0.5-1y	69%	43%	67%	
	2-6y	69%	43%	67%	
	7-17y	73%	35%	77%	
	18-64y	73%	35%	77%	
	65+y	62%	24%	52%	

Table 1: Characteristics of the main parameters used for in the dynamic transmission model.

5.3.2 Probability of outcome

The likelihood of symptomatic infection given the infection and subsequent General Practitioner (GP) or Emergency Room (ER) visit by age group was obtained from the scientific literature [191, 192, 193]. Influenza hospitalisation rates by age group were collected from the same studies [192, 193]. Influenza-related mortality was estimated using the fraction of all-cause deaths associated with influenza [165]. All the above estimates were drawn from national data. All the probabilities relating to the natural history of influenza disease have been drawn from the international scientific literature [173, 174].

5.3.3 Direct and indirect costs

All the average costs of the previous years were weighted to 2020 using the Italian consumer price index [194]. The total cost per dose administered is €12.31 for the eQIV, including the cost of the vaccine equal to €5.70, based on the average of the latest regional competitions available, and a cost for administration of €6.61. [195]. For qLAIV, the total cost per vaccine dose administered was set at €27.61 corresponding to €20.40 for vaccine costs and €6.61 for administration costs. For the eQIV vaccine it was considered that children aged 6 months <9 years should receive 2 doses, while for the qLAIV vaccine a single dose was assumed to be administered in that age group, in accordance with the recommendations in the UK [159].

Costs related to influenza diseases and related complications were estimated using data from literature and other national sources [173, 174]. The direct health care costs

of influenza include the costs related to GP's visits, which also include prescribed medications and referral to the specialist, and the costs of access to the emergency room and hospitalisation. Indirect health costs (i.e. non-influenza related health costs over life years gained) were also considered. These costs were estimated using the remaining life expectancy at the age of death and the age-specific annual health care cost unrelated to influenza or pneumonia. Productivity losses include costs due to the sick (15-69 years) or care of a sick child (<15 years) from paid work. Productivity losses of premature deaths were assessed using the friction method [196], assuming that absence from work was limited to a friction period of 85 days [197].

5.3.4 Years of life weighted for quality

The *Quality-Adjusted Life Years* (QALY) losses due to influenza diseases are based on international scientific literature [198]. QALY losses due to premature death associated with influenza were estimated using life expectancy at the age of death and quality of life in relation to the health status of the Italian population by age group [199, 200].

5.3.5 Cost-effectiveness analysis

The stochastic transmission model generated 1000 simulated series of 10 consecutive seasons. For each simulation, a set of economic-health parameters was used. Subsequently, simulations of discounted costs and QALY losses over the analysed 10-year period were averaged. The *incremental cost-effectiveness ratio* (ICER) was calculated by dividing the difference in costs between two strategies by the difference in QALY. The vaccination program considered by increasing the paediatric vaccination rate was considered convenient when the ICER was less than €30,000 per QALY earned.

5.3.6 Sensitivity analysis

The replacement of QIVe with qLAIV (in the age group 2-6 years) was subjected to both deterministic (univariate; DSA - Deterministic Sensitivity Analysis) and probabilistic (multivariate; PSA - Probabilistic Sensitivity Analysis) sensitivity analysis. A deterministic and probabilistic sensitivity analysis was also carried out when the sale price of the qLAIV vaccine changed up to €18.00, the price indicated in the most recent regional tenders awarded.

5.4 Results

Table 2 shows the average number of flu cases and complications in a flu season, by hypothesised scenario.

Under the current vaccination program, we estimated an average of 4,955,026 (95% CI 4,954,263-4,955,788) confirmed cases in 1000 simulations; 1,984,083 (95% CI 1,190,450-2,777,716) medical visits and access to the emergency room; 45,167 (95% CI 27,100-63,234) Hospitalisations; and 1576 (95% CI 946-2.206) deaths per year. The introduction

	Cases of confirmed flu		Complicated cases	
	Average	**95% CI**	**Average**	**95% CI**
In the general population				
Basic scenario	4,955,026	4,954,263-4,955,788	1,984,083	1,190,450-2,777,716
Alternative scenario	1,708,786	1,708,325-1,709,248	945.747	567.448-1.324.046
Reduction	3,246,240	3,656,530-6,253,522	1,038,336	623.002-1.453.670
In subjects 2-6 years				
Basic scenario	844.355	843.652-845.057	127413	76,448-178,378
Alternative scenario	212.735	213.754-211.717	38.998	23,399-54,597
Reduction	631.619	378.972-884.267	88.415	53.049-123.781
	Hospitalisations		**Death**	
	Average	**95% CI**	**Average**	**95% CI**
In the general population				
Basic scenario	45.167	27.100-63.234	1,576	946-2.206
Alternative scenario	20,537	12.322-28.752	912	547-1277
Reduction	24,630	14.778-34.482	664	398-930
In subjects 2-6 years				
Basic scenario	3,478	2.087-4.869	26	16-36
Alternative scenario	1,064	638-1.490	8	5-11
Reduction	2,414	1,448-3,380	18	11-25

Table 2: Confirmed influenza cases, complicated cases, Hospitalisations and deaths in the target population and in the general population by scenario considered. The data estimates what could happen in a hypothetical next flu season.

of the qLAIV vaccine in children aged 2 to 6 years at 40% vaccination coverage would avoid 3,246,240 (95% CI 3,656,530-6,253,522) symptomatic cases; 1,038,060 (95% CI 623,002-1,453,670) medical visits and access to the emergency room; 24,630 (95% CI 14,778-34,482) Hospitalisations; and 664 (95% CI 398-930) deaths per year. When only the outcomes among children aged 2 to 6 years were considered, the mean reduction was estimated in 631,619 (378,972-884,267) symptomatic cases; 88,418 (53,049-123,781) medical visits and access to the emergency room; 2,414 (1,448-3,380) Hospitalisations; and 18 (11-25) deaths per year. Thus, respectively, 22% and 48% of symptomatic cases were avoided in the target group and in subjects age >18 years, while 40% of deaths were avoided in subjects >65 years.

5.5 Cost effectiveness analysis

Table 3 shows the economic impact and cost-effectiveness of introducing the qLAIV vaccine in children aged between 2 and 6 years with a vaccination coverage of 40% in Italy.

The introduction of the qLAIV vaccine produced an average gain of 33,831 QALYs, of which 93% due to a reduction in complicated cases and 5.5% to the prevention of mor-

	General population		
	Basic scenario	**Alternative scenario**	**Difference**
QALY lost			
- for the disease	16,045	5,495	10,550
- for mortality	2,498	829	1,669
QALY tot. lost	33,831	11,612	22,219
Costs			
Vaccination	196,624,666	215,331,326	-18,706,660
Direct costs	196,624,665	215,331,326	-18,706,661
Loss of productivity	35,748,135	11,526,246	24,221,889
Indirect costs	116,067,084	37,643,010	78,424,074
Total costs	716,660,209	389,634,739	327,025,470
Cost effective			
ICER SSN (euro/QALY earned)			11,189
ICER Soc. (euro/QALY earned)			14,718
	Children 2-6 years		
	Basic scenario	**Alternative scenario**	**Difference**
QALY lost			
- for the disease	3,998	1,516	2,482
- for mortality	71	18	53
QALY tot. lost	5,057	1,274	3,783
Costs			
Vaccination	1,435,204	20,141,864	-18,706,660
Direct costs	1,435,203	20,141,864	-18,706,661
Loss of productivity	1,261,763	317,901	943,862
Indirect costs	na	na	na
Total costs	41,363,072	30,201,695	11,161,377
Cost effective			
ICER SSN (euro/QALY earned)			2,701
ICER Soc. (euro/QALY earned)			2,951

Table 3: Estimation of lost QALYs, costs and ICER for the general population and in the age group 2-6 years by scenario considered.

tality in all age groups considered against a reduction in costs, a total of approximately 327 million euros.

Dividing the average net cost by the average number of QALYs saved results in an ICER of €11,189 per QALY earned for the SSN perspective and €14,718 per QALY earned for the society perspective. When only the outcomes among children aged 2 to 6 were considered, the infant vaccination program resulted in an average gain of 5,057 QALYs, of which 20% was due to the prevention of overall mortality. Average total costs were estimated to rise by 11 million euros, with most of the cost savings due to

productivity losses avoided.

In both perspectives considered, the strategy with qLAIV is cost-effective in the whole population considered, in particular, in children aged between 2 and 6 years it is particularly cost-effective (ICER SSN: €2,701/QALY) and the indirect effects of the alternative strategy on the non-directly treated population are even cost effective dominant.

5.6 Sensitivity analysis

5.6.1 Deterministic sensitivity analysis

The DSA reported in Figure 1 demonstrates that the main drivers of the observed ICER (regardless of the study perspective) are: the total number of infections (and therefore the efficacy of vaccines), the likelihood of complications, Hospitalisations and medical visits.

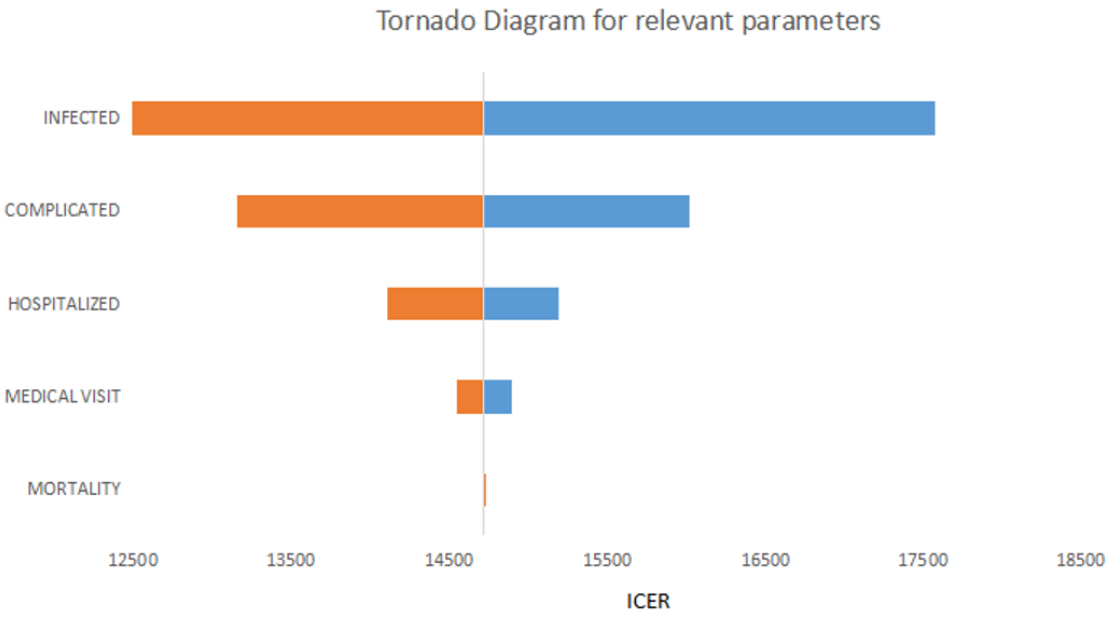

Figure 1: Deterministic sensitivity analysis.

The tornado diagram shows that the risk of infection determines the greatest variability of the ICER (from a lower limit of 12,252 to an upper limit of 17,566) followed by the probability of complications (from a lower limit of 13,154 to an upper limit of 16,013) and the probability of hospitalization (from a lower limit of 14,102 to an upper limit of 15,194).

5.6.2 Probabilistic sensitivity analysis

Figure 2 shows the results of the probabilistic sensitivity analysis using 1000 simulations.

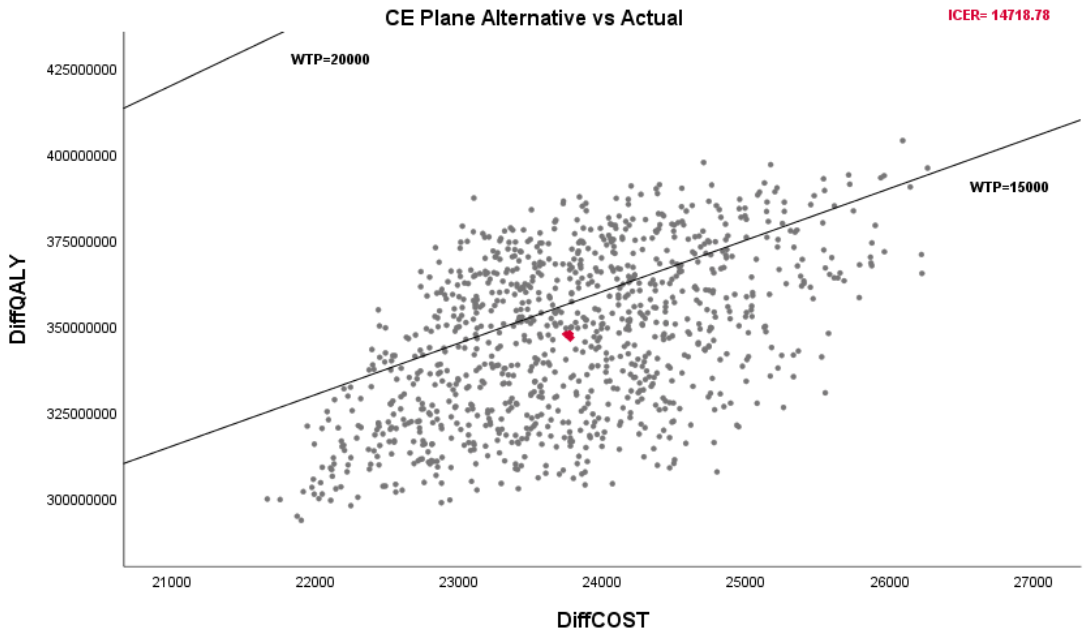

Figure 2: Probabilistic sensitivity analysis from the perspective of society, alternative scenario to the base scenario (the red dot represents the average ICER value).

The cost-effectiveness analysis indicates that the economic impact of the qLAIV vaccination program is also substantial from the societal perspective. Vaccination with qLAIV in 40% of children aged 2 to 6 years was found to be cost effective in 100% of the simulations. Although the cost of vaccination is higher in the alternative strategy (215,331,326 euros) than the current strategy (196,624,666 euros), considering the overall economy over 1000 simulations, the alternative strategy is the convenient option with a lower average cost and greater effectiveness for a willingness to pay of €30,000/QALY in all simulations.

By making the price of qLAIV oscillate between €12.0 and €30.0, the ICER thresholds (SSN perspective) €30,000/QALY are reached, respectively, with a price of €22.5 and €28.0 (Figure 3).

5.7 Discussion

The main results of this modelling study indicate that the introduction of influenza vaccination with qLAIV at 40% vaccination coverage in children aged 2 to 6 years in Italy is convenient for the conventional threshold of €30,000 per QALY both in perspective of the SSN and that of the society.

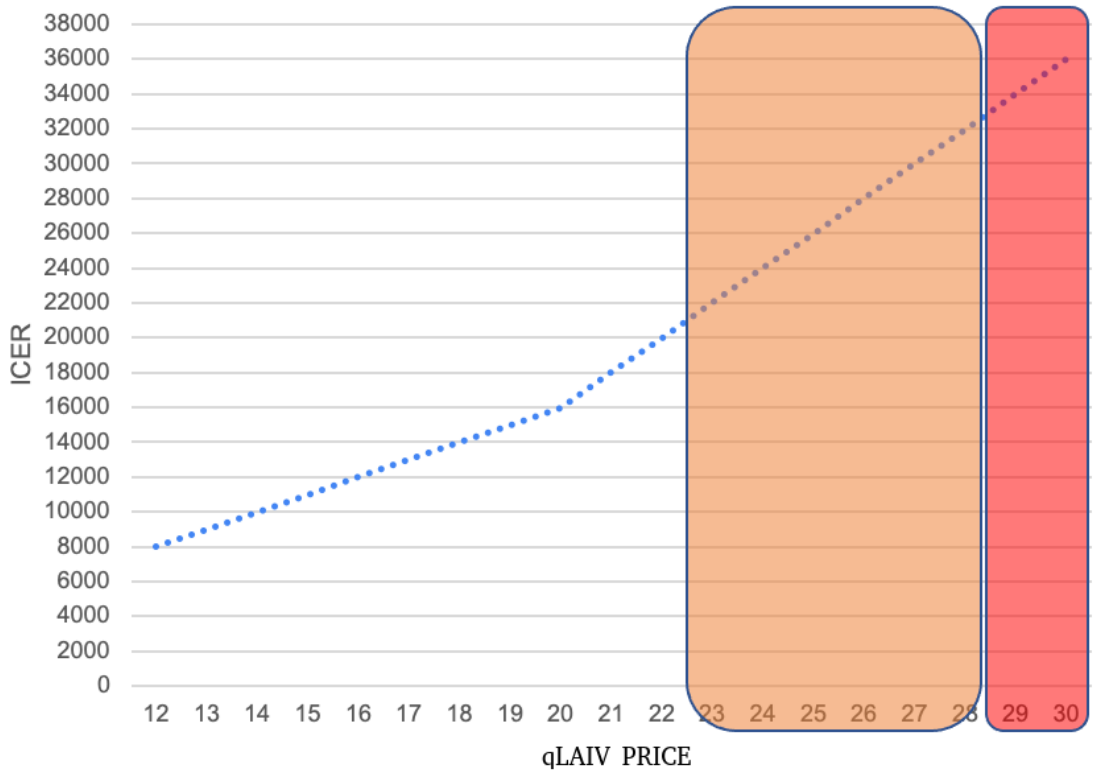

Figure 3: Break-even sensitivity analysis as the qLAIV purchase price changes.

The robustness of the base case was amply confirmed by the sensitivity analyses: qLAIV remains cost-effective (at WTP value <€30,000/QALY) in 100% of the simulations. Although the commercialisation of qLAIV may require some initial investment, from a public health point of view its impact in terms of influenza-related events is particularly significant in the age groups that are not affected by the alternative strategy.

Furthermore, considering that the average award price of the regional tenders was €18.0, we conducted an additional sensitivity analysis to demonstrate that up to a cost of €22.5 the use of the qLAIV vaccine represents a cost effective strategy in Italy.

For cost-effectiveness estimation we used an influenza transmission model that captures the dynamics of the infection, as well as the seasonal variability of epidemic size and vaccine efficacy. Taking these aspects into account is essential for estimating the effects of influenza vaccination programs [201]. The transmission model was calibrated on the number of visits made by sentinel doctors of the INFLUNET surveillance network with flu-like illness in Italy over 10 seasons (from 2010/2011 to 2019/2020) [177]. The result was subjected to an extensive sensitivity analysis, which made it possible to identify the main drivers of the alternative vaccination program considered. In this study, we measured protection against specific types of influenza viruses A and B and subtypes A/H1N1pdm09 and A/H3N2. This approach has been used in cost effective-

ness analyses conducted on other types of vaccinations by applying different scenarios that did not consider paediatric age groups as widely [173, 174]. The effect of including different types and subtypes of influenza is simple when one assumes independence between them. We hypothesised that there is no significant evidence that one type of vaccine is more effective than another and considered substantial efficacy after a single dose in previously unvaccinated children aged 2 to 6 years also in the light of studies published in the literature [161, 162] and of what was decided in the UK [159] and in Italy [160] during the last flu season.

On the other hand, some potential benefits of qLAIV were not considered, such as greater adherence to pediatric vaccination mainly due to the needle-free administration of qLAIV. Several limitations need to be described for this study. First of all we considered a constant vaccine efficacy across different flu seasons and this could affect the results especially in flu seasons for which there is a mismatch between circulating strains and vaccine composition . However, we estimated cost effectiveness in a standard season without considering the potential presence of circulating influenza virus strains other than those contained in the vaccine. We also haven't considered some possible long-term effects of influenza, such as acute respiratory distress syndrome (ARDS) which can cause lifelong disability. However, this complication is rare and its exclusion reflects a conservative approach.

Our results highlight that vaccination against influenza with the qLAIV vaccine in subjects aged 2 to 6 years is consistent with what has been published in the literature in studies conducted in England and Wales and in Germany with a very similar approach to the one used for the present study, which demonstrated the benefits of introducing an extensive vaccination program in children [202, 203, 204, 205].

The results of this study are of direct interest to those involved in public health policies. We expect a childhood flu vaccination program with the qLAIV vaccine to prevent a significant burden of disease in all age groups and be cost-effective for the entire population.

A decision on the introduction of the qLAIV vaccine requires more than a single cost-effectiveness analysis such as considering the acceptability of vaccination [206]. Most of the disease burden prevented by paediatric vaccination is not among those vaccinated but among the elderly through indirect protection. In fact, most of the disease burden prevented thanks to the use of qLAIV in the paediatric population of 2-6 years with a vaccination coverage of 40% was observed above all in the other adult and elderly age groups through the indirect protection guaranteed by the vaccine's strategy.

5.8 Conclusions

The introduction of qLAIV in Italy is highly cost-effective and can represent a valid alternative for the prevention of seasonal influenza in the paediatric population aged between 2 and 6 years. Achieving vaccination coverage of 40% in the age group considered could lead to a decrease in the morbidity and mortality of influenza even in adults and the elderly thanks to the effect linked to the phenomenon of community immunity

(*herd-immunity*). In particular, the qLAIV vaccine represents an important novelty in the panorama of vaccines to be administered in paediatric age also for its ease of use in the medical offices of general practitioners and paediatricians of free choice and for the opportunities it could offer through the administration of a single dose with a net saving both in logistical and organisational terms.

6. An Economic Evaluation of the Adjuvanted Quadrivalent Influenza Vaccine Compared with Standard-Dose Quadrivalent Influenza Vaccine in the Spanish Older Adult Population

6.1 Introduction

Over the last few decades, vaccination has been a successful public health strategy to prevent various infectious diseases worldwide, effectively helping reduce the burden of vaccine-preventable diseases [207, 208]. Influenza is an acute viral infection, highly transmissible, observed around the globe every year, with peak spread during the winter season [209]. Seasonal influenza is a vaccine-preventable disease. Influenza's public health burden can be serious because of high transmissibility, accompanying comorbidities (e.g., pneumonia), and higher mortality, especially among the higher-risk population, such as the elderly [210]. Furthermore, in addition to disease management costs, influenza can have an increased socioeconomic impact due to productivity loses associated with missing work or absenteeism [211].

The clinical efficacy of vaccines against influenza has been improving steadily over the years, e.g., by going from trivalent to quadrivalent vaccines (the latter offers protection against all four viral strains), through the addition of vaccine adjuvants or by increasing antigen concentration [212]. Alongside the increased clinical efficacy, there is a growing amount of evidence on the cost-effectiveness of vaccination strategies against influenza, particularly if improved vaccines are used, such as quadrivalent influenza vaccines (QIV) [210].

Results from a recent modelling exercise across European settings support using enhanced influenza vaccines for the high-risk population (e.g., elderly patients) [213]. Economic modelling studies in Spanish settings have found cell-based QIVs (QIVc) to be

cost-effective compared with traditional egg-based QIVs (QIVe) for adult patients (aged 9-64 years and at high-risk of complications) [214]; furthermore, for individuals aged 65 or older, adjuvanted QIV (aQIV) was cost-saving compared with high-dose (HD)-QIV [209], and adjuvanted trivalent influenza vaccine (aTIV) was found to be cost-effective compared with TIV [215, 216]. Immunosenescence refers to the biological aging process associated with progressive decline in systemic immunity and increased prevalence of autoimmune and chronic diseases, increased vulnerability to common infectious, and poor responses to vaccination [217]. aQIV is indicated for individuals aged 65 years or older. aQIV combines MF59® adjuvant (an oil-in-water emulsion of squalene oil) and a standard dose of antigen, and is designed to produce stronger and longer immune response, especially in the elderly where immunosenescence reduces vaccine effectiveness; compared with younger adults (18-64 years), vaccine effectiveness for the elderly was found to be 27% lower (37% for the elderly versus 51% for younger adults) [218]. Real-world evidence has shown that adjuvanted influenza vaccines results in statistically significantly fewer influenza-related medical encounters compared with non-adjuvanted influenza vaccines [218, 219, 220].

This study used a dynamic transmission model aimed to evaluate the cost-effectiveness of aQIV vs. QIVe in the elderly population (65+ years) in Spain. Given the dynamic nature of the model (i.e., accounting for indirect effect of vaccination), and similarly to several other models [221, 222], the whole Spanish population is included so that herd protection can be accounted for; it has been reported that the indirect effects of vaccination can be more significant than the direct effects [223]. The model is used to project both costs and clinical benefits of competing vaccination strategies for the elderly, from the payer and societal perspectives.

6.2 Materials and Methods

6.2.1 Model structure

The World Health Organization (WHO) guidelines were followed to conduct a cost-effectiveness analysis of the influenza vaccines in the Spanish older adult population [224]. Influenza transmission and burden was simulated by adapting a SEIR (Susceptible - Exposed - Infectious - Recovered) model that was developed previously to evaluate the cost-effectiveness of aQIV in the Italian setting (see e.g. [174, 225]), explained yet in details in Section 5.2.1. The model was structured in two modules: epidemiological and disease burden. The epidemiological module is a dynamic compartment model that allows to estimate the number of influenza cases by season. The output of the epidemiological model is the number of infections due to the influenza viral subtypes A(H1N1), A(H3N2), and B; both symptomatic and asymptomatic cases are predicted. The dynamic nature of the epidemiological module allows to incorporate the indirect effect of influenza vaccination, i.e., herd protection.

The burden module is a decision tree starting from the final output of the epidemiological model and simulating the natural history of the disease, i.e., among patients

infected with influenza, the model estimates potential complications, which may require treatment, including hospitalisation, and may also cause the subject's death (Figure 1). The burden module model estimates the expected number of clinical events associated with influenza and the corresponding costs and quality-adjusted life years (QALY) estimated for each of the two influenza vaccines analysed in the current assessment.

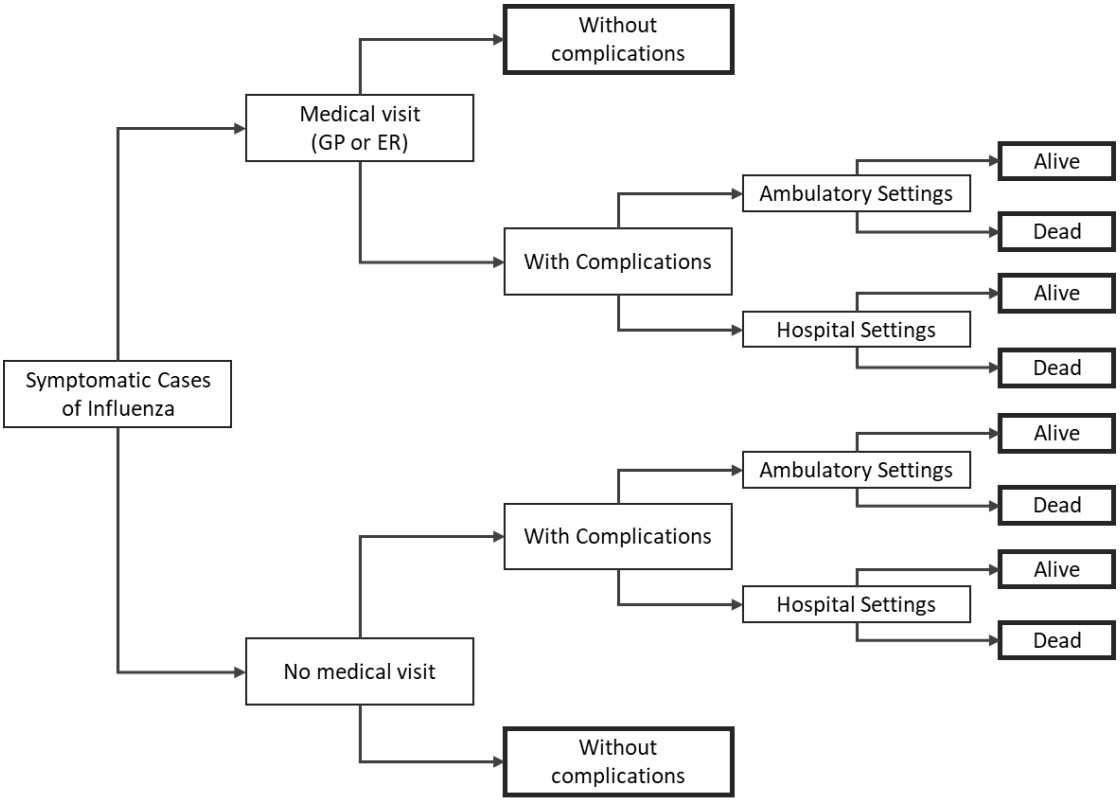

Figure 1: Decision-tree structure for the disease burden module. Note: bold rectangles represent terminal nodes. ER = emergency room; GP = general practitioner.

6.3 Epidemiological Model Inputs

6.3.1 Population

he model was stratified into 86 age groups/classes. Contacts among age classes followed a published contact matrix for Spain, part of a larger study that analysed 26 European countries [184]. The latent period was set to 1.5 days and the infectious period to 1.2 days; hence, the influenza generation time was 2.7 days [226]. The distribution of contact rates was chosen on the basis of the dominant (or codominant) strains in Spain in the years 2010-2019 [226, 227]. In the absence of transmission rates for Spain, Italian transmission rates for the overall population were used as a proxy, using data for the

same years in which matching strains were observed in the two markets (Table 1). In the only case in which the strains did not match (2017/2018 season), H3N2 data of the following year were used.

Season	Strain Circulation in Spain	Strain Circulation in Italy
2010/11	**H1N1**	**H1N1**/B
2011/12	**H3N2**	**H3N2**
2012/13	**B**	H1N1/**B**
2013/14	**H1N1/H3N2**	**H1N1/H3N2**
2014/15	**H3N2**	H1N1/**H3N2**/B
2015/16	**H1N1**	**H1N1**/H3N2/B
2016/17	**H3N2**	**H3N2**
2017/18	**B**/H3N2	H1N1/**B**
2018/19	Not available	H1N1/H3N2

Table 1: Influenza strains for influenza seasons after 2010/11.
Note: **Bold** font highlights the correspondence of strains between Spain and Italy by season. Underlined text indicates data from a different season used as a proxy.

No estimates of $\mathcal{R}_0$ for influenza in Spain were identified, hence Italian estimates were used [226], assuming that in each season the contact rate for the dominant strains in Spain were the same as that of the corresponding strains in Italy. It should be noted that using the Spanish contact matrix and population structure combined with the contact rates estimated for Italy resulted in lower values of $\mathcal{R}_0$, and hence the average number of influenza infections predicted by the model per season would have been lower than published data for Spain [227]. Hence, a rescaled distribution of the Italian transmission rates was applied, using a factor of 1.05. This factor was found empirically to result in an average number of reported infections matching observed outcomes for Spain, reported in a study on transmissibility of influenza [227]. Furthermore, the 2014/2015 season (H3N2) was excluded from the analysis because the procedure estimating $\mathcal{R}_0$ for this season yielded a value below 1, in which case an epidemic cannot occur. A summary of the population included in the model is presented in Table 2. The Spanish population was sourced from the National Statistics Institute, Spanish Statistical Office (population reflects official data up to 2021) [228].

6.3.2 Vaccine Coverage

Two different sources were used for vaccine coverage: one for individuals with ages between 0 and 64 (2012) [212], and another for those older than 65 years (2020) [229]. Coverage data for the 0-64 age category is aligned with a previous publication that evaluated the cost-effectiveness of quadrivalent influenza vaccine in Spain; the coverage for healthy individuals was reported as 0% (since in Spain vaccination is not recommended for healthy individuals) [212]. For the 65+ population, the model considers all individuals are at high risk for influenza infection, which is aligned with Spanish government

Age	N	% Healthy	% at Risk	At-Risk — Coverage	Overall - Coverage
0-8	3,662,079	79.93%	20.07%	24.20%	4.86%
9-17	4,500,901	78.63%	21.37%	24.24%	5.18%
18-64	29,719,673	57.46%	42.54%	17.15%	7.29%
≥65	9,444,037	0 %	100%	67.7%	67.7%

Table 2: Summary of Spanish population structure.
Note: Based on the Spanish Ministry of Health, the 'at-risk' population included individuals with chronic cardiovascular or lung disease, metabolic disease, morbid obesity, chronic renal disease, hemoglobin disorders and anemia, asplenia, chronic liver disease, severe neuromuscular diseases, immunosuppressed, cochlear implanted, cognitive dysfunction, people living in closed institutions, pregnant women, and children from 6 months to 18 years receiving long-term treatment with acetylsalicylic acid. Individuals without these conditions are considered healthy, i.e., influenza vaccination is not recommended to them [212].

guidelines for vaccination [230]. A summary of the coverage data used by the model is presented Table 3.

Age Category	0-4	5-17	18-49	50-64	65-69	70-74	75-79	80-84	85+
Vaccine coverage	4.55%	5.18%	2.91%	15.66%	59.84%	67.41%	68.36%	76.39%	72.23%

Table 3: Overall vaccine coverage.

6.3.3 Effectiveness

Estimates of QIVe effectiveness came from a recent systematic review and meta-analyses, which took into account differences between age groups and viral type. The meta-analysis results were summarized in a recent health-technology assessment (HTA) and are presented in Table 4 [184, 59].

Age Category	Viral Strain		
	H1N1	H3N2	B
0.5-1	69.0 (49.0-81.0)	43.0 (28.0-55.0)	66.5 (57.7-73.6)
2-6	69.0 (49.0-81.0)	43.0 (28.0-55.0)	66.5 (57.7-73.6)
7-17	73.0 (52.0-84.0)	35.0 (14.0-41.0)	77.0 (18.0-94.0)
18-64	73.0 (49.0-81.0)	35.0 (14.0-41.0)	77.0 (18.0-94.0)
≥65	62.0 (36.0-78.0)	24.0 (-6.0-45.0)	52.1 (41.5-60.8)

Table 4: QIVe absolute vaccine effectiveness.
Note: Effectiveness reported as mean% (95% confidence interval).

The relative vaccine effectiveness (rVE) of aQIV compared with QIVe was sourced from two published meta-analyses (Table 5). These meta-analyses reported on the rVE

of aTIV vs. TIV. These results are extrapolated for the comparison of aQIV vs. QIV; the extrapolation is needed because to date, there are no real-world evidence aQIV studies [231]. Although the meta-analyses compared aTIV vs. TIV, these results are appropriate for aQIV as the European Medicines Agency (EMEA) established that observational effectiveness studies performed with aTIV are relevant to aQIV because both vaccines are manufactured using the same process and have overlapping compositions [232].

Meta-Analysis	rVE	Notes
Calabrò et al., 2021 [174]	34.6% (95% CI: 2.0–66.0%)	Synthesised three studies that reported the relative effectiveness of aTIV against TIV, based on laboratory-confirmed influenza studies.
Coleman et al., 2021 [218]	13.9% (95% CI 4.2–23.5%)	Studied the effectiveness of aTIV relative to vaccination with TIV. It included influenza-like-illness outcomes using influenza-related medical encounters for influenza with or without pneumonia in various clinical settings including outpatient, hospital, or emergency department.

Table 5: aQIV relative vaccine effectiveness (extrapolated from aTIV).
aQIV = adjuvanted quadrivalent influenza vaccine; aTIV = adjuvanted trivalent influenza vaccine; CI = confidence interval; rVE = relative vaccine effectiveness; TIV = trivalent influenza vaccine.

6.4 Disease Burden Module Inputs

6.4.1 Rates of Clinical Events

Table 6 shows the probability of patients with a symptomatic case of influenza seeking different types of medical support. Visits to the general practitioner (GP) are further stratified as ambulatory (patient visits a doctor's office) or a home visit (doctor visits the patient at home). Table 7 details the probability of developing complications and the distribution around the type of complications. These probabilities were not available from the literature specific to the Spanish settings, hence Italian data were used as a surrogate.

Age Category	Probability of Medical Support Seeking, by Type			
	GP Visit [191]	GP Ambulatory [193]	GP Home Visit [193]	ER[192, 193]
0–8	65.63%	34.02%	65.98%	3.04%
9–17	57.63%	34.02%	65.98%	1.65%
18–64	32.03%	34.02%	65.98%	0.02%
≥65	36.89%	34.02%	65.98%	0.02%

Table 6: Medical support seeking by patients with a symptomatic case of influenza.
GP = general practitioner; ER = Emergency Room.
Note: ambulatory and home visit correspond to the distribution of GP visit types; i.e., 34% of the total GP visits are considered ambulatory, whereas 66% are home visits.

Age Category	Probability of Complications [193, 233, 234]	Distribution of Influenza Complications [192, 193]			
		URTI	Bronchitis	Pneumonia	Other Respiratory
0–8	22.21%	54.46%	43.31%	2.23%	0.00%
9–17	15.09%	54.55%	43.64%	1.82%	0.00%
18–64 LR	29.98%	52.33%	39.52%	3.63%	4.52%
18–64 HR	55.33%	52.33%	39.52%	3.63%	4.52%
≥65	63.65%	52.33%	39.52%	3.63%	4.52%

Table 7: Influenza-related complications.
HR = high risk; LR = low risk; URTI = upper respiratory tract infection.

As patients experience influenza-related complications these may result in hospitalisations. Table 8 shows the probability of being hospitalised, and the distribution of hospitalisations by type of complication. hospitalisations data were not identified specific to the Spanish settings, hence Italian data were used as a proxy.

		hospitalisations by Complications [235, 236]					
Age Category	Prob. Hosp. [192, 193]	URTI	Bronchitis	Pneumonia w/o Comp.	Pneumonia with Comp.	COPD	Cardiac
0–8	4.14%	0.00%	0.00%	100.00%	0.00%	0.00%	0.00%
9–17	2.73%	0.00%	0.00%	100.00%	0.00%	0.00%	0.00%
18–64 LR	0.41%	23.53%	5.88%	29.41%	41.18%	0.00%	0.00%
18–64 HR	2.96%	23.53%	5.88%	29.41%	41.18%	0.00%	0.00%
≥65	2.96%	15.38%	3.85%	19.23%	26.92%	19.23%	15.38%

Table 8: Influenza-related hospitalisations.
COPD = chronic obstructive respiratory diseases; comp. = complications; hosp. = hospitalisations; HR = high risk; LR = low risk; URTI = upper respiratory tract infection; w/o = without.

6.4.2 Mortality

Only subjects who incur influenza-related complications face an influenza-specific risk of death. In absence of influenza-related death rates for Spain, data from the UK (previously used by Garcia et al. [212] when evaluating QIVs in Spain) and Italy were used. The risk of death (mortality likely attributable to influenza) was stratified by age categories and risk level (where applicable): ages 0-8 = 0.03%, 9-17 = 0.01%, 18-64 low risk = 0.15%, and high risk = 0.19%; 65+ = 2.67% [234, 165].

6.4.3 Costs

All costs are expressed in 2021 euros. It should be noted that in Spain, costs informed by the autonomous communities bulletins remain current from the time of their publication, until a new version is posted by the Spanish government, i.e., these official costs should not be inflated. The per-dose cost of each vaccine was €9.50 and €13 for QIVe and

aQIV, respectively. These figures correspond to official tender prices set by the Spanish Ministry of Health [237]. The administration cost, evaluated from the public healthcare perspective, was €25.94 [238]. The disease management cost of influenza without complications considers the cost of GP visits (ambulatory or at home), priced at €59 and €83, respectively; the cost of pharmaceuticals at €3.21 (includes antivirals, drugs used for the symptomatic therapy of influenza, and antibiotics); and visits to the emergency room at €183 [215, 239]. The disease management costs associated with ambulatory complications are detailed in Table 9. It should be noted that for individuals ≥18 years, there were data to inform the probability of different medical interventions in case of ambulatory complications following influenza; the probability of medical interventions was combined with unit local (Spanish) costs to inform the model. For the 0-17 age category however, detailed data on medical interventions were not available, hence overall costs were used.

Age Category	**Resource**	**Probability (%)**	**Cost**
0–17	URTI costs	N/A	€59.00 [239]
	LRTI costs		€171.45 [238]
≥ 18 [239]	Antibiotic treatment (×5 days)	95.48%	€3.00
	Specialist visit	1.04%	€215.00
	X-ray thorax	7.72%	€23.34
	X-ray sinuses	0.52%	€23.34
	X-ray others	0.28%	€23.34
	Hematology	0.61%	€4.00
	ECG	0.24%	€15.00
	Blood analysis	0.09%	€5.00
	Throat swab	0.05%	€18.00
	Audiometry	0.05%	€62.00

Table 9: Ambulatory complications cost.
ECG = electrocardiogram; LRTI = lower respiratory tract infections; N/A = not applicable; URTI = upper respiratory tract infections.

hospitalisations costs by type of complication were as follows: upper-respiratory tract infection €2607.94; pneumonia €3393.23; chronic obstructive respiratory disease €3277.45; bronchitis €2507.91; and cardiac €3439.30 [240]. The model accounts for two categories of indirect costs: loss of productivity of workers due to influenza or resulting from premature death. Both categories of indirect costs have been estimated using the friction cost method [174]. The estimation of indirect cost combines the number of working hours per week (40) and the average pay per-hour (€17.34) [214], the employment rate (58.65% for 18-64 years individuals, 1.2% for those aged 65-69 years, and 0.3% for those aged 70+), sourced from official data from the Spanish Statistics National Institute [228]; the average number of working days lost for cases that did not require hospitalisations (4.7 days) [241], and those that resulted in hospitalisations (13.25) [235]; the probability of patients remaining at home as a result of developing

influenza-like symptoms (48.32%) [241]; and probability of parents having to take care of sick children (35%) [214].

6.4.4 Utilities

Table 10 shows the reference utilities (for healthy individuals) stratified by age categories [199, 200]. As patients experience the disease, disutilities are applied associated with different clinical events. The disutility for influenza-related symptoms not requiring a medical visit was 0.005 [198]; for influenza-related symptoms requiring a GP visit was 0.06 [198]; for influenza-related symptoms with associated complications was 0.0075 [198]; and for cases requiring hospitalisations, the disutility was 0.0090 [198]. Influenza-related disutilities were not available specifically for Spain, hence these were sourced from a burden of illness study sampling more than 2200 individuals from the general population in Belgium who had experienced influenza-like-illness [198].

Age Category	**Utility [199, 200]**
0–8	0.95
9–17	0.95
18–64	0.93
$\geq$65	0.87

Table 10: Utilities (for healthy individuals).

As patients' QALYs are accrued over several years in the future, the QALYs accrued after the first year were discounted at a 3.0% annual rate, following Spanish guidelines for health economics [242]. The same discount rate was used to accrue future indirect costs associated with averted deaths.

6.5 Analysis

The model allows for the calculation of burden of illness (i.e., number of symptomatic cases, medical help-seeking events with and without complications and with and without hospitalisations, quality-adjusted life-years, and deaths), costs (direct: vaccine acquisition and administration and disease management, and indirect: productivity lost), and incremental analysis (cost per-QALY gained). From the public payer perspective, only direct medical costs are included, whereas for the societal perspective, the productivity lost costs were added to the direct medical costs. Incremental cost-effectiveness ratios (ICERs) were calculated to compare aQIV versus QIVe. The base case considers two main scenarios around relative vaccine effectiveness (rVE) of aQIV versus QIVe, given that two relevant published meta-analyses were identified providing quite different estimates for rVE: 34.6% and 13.9%. Additional scenario analyses were conducted testing the impact of changes to model inputs and/or assumptions on the model results. A one-way deterministic sensitivity analysis (DSA) was used to identify the parameters that are key drivers of the ICER. In the DSA, parameters were changed using a $\pm$20%

variation from their base case value. A probabilistic sensitivity analysis (PSA) was also conducted by varying parameters based on their underlying probability distribution (the contact rate (beta) varied according to the expected distribution in the past 10 seasons; in alignment with previous publications, costs and disutilities were assumed to follow a gamma distribution using a coefficient of variation of 22%) [225, 174]; 10,000 PSA iterations of the model were run to assess the effect of uncertainty on the ICERs (additional details regarding the sensitivity analysis are included in the Appendix 6.A - Tables 6.A.4-6.A.11). A willingness-to-pay threshold of €25,000 per QALY gained, relevant to Spain as per published literature, was used as the threshold to determine the cost-effectiveness of the interventions [243, 244].

6.6 Results

The total number of people vaccinated was 9,150,385. Replacing QIVe with aQIV in the Spanish elderly population would on average prevent 43,664 influenza complicated cases, 1111 hospitalisations, and 569 deaths (with a rVE = 34.6%) or 19,104 influenza complicated cases, 486 hospitalisations, and 252 deaths (with a rVE = 13.9%). Additional details on the outcomes for the clinical events simulated are presented in Table 11. The incremental results for total costs and QALYs are shown in Table 12. Based on the incremental results, the ICER for the scenario using an rVE = 34.6% was €2240 per QALY gained from the payer perspective, and from the societal perspective aQIV was cost-saving; when using an rVE = 13.9%, the ICERs were €6694 and €3936 from the payer and societal perspectives, respectively. Therefore, using either estimate of relative-efficacy and from both perspectives, the results indicate that using aQIV as the vaccination strategy for the elderly population in Spain is cost-effective compared to QIVe. Table 13 shows the costs that the payer will incur for the vaccination of eligible individuals in Spain according to the population structure, vaccine coverage, and vaccines' prices. Direct and indirect costs are detailed in the Appendix 6.A (Tables 6.A.1 and 6.A.2, respectively). Finally, QALYs stratified by age and type of clinical event are also presented in the Appendix 6.A (Table 6.A.3).

Results from the DSA are presented in Figure 2 as tornado charts displaying the impact on the ICER of those parameters whose change caused the largest variations from the base-case ICER (from the payer's perspective). DSA results are presented for both aQIV scenarios (i.e., for both estimations of rVE). Vaccine effectiveness, vaccine cost, and coverage were the most influential parameters in the dynamic model. Since aQIV is more effective than QIVe, a decrease of aQIV's price makes it even more economically attractive than QIVe. In contrast, an increase in QIVe's price impacts the cost-effectiveness analysis in the opposite way: since QIVe is less effective, increasing its price makes it less economically justifiable. It should also be noted that even for the scenarios with the largest variations in the ICERs, the value remained under the Spanish WTP threshold (€25,000 per QALY gained).

Results from the PSA indicate that from the payer's perspective, the probability of aQIV being cost-effective compared with QIVe is 65% for the scenario using rVE =

Age Category	Medical Visits without Complications		Medical Visits with Complications	
	aQIV rVE = 34.6%	aQIV rVE = 13.9%	aQIV rVE = 34.6%	aQIV rVE = 13.9%
0–8	7253	3110	3015	1293
9–17	6964	3021	2089	906
18–64	8833	3847	18,529	8070
≥65	4221	1862	20,031	8835
Total	27,271	11,840	43,664	19,104
Age Category	**hospitalisations**		**Deaths**	
	aQIV rVE = 34.6%	aQIV rVE = 13.9%	aQIV rVE = 34.6%	aQIV rVE = 13.9%
0–8	124	53	1	1
9–17	57	25	1	1
18–64	338	147	32	14
≥65	592	261	535	236
Total	1111	486	569	252

Table 11: Clinical events prevented—aQIV vs. QIVe.
aQIV = adjuvanted quadrivalent influenza vaccine; QIVe = standard-dose quadrivalent influenza vaccine.

Age Category	Direct Medical Costs (Thousands)		Indirect Costs (Thousands)		QALYs	
	rVE 34.6%	rVE 13.9%	rVE 34.6%	rVE 13.9%	rVE 34.6%	rVE 13.9%
0–8	-€1497	-€642	-€1905	-€1023	112.8	64.9
9–17	-€1074	-€467	-€1294	-€828	109.8	63.4
18–64	-€2540	-€1109	-€13,507	-€5905	992.4	433.6
≥65	€19,224	€20,990	-€1103	-€487	5083.8	2242.6
Total	€14,112	€18,773	-€17,808	-€8243	6298.7	2804.5

Table 12: Incremental costs and QALYs results aQIV vs. QIVe.
aQIV = adjuvanted quadrivalent influenza vaccine; QIVe = standard-dose quadrivalent influenza vaccine; QALY = quality-adjusted life years; rVE = relative vaccine effectiveness (aQIV vs. QIVe).

34.6%, and 52.4% for the scenario using rVE = 13.9%. Figure 3 shows the results from the PSA as scatter plots (incremental QALYs versus incremental costs) from the payer perspective. Because of the nonlinearities of the system the majority of the simulations

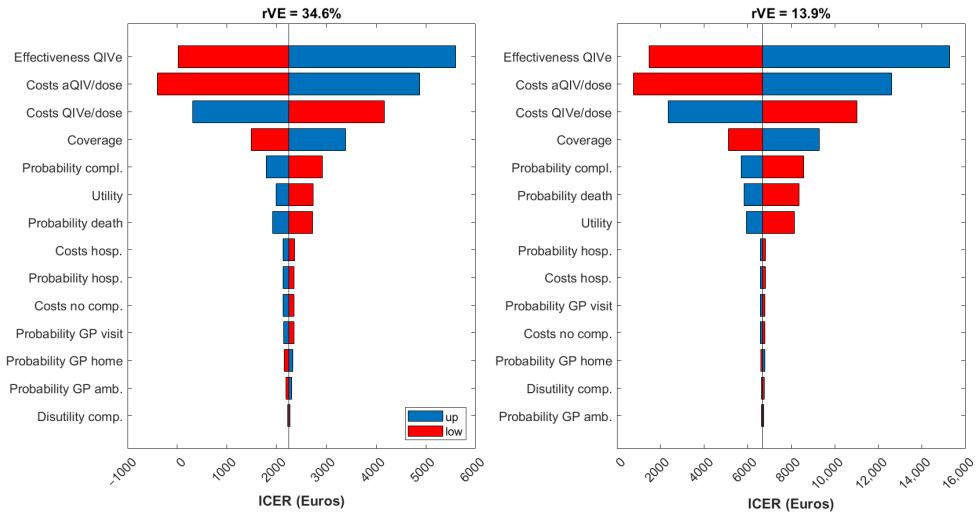

Figure 2: Tornado diagrams for the ICER from the payer perspective. aQIV = adjuvanted quadrivalent influenza vaccine; amb. = ambulatory; comp. = complications; hosp. = hospitalisations; QIVe = standard-dose quadrivalent influenza vaccine; rVE = relative vaccine effectiveness.

have a number of infected individuals lower than the mean.

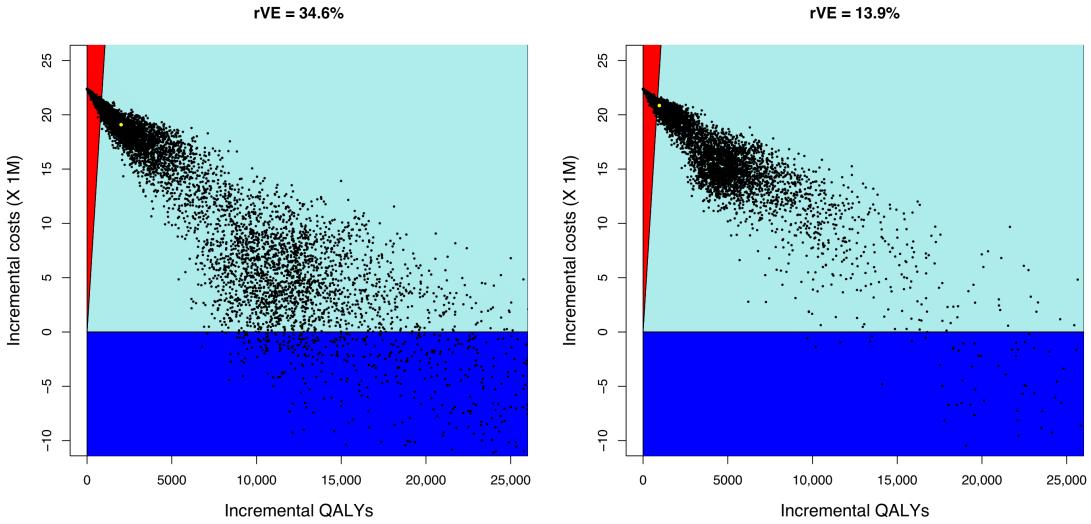

Figure 3: Cost-effectiveness scatter plots—incremental QALYs versus incremental costs (payer perspective). Note: dark blue represents cost-saving scenarios, the light blue sector represents results under €25,000/QALY; red represents results over €25,000/QALY; aQIV = adjuvanted quadrivalent influenza vaccine; QALY = quality-adjusted life-years.

Age Category	Administration (Thousands)	Acquisition (Thousands)	
		QIVe	aQIV
0–8	€9227	€3379	€3379
9–17	€6048	€2215	€2215
18–64	€56,236	€20,595	€20,595
≥65	€165,850	€60,739	€83,117
Total	€237,361	€86,929	€109,306

Table 13: Vaccine acquisition and administration costs.
aQIV = adjuvanted quadrivalent influenza vaccine; QIVe = standard-dose quadrivalent influenza vaccine.

6.7 Discussion

Given that healthcare payers have limited resources to fund the reimbursement of new healthcare interventions, including vaccination strategies against preventable infectious diseases, cost-effectiveness analyses are needed to support decision making regarding the use of these limited funding resources. Improvements in the effectiveness from new healthcare interventions typically come accompanied with a price premium to acquire these new interventions. From a payer's perspective, it becomes critical to assess whether the higher cost of a new technology is worth paying when compared with its benefits. In most markets, new healthcare technologies undergo economic evaluations as one of several regulatory steps to achieve reimbursement, and to support pricing and purchasing decisions [245]. In particular, cost-effectiveness analyses are used regularly to assess the value of new vaccines and vaccination strategies [210]. The WHO provides recommendations twice a year regarding the composition of the vaccines for the influenza season, i.e., which virus strains should the influenza vaccines protect against [246]. Different vaccine types can then be selected matching the protection against particular viral strains recommended by the WHO. These different vaccines will have a range of effectiveness and be available at different prices, hence raising the question of which vaccines should be preferred by a payer interested in getting the best possible value from their investment, potentially stratifying the decision by subpopulations, e.g., by age, or depending on the level of risk experienced. Even within the same class of vaccines (e.g., among quadrivalent vaccines), there will be different options to select from. This analysis focused on replacing QIVe with aQIV in the Spanish elderly population, making use of a dynamic transmission model that allowed accounting for indirect (herd) protection across the entire Spanish population. A majority of published economic analysis reports adult vaccinations strategies to be cost-effective [247]. In alignment with prior literature, results from the present study indicate that replacing QIVe with aQIV in the Spanish elderly population is a cost-effective strategy. The cost-effectiveness result holds even when using a lower rVE (i.e., 13.9% vs. 34.6%) for aQIV. The lower rVE was informed by published relative effectiveness outcomes that included different

real world evidence influenza-related medical encounters outcomes, as complementary to laboratory-confirmed influenza studies only. Although the acquisition cost of aQIV is higher compared with QIVe (27% higher), the better effectiveness of aQIV (using estimates from both meta-analyses) results in cost saving on disease management and better clinical outcomes which translate into increased QALYs. The net effect of increased total costs accompanied by QALY gains results in ICERs well below the cost-effectiveness threshold deemed to be appropriate in Spain (€25,000 per QALY gained). The elderly population have a higher risk of experiencing the worse clinical outcomes derived from influenza, hence offering elderly patients the most effective vaccine results in tangible clinical and economic benefits. A key strength of the analysis was the use of a dynamic model, making it possible to account for herd protection within the elderly group and other age groups of the Spanish population (<65yrs). Vaccination against infectious diseases has an indirect benefit on non-vaccinated individuals, a benefit that cannot be captured by static models. In fact, using dynamic models is currently recommended as the framework to be used for economic evaluations of vaccines [224]. Conducting the analysis faced several limitations as well. First, although every attempt was made to inform the model with data that was specific to the Spanish settings, this was not always possible due to the paucity of data. This was the case for disease transmission rates, where Italian data were used as a proxy; the viral strains circulating in both countries were similar most seasons, however, which should increase the validity of the approach. Italian data were also used to inform $\mathcal{R}_0$, and upon further examination, a rescaled distribution of the Italian transmission rates was used to better match the number of infections predicted by the model with published figures for Spain. Italian data were also used to inform the rates of clinical events among patients with symptomatic influenza. Second, a key model parameter, rVE, was subject to relatively high uncertainty as two published meta-analyses proposed rather different estimates for rVE. Furthermore, the meta-analyses used provided a comparison of aTIV vs. TIV that was extrapolated to be used for aQIV; given that these two vaccines (aTIV and aQIV) have overlapping compositions and undergo similar manufacturing processes, the extrapolation has been deemed appropriate by the EMEA. Nonetheless, analysis using either estimation of rVE resulted in aQIV being cost-effective (or cost saving) from both perspectives (payer and societal), hence even using the more conservative estimation of relative effectiveness, the conclusion is still that it is worth replacing QIVe with aQIV for the elderly population in Spain. In spite of these limitations, the model clinical results were validated versus relevant published results for Spain, hence increasing the model's face validity. In fact, results from the current analysis are aligned with prior analysis mentioned earlier that were conducted for Spain in which aTIV was found to be cost-effective compared with TIV [215, 216].

6.8 Conclusions

Considering the potential negative impacts on clinical outcomes and disease management that influenza can have in the elderly population, and the benefits derived from the use of

an influenza vaccine with better relative effectiveness, results for the analysis have shown that aQIV represents an affordable and highly cost-effective alternative to vaccinate the elderly in Spain. Results from these analyses should help inform regional decision makers in Spain as they determine which vaccination strategies should be funded that will provide the highest health outcomes for the older adult population.

Appendix

6.A Tables

Age Category	Medical Visits without Complications (Thousands)		Medical Visits with Complications (Thousands)		Hospitalisations (Thousands)		GP Ambulatory and Home Visits (Thousands)	
	aQIV rVE = 34.6%	aQIV rVE = 13.9%	aQIV rVE = 34.6%	aQIV rVE = 13.9%	aQIV rVE = 34.6%	aQIV rVE = 13.9%	aQIV rVE = 34.6%	aQIV rVE = 13.9%
0–8	-€23	-€10	-€311	-€133	-€421	-€180	-€742	-€318
9–17	-€22	-€10	-€220	-€96	-€193	-€85	-€638	-€277
18–64	-€28	-€12	-€338	-€147	-€1067	-€468	-€1106	-€482
≥65	-€14	-€6	-€362	-€160	-€1908	-€838	-€870	-€384
Total	-€88	-€38	-€1232	-€536	-€3589	-€1570	-€3356	-€1460

Table 6.A.1: Total (population) incremental direct medical costs.
aQIV = adjuvanted quadrivalent influenza vaccine; GP = general practitioner; QIVe = standard-dose quadrivalent influenza vaccine.

Age Category	Due to Deaths (Thousands)		Due to Workdays Lost by Diseased Workers (Thousands)		Due to Workdays Lost by Parents Assisting Diseased Children (Thousands)	
	aQIV rVE = 34.6%	aQIV rVE = 13.9%	aQIV rVE = 34.6%	aQIV rVE = 13.9%	aQIV rVE = 34.6%	aQIV rVE = 13.9%
0–8	-€361	-€361	€0	€0	-€1544	-€662
9–17	-€471	-€471	€0	€0	-€823	-€357
18–64	-€11,509	-€5035	-€14	-€6	€0	€0
≥65	-€1090	-€481	€0	€0	€0	€0
Total	-€13,431	-€6348	-€14	-€6	-€2367	-€1019

Table 6.A.2: Total (population) incremental indirect costs (productivity losses).
aQIV = adjuvanted quadrivalent influenza vaccine; GP = general practitioner; QIVe = standard-dose quadrivalent influenza vaccine.

Age Category	Influenza without Complications		Influenza with Complications		hospitalisations		Deaths Avoided	
	aQIV rVE = 34.6%	aQIV rVE = 13.9%	aQIV rVE = 34.6%	aQIV rVE = 13.9%	aQIV rVE = 34.6%	aQIV rVE = 13.9%	aQIV rVE = 34.6%	aQIV rVE = 13.9%
0–8	60.1	25.8	22.6	9.7	1.1	0.5	29.0	29.0
9–17	65.7	28.5	15.7	6.8	0.5	0.2	27.9	27.9
18–64	146.8	63.9	138.7	60.4	3.0	1.3	703.8	307.9
≥65	61.4	27.1	150.2	66.3	5.3	2.3	4866.8	2146.9
Total	334.0	145.3	327.2	143.2	10.0	4.4	5627.5	2511.6

Table 6.A.3: Total (population) incremental quality-adjusted life years.
aQIV = adjuvanted quadrivalent influenza vaccine; GP = general practitioner; QIVe = standard-dose quadrivalent influenza vaccine.

	Base Case		Lower Bound		Upper Bound	
Age Category	**At Risk Influenza Coverage**	**Overall Coverage**	**At Risk Coverage**	**Overall Coverage**	**At Risk Coverage**	**Overall Coverage**
0–8	24.20%	4.86%	19.36%	3.89%	29.04%	5.83%
9–17	24.24%	5.18%	24.24%	5.18%	24.24%	5.18%
18–64	17.15%	7.29%	13.72%	5.84%	20.58%	8.75%
≥65	67.70%	67.70%	54.16%	54.16%	81.24%	81.24%

Table 6.A.4: Lower and upper bounds for vaccine coverage in DSA.

Base Case									
Age Category	**H1N1**			**H3N2**			**B**		
	QIVe	**aQIV (rVE = 34.6%)**	**AQIV (rVE = 13.9%)**	**QIVe**	**aQIV (rVE = 34.6%)**	**AQIV (rVE = 13.9%)**	**QIVe**	**aQIV (rVE = 34.6%)**	**AQIV (rVE = 13.9%)**
0.5–1	69.00%	69.00%	69.00%	43.00%	43.00%	43.00%	67.00%	67.00%	67.00%
2–6	69.00%	69.00%	69.00%	43.00%	43.00%	43.00%	67.00%	67.00%	67.00%
7–17	73.00%	73.00%	73.00%	35.00%	35.00%	35.00%	77.00%	77.00%	77.00%
18–64	73.00%	73.00%	73.00%	35.00%	35.00%	35.00%	77.00%	77.00%	77.00%
≥65	62.00%	75.20%	67.30%	24.00%	50.40%	34.60%	52.00%	68.70%	58.70%
Lower Bound									
0.5–1	49.00%	49.00%	49.00%	28.00%	28.00%	28.00%	57.70%	57.70%	57.70%
2–6	49.00%	49.00%	49.00%	28.00%	28.00%	28.00%	57.70%	57.70%	57.70%
7–17	49.00%	49.00%	49.00%	28.00%	28.00%	28.00%	57.70%	57.70%	57.70%
18–64	52.00%	52.00%	52.00%	14.00%	14.00%	14.00%	18.00%	18.00%	18.00%
≥65	36.00%	62.76%	63.60%	-6.00%	25.52%	27.19%	41.00%	52.96%	54.02%
Upper Bound									
0.5–1	81.00%	81.00%	81.00%	55.00%	55.00%	55.00%	73.60%	73.60%	73.60%
2–6	81.00%	81.00%	81.00%	55.00%	55.00%	55.00%	73.60%	73.60%	73.60%
7–17	81.00%	81.00%	81.00%	55.00%	55.00%	55.00%	73.60%	73.60%	73.60%
18–64	84.00%	84.00%	84.00%	41.00%	41.00%	41.00%	94.00%	94.00%	94.00%
≥65	78.00%	87.08%	70.93%	45.00%	74.16%	41.86%	60.80%	83.68%	63.28%

Table 6.A.5: Lower and upper bounds for vaccine effectiveness in DSA.
aQIV = adjuvanted quadrivalent influenza vaccine; GP = general practitioner; QIVe = standard-dose quadrivalent influenza vaccine.

PSA implementation

Using the base values for probability of complications and for costs, a linear regression was developed for direct and indirect costs (excluding those of vaccination) and QALYs as a function of the number of infections in the various age classes. The PSA was then performed by varying each of these coefficients, sampling them from a gamma distribution with the mean given by the estimated mean value and using a coefficient of variation equal to 22% [225].

The transmission rates were varied according to the a posteriori distribution (beta) estimated from the Italian data source informing the transmission rates [225].

Age Category	GP Visit	ER Visit	Probability of Complications	Probability hospitalisations	Probability of Death
Base Case					
0–8	65.63%	3.04%	22.21%	4.14%	0.03%
9–17	57.63%	1.65%	15.09%	2.73%	0.01%
18–64 LR	32.03%	0.02%	29.98%	0.41%	0.15%
18–64 HR	32.03%	0.02%	55.33%	2.96%	0.19%
≥65	36.89%	0.02%	63.65%	2.96%	2.67%
Lower Bound					
0–8	52.50%	2.43%	17.77%	3.31%	0.02%
9–17	46.10%	1.32%	12.07%	2.18%	0.01%
18–64 LR	25.62%	0.01%	23.99%	0.33%	0.12%
18–64 HR	25.62%	0.01%	44.26%	2.37%	0.15%
≥65	29.51%	0.01%	50.92%	2.37%	2.13%
Upper Bound					
0–8	78.75%	3.65%	26.65%	4.97%	0.03%
9–17	69.15%	1.98%	18.11%	3.27%	0.02%
18–64 LR	38.43%	0.02%	35.98%	0.50%	0.18%
18–64 HR	38.43%	0.02%	66.39%	3.55%	0.23%
≥65	44.26%	0.02%	76.38%	3.55%	3.20%

Table 6.A.6: ER = emergency room; GP = general practitioner; HR = high risk; LR = low risk.

	Base Case	Lower Bound	Upper Bound
Cost QIVe per dose	€9.50	€7.60	€11.40
Cost aQIV per dose	€13.00	€10.40	€15.60
Vaccine administration cost	€25.94	€20.75	€31.13
Cost flu without complication (all components: GP ambulatory, GP home, pharmaceutical costs, ER)			
Cost GP visit at ambulatory (winter)	€59.00	€47.20	€70.80
Cost GP visit at home (winter)	€83.00	€66.40	€99.60
Cost pharmaceuticals	€3.21	€2.57	€3.85
Cost ED visit per equivalent patient	€183.00	€146.40	€219.60
Cost flu with ambulatory complications 0–17 years (URTI + LRTI)			
URTI	€59.00	€47.20	€70.80
LRTI	€171.45	€137.16	€205.74
Costs flu with ambulatory complications ≥18 years (cost of all resources)			
Antibiotic treatment (× 5 days)	€15.00	€12.00	€18.00
Specialist visit	€215.00	€172.00	€258.00
X-ray thorax	€23.34	€18.67	€28.01
X-ray sinuses	€23.34	€18.67	€28.01
X-ray others	€23.34	€18.67	€28.01
Hematology	€4.00	€3.20	€4.80
ECG	€15.00	€12.00	€18.00
Blood analysis	€5.00	€4.00	€6.00
Throat swab	€18.00	€14.40	€21.60
Audiometry	€62.00	€49.60	€74.40
hospitalisations costs (all conditions: URTI, pneumonia, COPD, bronchitis, cardiac)			
URTI	€2607.94	€2086.35	€3129.52
Pneumonia	€3393.23	€2714.59	€4071.88
COPD	€3277.45	€2621.96	€3932.94
Bronchitis	€2507.91	€2006.33	€3009.49
Cardiac	€3439.30	€2751.44	€4127.16

Table 6.A.7: Lower and upper bounds for unit resource costs in DSA.
aQIV = adjuvanted quadrivalent influenza vaccine; COPD = chronic obstructive respiratory diseases; ECG = electrocardiogram; ER = emergency room; GP = general practitioner; LRTI = lower respiratory tract infection; QIVe = standard-dose quadrivalent influenza vaccine; URTI = upper respiratory tract infection.

Age Category	Base Case	Lower Bound	Upper Bound
0–8	0.95	0.76	1.00
9–17	0.95	0.76	1.00
18–64	0.93	0.75	1.00
≥65	0.87	0.70	1.00

Table 6.A.8: Lower and upper bounds for reference utilities (healthy individuals).

Influenza-Related Complication	Base Case	Lower Bound	Upper Bound
Influenza symptoms without medical visit	0.005	0.0040	0.0060
Influenza symptoms with medical visit	0.006	0.0048	0.0072
Influenza symptoms with complications	0.0075	0.0060	0.0090
Influenza symptoms with complications and hospitalisations	0.0090	0.0072	0.0108

Table 6.A.9: Lower and upper bounds for influenza-related complications disutilities.

	Lower $\mathcal{R}_0$	**Mean $\mathcal{R}_0$**	**Upper $\mathcal{R}_0$**
B	1.0881	1.0968	1.1055
H1N1	1.0029	1.0548	1.1330
H3N2	0.9734	1.0439	1.1416

Table 6.A.10: Lower and upper bounds for $\mathcal{R}_0$ (QIVe).

Variable	**Direct Costs**	**Indirect Costs**	**QALYs**
Infections in age-classes 0–8	110.47	245.86	7.91
Infections in age-classes 9–17	77.64	146.52	6.48
Infections in age-classes 18–64	55.03	346.52	21.44
Infections in age-classes $\geq$65	100.27	135.04	161.45

Table 6.A.11: Linear regression coefficients.
QALY = quality-adjusted life years.

7. Conclusions and future directions

The thesis collects most of the research I carried out throughout my PhD, and hence covers various topics of mathematical models applied to epidemiology.

The thesis is divided into two main parts: the first, corresponding to Chapters 2 and 3, regards the global stability analysis of epidemic models which include the class of asymptomatic individuals.

The second part, corresponding to Chapter 4-6, concerns the analysis of heterogeneous humans interactions in epidemics, mainly through numerical simulations and using real data.

In the first part of the thesis, the role of asymptomatic individuals during an epidemics is studied using a SAIRS-type epidemic model. Both the cases of a single population and a network of different communities are considered. The rigorous proof of global stability analysis of the equilibria, in particular for the endemic equilibrium, has proven to be a challenging problem. Indeed, the main results in this context regard the rigorous global stability analysis of the endemic equilibrium, and the most general result is still not a completely comprehensive one. These results are obtained by using Lyapunov theory, a geometric approach which generalises the Poincaré-Bendixson theorem and, in the case of network, a graph-theoretic approaches to find Lyapunov functions. However, the use of these mathematical tools resulted in an artificial additional hypothesis on the parameters, which stopped us from providing a general statement concerning only the Basic Reproduction Number.

The second part of the thesis is itself divided in two parts.

First, a stochastic SIR model on a scale-free network is proposed to determine the probability of having a minor epidemic in a network, i.e. an epidemic with a low number of infectious that ends with the elimination of the disease. The most important tool used in this work is a specialised and computationally less expensive version of the Gillespie algorithm. This algorithm proved to be remarkably efficient, and we plan on generalising it to more complex compartmental models, to describe more realistic infectious diseases.

Then, a cost-effectiveness analysis of paediatric influenza vaccination in Italy is performed based on a multi-group SEIR epidemic model divided by age classes. This approach has been also adapted to study the case of elderly influenza vaccination in Spain.

As a future directions, it would be interesting to incorporate more realistic features into the models considered in this thesis. First, Chapters 2 and 3 leave some open problems on the global asymptotic stability of the endemic equilibrium. The most general analytical result is achieve with artificial restrictions on the parameters, even though extensive numerical simulations seem to indicate that these could be relaxed. Models which include asymptomatic infections are useful to adapt classic control strategies, e.g. quarantine of infectious individuals, also in presence of diseases which present an asymptomatic stage, and we believe these deserve a much more extensive role in the field of mathematical modelling of infectious diseases. Remarkably, both for the single population and the network case, the SAIRS model does not show a periodic behaviour, despite its complexity. This clashes with the observation of real-world diseases which periodically exhibit peaks of infections. In this context, other elements could be included in further generalisations to increase realism, e.g. the vital dynamics of the population, in order to find a minimal ODE model in which limit cycles appear. Models which include asymptomatic infections could be also studied from the stochastic point of view on networks: the Gillespie algorithm presented in Chapter 4 can be modified in order to include the asymptomatic stage, and a heterogeneous infectivity between symptomatic and asymptomatic individuals.

Another interesting generalisation could be considering other compartments. First, one can think to distinguish between the loss of immunity after a recovery o after a vaccination; in this framework, it can be useful to add a "Vaccinated" compartment in the model. Moreover, a distinction between asymptomatic and pre-symptomatic individuals can be achieved by including the "Exposed" compartment. This last model could be used to generalise the multi-age SEIR model used for the cost-effectiveness analysis of influenza.

We leave these, and other interesting research questions, as future works.

Bibliography

[1] W.O. Kermack and A.G. McKendrick. Contributions to the mathematical theory of epidemics—I. *Bltn Mathcal Biology*, 53:33–55, 1991.

[2] A. Aleta and Y. Moreno. Evaluation of the potential incidence of COVID-19 and effectiveness of containment measures in Spain: a data-driven approach. *BMC medicine*, 18:1–12, 2020.

[3] M. Gatto, E. Bertuzzo, L. Mari, S. Miccoli, L. Carraro, R. Casagrandi, and A. Rinaldo. Spread and dynamics of the COVID-19 epidemic in Italy: Effects of emergency containment measures. *Proceedings of the National Academy of Sciences*, 117(19):10484–10491, 2020.

[4] J.A. Backer and J. Wallinga. Spatiotemporal analysis of the 2014 Ebola epidemic in West Africa. *PLoS computational biology*, 12(12):e1005210, 2016.

[5] M.J. Ferrari, R.F. Grais, N. Bharti, A.J.K. Conlan, O.N. Bjωrnstad, L.J. Wolfson, P.J. Guerin, A. Djibo, and B.T. Grenfell. The dynamics of measles in sub-Saharan Africa. *Nature*, 451(7179):679–684, 2008.

[6] M. Tizzoni, P. Bajardi, C. Poletto, J.J. Ramasco, D. Balcan, B. Gonçalves, N. Perra, V. Colizza, and A. Vespignani. Real-time numerical forecast of global epidemic spreading: case study of 2009 A/H1N1pdm. *BMC medicine*, 10(1):1–31, 2012.

[7] H.W. Hethcote and H.R. Thieme. Stability of the endemic equilibrium in epidemic models with subpopulations. *Mathematical Biosciences*, 75(2):205–227, 1985.

[8] M. Iannelli and A. Pugliese. *An Introduction to Mathematical Population Dynamics: Along the Trail of Volterra and Lotka*, volume 79. Springer, 2015.

[9] H.W. Hethcote, H.W. Stech, and P. van den Driessche. Differential equations and applications in ecology, epidemics and population problems, 1981.

[10] H.W. Hethcote. Qualitative analyses of communicable disease models. *Mathematical biosciences*, 28(3-4):335–356, 1976.

[11] F. Brauer. Mathematical epidemiology: Past, present, and future. *Infectious Disease Modelling*, 2(2):113–127, 2017.

[12] Z. Shuai and P. van den Driessche. Global stability of infectious disease models using Lyapunov functions. *SIAM Journal on Applied Mathematics*, 73(4):1513–1532, 2013.

[13] A. Korobeinikov. Lyapunov functions and global stability for SIR and SIRS epidemiological models with non-linear transmission. *Bulletin of Mathematical Biology*, 68(3):615–626, 2006.

[14] J. Mena-Lorcat and H.W. Hethcote. Dynamic models of infectious diseases as regulators of population sizes. *Journal of Mathematical Biology*, 30(7):693–716, 1992.

[15] G.W. Harrison. Global stability of predator-prey interactions. *Journal of Mathematical Biology*, 8(2):159–171, 1979.

[16] E. Beretta and Y. Takeuchi. Global asymptotic stability of Lotka–Volterra diffusion models with continuous time delay. *SIAM Journal on Applied Mathematics*, 48 (3):627–651, 1988.

[17] M.Y. Li and J.S. Muldowney. A geometric approach to global-stability problems. *SIAM Journal on Mathematical Analysis*, 27(4):1070–1083, 1996.

[18] M.Y. Li and J.S. Muldowney. Dynamics of differential equations on invariant manifolds. *Journal of Differential Equations*, 168(2):295–320, 2000.

[19] M.Y. Li, J.R. Graef, L. Wang, and J. Karsai. Global dynamics of a SEIR model with varying total population size. *Mathematical Biosciences*, 160(2):191–213, 1999.

[20] M.Y. Li and J.S. Muldowney. Global stability for the SEIR model in epidemiology. *Mathematical biosciences*, 125(2):155–164, 1995.

[21] P. van den Driessche, M. Li, and J. Muldowney. Global stability of SEIRS models in epidemiology. *Canadian Applied Mathematics Quarterly*, 7:409–425, 1999.

[22] B. Buonomo and D. Lacitignola. On the use of the geometric approach to global stability for three dimensional ODE systems: a bilinear case. *Journal of Mathematical Analysis and Applications*, 348(1):255–266, 2008.

[23] B. Buonomo, A. d'Onofrio, and D. Lacitignola. Global stability of an SIR epidemic model with information dependent vaccination. *Mathematical biosciences*, 216(1): 9–16, 2008.

[24] B. Buonomo, A. d'Onofrio, and D. Lacitignola. Modeling of pseudo-rational exemption to vaccination for SEIR diseases. *Journal of Mathematical Analysis and Applications*, 404(2):385–398, 2013.

[25] G. Lu and Z. Lu. Geometric approach for global asymptotic stability of three-dimensional Lotka–Volterra systems. *Journal of Mathematical Analysis and Applications*, 389(1):591–596, 2012.

[26] H.R. Thieme. Local stability in epidemic models for heterogeneous populations. In *Mathematics in biology and medicine*, pages 185–189. Springer, 1985.

[27] R.N. Mohapatra, D. Porchia, and Z. Shuai. Compartmental Disease Models with Heterogeneous Populations: A Survey. *Mathematical Analysis and its Applications*, 143:619, 2015.

[28] H. Guo, M.Y. Li, and Z. Shuai. Global stability of the endemic equilibrium of multigroup SIR epidemic models. *Canadian applied mathematics quarterly*, 14(3): 259–284, 2006.

[29] H. Guo, M. Li, and Z. Shuai. A graph-theoretic approach to the method of global Lyapunov functions. *Proceedings of the American Mathematical Society*, 136(8): 2793–2802, 2008.

[30] M.Y. Li and Z. Shuai. Global-stability problem for coupled systems of differential equations on networks. *Journal of Differential Equations*, 248(1):1–20, 2010.

[31] Y. Muroya, Y. Enatsu, and T. Kuniya. Global stability for a multi-group SIRS epidemic model with varying population sizes. *Nonlinear Analysis: Real World Applications*, 14(3):1693–1704, 2013.

[32] Y. Muroya and T. Kuniya. Further stability analysis for a multi-group SIRS epidemic model with varying total population size. *Applied Mathematics Letters*, 38:73–78, 2014.

[33] D. Fan, P. Hao, D. Sun, and J. Wei. Global stability of multi-group SEIRS epidemic models with vaccination. *International Journal of Biomathematics*, 11(01): 1850006, 2018.

[34] T. Alamo, D.G. Reina, V.M. Gata, P.M.and Preciado, and G. Giordano. Data-driven methods for present and future pandemics: Monitoring, modelling and managing. *Annual Reviews in Control*, 52:448–464, 2021.

[35] J.T. Kemper. The effects of asymptomatic attacks on the spread of infectious disease: a deterministic model. *Bulletin of mathematical biology*, 40(6):707–718, 1978.

[36] E.J. Nelson, J.B. Harris, J.G. Morris, S.B. Calderwood, and A. Camilli. Cholera transmission: the host, pathogen and bacteriophage dynamic. *Nature Reviews Microbiology*, 7(10):693–702, 2009.

[37] N.I. Stilianakis, A.S. Perelson, and F.G. Hayden. Emergence of drug resistance during an influenza epidemic: insights from a mathematical model. *Journal of Infectious Diseases*, 177(4):863–873, 1998.

[38] F. Débarre, S. Bonhoeffer, and R.R. Regoes. The effect of population structure on the emergence of drug resistance during influenza pandemics. *Journal of the Royal Society Interface*, 4(16):893–906, 2007.

[39] R.M. Anderson and R.M. May. Spatial, temporal, and genetic heterogeneity in host populations and the design of immunization programmes. *Mathematical Medicine and Biology: A Journal of the IMA*, 1(3):233–266, 1984.

[40] H. Andersson and T. Britton. Heterogeneity in epidemic models and its effect on the spread of infection. *Journal of applied probability*, 35(3):651–661, 1998.

[41] A.L. Lloyd and R.M. May. Spatial Heterogeneity in Epidemic Models. *Journal of Theoretical Biology*, 179(1):1–11, 1996. ISSN 0022-5193.

[42] H.W. Hethcote. An immunization model for a heterogeneous population. *Theoretical Population Biology*, 14(3):338–349, 1978. ISSN 0040-5809.

[43] R. Pastor-Satorras, C. Castellano, P. Van Mieghem, and A. Vespignani. Epidemic processes in complex networks. *Reviews of modern physics*, 87(3):925, 2015.

[44] G. Strona, C.J. Carstens, P.S.A. Beck, and B.A. Han. The intrinsic vulnerability of networks to epidemics. *Ecological modelling*, 383:91–97, 2018.

[45] G.M. Knight, N.J. Dharan, G.J. Fox, N. Stennis, A. Zwerling, R. Khurana, and D.W. Dowdy. Bridging the gap between evidence and policy for infectious diseases: How models can aid public health decision-making. *International journal of infectious diseases*, 42:17–23, 2016.

[46] Influenzanet, 2005. URL `https://influenzanet.info/#page/home`.

[47] Flu Near You, 2011. URL `http://www.flunearyou.orghttp://www.flunearyou.org`.

[48] A. Pandey, K.E. Atkins, J. Medlock, N. Wenzel, J.P. Townsend, J.E. Childs, T.G. Nyenswah, M.L. Ndeffo-Mbah, and A.P. Galvani. Strategies for containing ebola in west africa. *Science*, 346(6212):991–995, 2014.

[49] J.A. Firth, J. Hellewell, P. Klepac, S. Kissler, A.J. Kucharski, and L.G. Spurgin. Using a real-world network to model localized COVID-19 control strategies. *Nature medicine*, 26(10):1616–1622, 2020.

[50] C. Rizzo, G. Rezza, and W. Ricciardi. Strategies in recommending influenza vaccination in europe and us. *Human Vaccines & Immunotherapeutics*, 14(3):693–698, 2018.

[51] E.A. Belongia, M.D. Simpson, J.P. King, M.E. Sundaram, N.S. Kelley, M.T. Osterholm, and H.Q. McLean. Variable influenza vaccine effectiveness by subtype: a systematic review and meta-analysis of test-negative design studies. *The Lancet Infectious Diseases*, 16(8):942–951, 2016.

[52] R.M. Granich, C.F. Gilks, C. Dye, K.M. De Cock, and B.G. Williams. Universal voluntary hiv testing with immediate antiretroviral therapy as a strategy for elimination of hiv transmission: a mathematical model. *The Lancet*, 373(9657):48–57, 2009.

[53] L.E.C. Rocha, F. Liljeros, and P. Holme. Simulated epidemics in an empirical spatiotemporal network of 50,185 sexual contacts. *PLoS Comput Biol*, 7(3):e1001109, 2011.

[54] A. Brennan, S.E Chick, and R. Davies. A taxonomy of model structures for economic evaluation of health technologies. *Health economics*, 15(12):1295–1310, 2006.

[55] S. Kim and S.J. Goldie. Cost-effectiveness analyses of vaccination programmes. *Pharmacoeconomics*, 26(3):191–215, 2008.

[56] S. Ottaviano, M. Sensi, and S. Sottile. Global stability of SAIRS epidemic models. *Nonlinear Analysis: Real World Applications*, 65:103501, 2022.

[57] S. Ottaviano, M. Sensi, and S. Sottile. Global stability of multi-group SAIRS epidemic models.arxiv:2202.02993, 2022.

[58] S. Sottile, O. Kahramanoğulları, and M. Sensi. How network properties and epidemic parameters influence stochastic sir dynamics on scale-free random networks. *Journal of Simulation*, pages 1–14, 2022.

[59] S. Boccalini et al. Health technology assessment (hta) of the introduction of influenza vaccination for italian children with fluenz tetra®. *Journal of Preventive Medicine and Hygiene*, 2021.

[60] A. Fochesato, S. Sottile, A. Pugliese, S. Márquez-Peláez, H. Toro-Diaz, R. Gani, P. Alvarez, and J. Ruiz-Aragón. An Economic Evaluation of the Adjuvanted Quadrivalent Influenza Vaccine Compared with Standard-Dose Quadrivalent Influenza Vaccine in the Spanish Older Adult Population. *Vaccines*, 10(8):1360, 2022.

[61] M. Robinson and N.I. Stilianakis. A model for the emergence of drug resistance in the presence of asymptomatic infections. *Mathematical Biosciences*, 243(2): 163–177, 2013.

[62] M. Day. Covid-19: identifying and isolating asymptomatic people helped eliminate virus in Italian village. *BMJ: British Medical Journal (Online)*, 368, 2020.

[63] K. Mizumoto, K. Kagaya, A. Zarebski, and G. Chowell. Estimating the asymptomatic proportion of coronavirus disease 2019 (COVID-19) cases on board the Diamond Princess cruise ship, Yokohama, Japan, 2020. *Eurosurveillance*, 25(10): 2000180, 2020.

[64] D.P. Oran and E.J. Topol. Prevalence of asymptomatic SARS-CoV-2 infection: a narrative review. *Annals of internal medicine*, 173(5):362–367, 2020.

[65] D.P. Oran and E.J. Topol. The proportion of SARS-CoV-2 infections that are asymptomatic: a systematic review. *Annals of internal medicine*, 174(5):655–662, 2021.

[66] S. Ansumali, S. Kaushal, A. Kumar, M.K. Prakash, and M. Vidyasagar. Modelling a pandemic with asymptomatic patients, impact of lockdown and herd immunity, with applications to SARS-CoV-2. *Annual reviews in control*, 2020.

[67] V. Wiwanitkit. Unusual mode of transmission of dengue. *The Journal of Infection in Developing Countries*, 4(01):051–054, 2010.

[68] Y. Gu, N. Komiya, H. Kamiya, Y. Yasui, K. Taniguchi, and N. Okabe. Pandemic (H1N1) 2009 transmission during presymptomatic phase, Japan. *Emerging infectious diseases*, 17(9):1737, 2011.

[69] G. Lu and Z. Lu. Geometric approach to global asymptotic stability for the SEIRS models in epidemiology. *Nonlinear Analysis: Real World Applications*, 36:20–43, 2017.

[70] J.A. Yorke. Invariance for ordinary differential equations. *Theory of Computing Systems*, 1(4):353–372, 1967.

[71] R.M. Anderson and R.M. May. *Infectious diseases of humans: dynamics and control*. Oxford university press, 1992.

[72] O. Diekmann and J.A.P. Heesterbeek. *Mathematical epidemiology of infectious diseases: model building, analysis and interpretation*, volume 5. John Wiley & Sons, 2000.

[73] P. van den Driessche and J. Watmough. Further notes on the basic reproduction number. In *Mathematical Epidemiology*, pages 159–178. Springer, 2008.

[74] P. van den Driessche and J. Watmough. Reproduction numbers and sub-threshold endemic equilibria for compartmental models of disease transmission. *Mathematical Biosciences*, 180:29–48, 2002.

[75] L. Perko. Linear systems. In *Differential Equations and Dynamical Systems*, pages 1–63. Springer, 1991.

[76] H.I. Freedman, S. Ruan, and M. Tang. Uniform persistence and flows near a closed positively invariant set. *Journal of Dynamics and Differential Equations*, 6 (4):583–600, 1994.

[77] N.P. Bhatia and G.P. Szegö. *Dynamical systems: stability theory and applications*, volume 35. Springer, 2006.

[78] J.P. La Salle. *The stability of dynamical systems*. SIAM, 1976.

[79] M.M. Ballyk, C.C. McCluskey, and G.S.K. Wolkowicz. Global analysis of competition for perfectly substitutable resources with linear response. *Journal of mathematical biology*, 51(4):458–490, 2005.

[80] S. Bonaccorsi, S. Ottaviano, D. Mugnolo, and F. De Pellegrini. Epidemic outbreaks in networks with equitable or almost-equitable partitions. *SIAM Journal on Applied Mathematics*, 75(6):2421–2443, 2015.

[81] S. Ottaviano, F. De Pellegrini, S. Bonaccorsi, D. Mugnolo, and P. Van Mieghem. Community networks with equitable partitions. In *Multilevel Strategic Interaction Game Models for Complex Networks*, pages 111–129. Springer, 2019.

[82] S. Ottaviano and S. Bonaccorsi. Some aspects of the Markovian SIRS epidemic on networks and its mean-field approximation. *Mathematical Methods in the Applied Sciences*, 44(6):4952–4971, 2021.

[83] P. Van Mieghem. The N-intertwined SIS epidemic network model. *Computing*, 93 (2-4):147–169, 2011.

[84] A. Lajmanovich and J.A. Yorke. A deterministic model for gonorrhea in a nonhomogeneous population. *Mathematical Biosciences*, 28(3):221–236, 1976. ISSN 0025-5564.

[85] W. Huang, K.L. Cooke, and C. Castillo-Chavez. Stability and bifurcation for a multiple-group model for the dynamics of HIV/AIDS transmission. *SIAM Journal on Applied Mathematics*, 52(3):835–854, 1992.

[86] J. Yu, D. Jiang, and N. Shi. Global stability of two-group SIR model with random perturbation. *Journal of Mathematical Analysis and Applications*, 360(1):235–244, 2009.

[87] R.A. Horn and C.R. Johnson. *Matrix analysis*. Cambridge university press, 2012.

[88] S. Hongying, F. Dejun, and W. Junjie. Global stability of multi-group SEIR epidemic models with distributed delays and nonlinear transmission. *Nonlinear Analysis: Real World Applications*, 13(4):1581–1592, 2012.

[89] M.Y. Li and Z. Shuai. Global stability of an epidemic model in a patchy environment. *Canadian Applied Mathematics Quarterly*, 17(1):175–187, 2009.

[90] S. Ruoyan and S. Junping. Global stability of multigroup epidemic model with group mixing and nonlinear incidence rates. *Applied Mathematics and Computation*, 218(2):280–286, 2011.

[91] S.M. Moghadas and A.B. Gumel. Global stability of a two-stage epidemic model with generalized non-linear incidence. *Mathematics and computers in simulation*, 60(1-2):107–118, 2002.

[92] N. Sherborne, K.B. Blyuss, and I.Z. Kiss. Compact pairwise models for epidemics with multiple infectious stages on degree heterogeneous and clustered networks. *Journal of Theoretical Biology*, 407:387–400, 2016.

[93] Y. Wang and J. Cao. Global stability of a multiple infected compartments model for waterborne diseases. *Communications in Nonlinear Science and Numerical Simulation*, 19(10):3753–3765, 2014.

[94] L. Ferretti, C. Wymant, M. Kendall, L. Zhao, A. Nurtay, L. Abeler-Dörner, M. Parker, D. Bonsall, and C. Fraser. Quantifying SARS-CoV-2 transmission suggests epidemic control with digital contact tracing. *Science*, 368(6491), 2020.

[95] R. Pastor-Satorras, C. Castellano, P. Van Mieghem, and A. Vespignani. Epidemic processes in complex networks. *Rev.Mod.Phys.*, 87:925–979, Aug 2015.

[96] M. Keeling and K. Eames. Networks and Epidemic Models. *Journal of the Royal Society, Interface / the Royal Society*, 2:295–307, 10 2005.

[97] G.F. de Arruda, F.A. Rodrigues, and Y. Moreno. Fundamentals of spreading processes in single and multilayer complex networks. *Physics Reports*, 756:1–59, 2018.

[98] P. Erdös and A. Rényi. On Random Graphs I. *Publicationes Mathematicae Debrecen*, 6:290, 1959.

[99] M.E.J. Newman and J. Park. Why social networks are different from other types of networks. *Physical Review E*, 68:036122, 2003.

[100] R. Albert, H. Jeong, and A.L. Barabási. Diameter of the world-wide web. *Nature*, 401:130–131, 1999.

[101] R. Albert, H. Jeong, and A.L. Barabási. Error and attack tolerance of complex networks. *Nature*, 406:378.381, 2000.

[102] A.L. Barabási and R. Albert. Emergence of Scaling in Random Networks. *Science*, 286(5439):509–512, 1999.

[103] M.L. Bertotti and G. Modanese. The configuration model for Barabasi-Albert networks. *Applied Network Science*, 4(1):1–13, 2019.

[104] S.L. Chang, M. Piraveenan, and M. Prokopenko. Impact of network assortativity on epidemic and vaccination behaviour. *Chaos, solitons & fractals*, 140:110143, 2020.

[105] G. Thedchanamoorthy, M. Piraveenan, S. Uddin, and U. Senanayake. Influence of vaccination strategies and topology on the herd immunity of complex networks. *Social Network Analysis and Mining*, 4(1):213, 2014.

[106] G. Caldarelli and A. Vespignani. *Large Scale Structure and Dynamics of Complex Networks: From Information Technologyto Financeand Natural Science*. World Scientific Publishing Company, 2007.

[107] S. Boccaletti, V. Latora, Y. Moreno, M. Chavez, and D. Hwang. Complex networks: Structure and dynamics. *Physics Reports*, 424:175–308, 2006.

[108] E. Estrada. *The Structure of Complex Networks: Theory and Applications*. Oxford University Press, 2011.

[109] I. Kiss, J. Miller, and P. Simon. *Mathematics of epidemics on networks: from exact to approximate models*. Springer, 2017.

[110] M. Boguná, C. Castellano, and R. Pastor-Satorras. Nature of the epidemic threshold for the susceptible-infected-susceptible dynamics in networks. *Physical review letters*, 111(6):068701, 2013.

[111] M. López-García. Stochastic descriptors in an SIR epidemic model for heterogeneous individuals in small networks. *Mathematical biosciences*, 271:42–61, 2016.

[112] F. Ball, D. Sirl, and P. Trapman. Analysis of a stochastic SIR epidemic on a random network incorporating household structure. *Mathematical Biosciences*, 224(2):53–73, 2010.

[113] M. Draief, A. Ganesh, and L. Massoulié. Thresholds for virus spread on networks. In *Proceedings of the 1st international conference on Performance evaluation methodolgies and tools*, pages 51–es, 2006.

[114] A. Ganesh, L. Massoulié, and D. Towsley. The effect of network topology on the spread of epidemics. In *Proceedings IEEE 24th Annual Joint Conference of the IEEE Computer and Communications Societies.*, volume 2, pages 1455–1466. IEEE, 2005.

[115] M. Keeling. The implications of network structure for epidemic dynamics. *Theoretical population biology*, 67(1):1–8, 2005.

[116] H. Zhang, Z.H. Guan, T. Li, X.H. Zhang, and D.X. Zhang. A stochastic SIR epidemic on scale-free network with community structure. *Physica A: Statistical Mechanics and its Applications*, 392(4):974–981, 2013.

[117] M. Kitsak, L.K. Gallos, S. Havlin, F. Liljeros, L. Muchnik, H.E. Stanley, and H.A. Makse. Identification of influential spreaders in complex networks. *Nature physics*, 6(11):888–893, 2010.

[118] B. Min. Identifying an influential spreader from a single seed in complex networks via a message-passing approach. *The European Physical Journal B*, 91(1):1–6, 2018.

[119] F. Radicchi and C. Castellano. Leveraging percolation theory to single out influential spreaders in networks. *Physical Review E*, 93(6):062314, 2016.

[120] J. Hindes and I.B. Schwartz. Epidemic extinction and control in heterogeneous networks. *Physical review letters*, 117(2):028302, 2016.

[121] P. Holme. Extinction times of epidemic outbreaks in networks. *PloS one*, 8(12): e84429, 2013.

[122] P. Holme and L. Tupikina. Epidemic extinction in networks: insights from the 12 110 smallest graphs. *New Journal of Physics*, 20(11):113042, 2018.

[123] E. Cator and P. Van Mieghem. Second-order mean-field susceptible-infected-susceptible epidemic threshold. *Physical review E*, 85(5):056111, 2012.

[124] D. Chakrabarti, Y. Wang, C. Wang, J. Leskovec, and C. Faloutsos. Epidemic thresholds in real networks. *ACM Transactions on Information and System Security (TISSEC)*, 10(4):1–26, 2008.

[125] P. Van Mieghem, J. Omic, and R. Kooij. Virus spread in networks. *IEEE/ACM Transactions On Networking*, 17(1):1–14, 2008.

[126] J.C. Miller. Bounding the size and probability of epidemics on networks. *Journal of Applied Probability*, 45(2):498–512, 2008.

[127] J.C. Miller. A note on the derivation of epidemic final sizes. *Bulletin of mathematical biology*, 74(9):2125–2141, 2012.

[128] A. Aleta, D. Martin-Corral, A.P. y Piontti, M. Ajelli, M. Litvinova, M. Chinazzi, N.E. Dean, M.E. Halloran, I.M. Longini Jr, S. Merler, A. Pentland, A. Vespignani, E. Moro, and Y. Moreno. Modelling the impact of testing, contact tracing and household quarantine on second waves of COVID-19. *Nature Human Behaviour*, 4(9):964–971, 2020.

[129] K. Sun, W. Wang, L. Gao, Y. Wang, K. Luo, L. Ren, Z. Zhan, X. Chen, S. Zhao, Y. Huang, Q. Sun, Z. Liu, M. Litvinova, A. Vespignani, M. Ajelli, C. Vibound, and H. Yu. Transmission heterogeneities, kinetics, and controllability of SARS-CoV-2. *Science*, 371(6526), 2021.

[130] O.M. Cliff, N. Harding, M. Piraveenan, E.Y. Erten, M. Gambhir, and M. Prokopenko. Investigating spatiotemporal dynamics and synchrony of influenza epidemics in Australia: an agent-based modelling approach. *Simulation Modelling Practice and Theory*, 87:412–431, 2018.

[131] C. Zachreson, K.M. Fair, O.M. Cliff, N. Harding, M. Piraveenan, and M. Prokopenko. Urbanization affects peak timing, prevalence, and bimodality of influenza pandemics in Australia: Results of a census-calibrated model. *Science advances*, 4(12):eaau5294, 2018.

[132] T. Rogers. Assessing node risk and vulnerability in epidemics on networks. *EPL (Europhysics Letters)*, 109(2):28005, 2015.

[133] B. Karrer and M.E.J. Newman. Message passing approach for general epidemic models. *Physical Review E*, 82(1):016101, 2010.

[134] D.T. Gillespie. Exact stochastic simulation of coupled chemical reactions. *Journal of Physical Chemistry*, 81:2340–2361, 1977.

[135] I. Artico, I. Smolyarenko, V. Vinciotti, and E.C. Wit. How rare are power-law networks really? *Proceedings of the Royal Society A*, 476(2241):20190742, 2020.

[136] V.M. Eguiluz, D.R. Chialvo, G.A. Cecchi, M. Baliki, and A.V. Apkarian. Scale-free brain functional networks. *Physical review letters*, 94(1):018102, 2005.

[137] E. Fox Keller. Revisiting "scale-free" networks. *BioEssays*, 27(10):1060–1068, 2005.

[138] A.D Broido and A. Clauset. Scale-free networks are rare. *Nature communications*, 10(1):1–10, 2019.

[139] P. Holme. Rare and everywhere: Perspectives on scale-free networks. *Nature communications*, 10(1):1–3, 2019.

[140] R. Durrett. *Random Graph Dynamics*. Cambridge University Press, 2006.

[141] A.L. Barabási. *Network Science*. Cambridge University Press, 2015.

[142] M. Boguñá, R. Pastor-Satorras, and A. Vespignani. Cut-offs and finite size effects in scale-free networks. *European Physical Journal B*, 38:205–209, 2004.

[143] M. Newman. *Networks: An Introduction*. Oxford University Press, 2010.

[144] R. van der Hofstad. *Random Graphs and Complex Networks*, volume 1. Cambridge University Press, 2016.

[145] R.N. Thompson, C.A. Gilligan, and N.J. Cunniffe. Will an outbreak exceed available resources for control? estimating the risk from invading pathogens using practical definitions of a severe epidemic. *J.R.Soc.Interface*, 17, 2020.

[146] M.J. Keeling and P. Rohani. *Modeling infectious diseases in humans and animals*. Princeton university press, 2011.

[147] M. Iannelli and A. Pugliese. *An introduction to mathematical population dynamics*. Springer, 2014.

[148] M.J. Keeling and B.T. Grenfell. Individual-based perspectives on R0. *Journal of theoretical biology*, 203(1):51–61, 2000.

[149] D. Flanders and D.G. Kleinbaum. Basic models for disease occurrence in epidemiology. *International Journal of Epidemiology*, 1995.

[150] T.E. Harris. *The Theory of Branching Processes*. Springer-Verlag, Berlin, 1963.

[151] C.J. Mode. *Multitype branching processes.Theory and applications*. American Elsevier Pub.Co., New York, 1971.

[152] P. Windridge. The extinctiontime of a subcritical branching process related to the SIR epidemic on a random graph. *Journal of Applied Probability*, 2018.

[153] M. Piraveenan, M. Prokopenko, and L. Hossain. Percolation centrality: Quantifying graph-theoretic impact of nodes during percolation in networks. *PloS one*, 8 (1):e53095, 2013.

[154] Ministero della Salute. Circolare "prevenzione e controllo dell'influenza: raccomandazioni per la stagione 2021-2022", last access: 6 agosto 2021. URL `https://www.trovanorme.salute.gov.it/norme/renderNormsanPdf?anno=2021&codLeg=79647&parte=1%20&serie=null`.

[155] P. MacDonald. Extension of influenza immunization program to children in england–future plans. *Human Vaccines & Immunotherapeutics*, 12(10):2707–2708, 2016.

[156] Ministero della Salute. Circolare "prevenzione e controllo dell'influenza: raccomandazioni per la stagione 2020-2021", last access: 6 agosto 2021. URL `https://www.trovanorme.salute.gov.it/norme/renderNormsanPdf?anno=2020&codLeg=74451&parte=1%20&serie=null`.

[157] K.G.G Mohn, I. Smith, H. Sjursen, and R.J. Cox. Immune responses after live attenuated influenza vaccination. *Human vaccines & immunotherapeutics*, 14(3): 571–578, 2018.

[158] Ministero della Salute. Faq - influenza e vaccinazione antinfluenzale, last access: 2 agosto 2021. URL `https://www.salute.gov.it/portale/p5_1_2.jsp?id=103#:~:text=Vaccino%20vivo%20attenuato&text=I%20ceppi%20influenzali%20contenuti%20nel,che%20nel%20tratto%20respiratorio%20inferiore`.

[159] Public Health England. The national childhood flu immunisation programme 2020 to 2021, last access: 2 agosto 2021. URL `https://www.gov.uk/government/publications/childhood-flu-programme-qa-for-healthcare-professionals`.

[160] Ministero della Salute. Trasmissione nota aifa alla regione lombardia: chiarimenti sull'utilizzo del vaccino fluenz tetra nella campagna vaccinale 2020/21.protocollo 0038627-26/11/2020-dgpre-mds-p, last access: 2 agosto 2021.

[161] S.L. Block, S.L. Toback, T. Yi, and C.S. Ambrose. Efficacy of a single dose of live attenuated influenza vaccine in previously unvaccinated children: a post hoc analysis of three studies of children aged 2 to 6 years. *Clinical therapeutics*, 31 (10):2140–2147, 2009.

[162] H.B. Neto, C.K. Farhat, M.W. Tregnaghi, S.A. Madhi, A. Razmpour, G. Palladino, M.G. Small, W.C. Gruber, B.D. Forrest, D153-P504 LAIV Study Group, et al. Efficacy and safety of 1 and 2 doses of live attenuated influenza vaccine in vaccine-naive children. *The Pediatric infectious disease journal*, 28(5):365–371, 2009.

[163] Ministero della Salute. Prevenzione e controllo dell'influenza, last access: 2 agosto 2021. URL `http://www.salute.gov.it/portale/influenza/dettaglioContenutiInfluenza.jsp?lingua=italiano&id=685&area=influenza&menu=vuoto`.

[164] C. Rizzo, A. Bella, C. Viboud, L. Simonsen, M.A. Miller, M.C. Rota, S. Salmaso, and M.L. Ciofi Degli Atti. Trends for influenza-related deaths during pandemic and epidemic seasons, italy, 1969–2001. *Emerging infectious diseases*, 13(5):694, 2007.

[165] A. Rosano, A. Bella, F. Gesualdo, A. Acampora, P. Pezzotti, S. Marchetti, W. Ricciardi, and C. Rizzo. Investigating the impact of influenza on excess mortality in all ages in italy during recent seasons (2013/14–2016/17 seasons). *International Journal of Infectious Diseases*, 88:127–134, 2019.

[166] M.C. Weinstein, B. O'Brien, J. Hornberger, J. Jackson, M. Johannesson, C. McCabe, and B.R. Luce. Principles of good practice for decision analytic modeling in health-care evaluation: Report of the ispor task force on good research practices—modeling studies. *Value in health*, 6(1):9–17, 2003.

[167] F.A. Sonnenberg and J.R. Beck. Markov models in medical decision making: a practical guide. *Medical decision making*, 13(4):322–338, 1993.

[168] A. Briggs and M. Sculpher. An introduction to markov modelling for economic evaluation. *Pharmacoeconomics*, 13(4):397–409, 1998.

[169] Mohan V Bala and Josephine A Mauskopf. Optimal assignment of treatments to health states using a markov decision model. *Pharmacoeconomics*, 24(4):345–354, 2006.

[170] R.M. Anderson and R.M. May. Vaccination against rubella and measles: quantitative investigations of different policies. *Epidemiology & Infection*, 90(2):259–325, 1983.

[171] M.J. Keeling and J.V. Ross. On methods for studying stochastic disease dynamics. *Journal of the Royal Society Interface*, 5(19):171–181, 2008.

[172] D. Husereau, M. Drummond, S. Petrou, C. Carswell, D. Moher, D. Greenberg, F. Augustovski, A.H. Briggs, J. Mauskopf, and E. Loder. Consolidated health economic evaluation reporting standards (cheers) statement. *International journal of technology assessment in health care*, 29(2):117–122, 2013.

[173] G.E. Calabrò, S. Boccalini, P. Bonanni, A. Bechini, D. Panatto, P.L. Lai, D. Amicizia, C. Rizzo, M. Ajelli, F. Trentini, S. Merler, M.L. Di Pietro, C. Primieri, I. Giacchetta, S. Violi, and C. de Waure. Valutazione di health technology assessment (hta) del vaccino antinfluenzale quadrivalente adiuvato: Fluad tetra, last access: 6 agosto 2021. URL `https://www.ijph.it/hta-vaccino-antinfluenzale-quadrivalente-adiuvato-fluad-tetra`.

[174] G.E. Calabrò, S. Boccalini, M. Del Riccio, A. Ninci, F. Manzi, A. Bechini, P. Bonanni, D. Panatto, P.L. Lai, D. Amicizia, A.M. Ferriero, C. Rizzo, F. Trentini, S. Merler, S. Capri, M.L. Specchia, M.L. Di Pietro, S. Mancinelli, L. Sarnari, and C. de Waure. Valutazione di health technology assessment (hta) del vaccino antinfluenzale quadrivalente da coltura cellulare: Flucelvax tetra. *Ital.J.Public Health*, 10:97–122, 2021.

[175] S. Merler, M. Ajelli, B. Camilloni, S. Puzelli, A. Bella, M.C. Rota, A.E. Tozzi, M. Muraca, M. Meledandri, A.M. Iorio, et al. Pandemic influenza a/h1n1pdm in italy: age, risk and population susceptibility. *PLoS One*, 8(10):e74785, 2013.

[176] Istituto Superiore di Sanità. Flunews italia.rapporto della sorveglianza integrata dell'influenza, last access: 2 agosto 2021. URL `https://www.epicentro.iss.it/influenza/flunews`.

[177] Istituto Superiore di Sanità. Sistema di sorveglianza integrata dell'influenza, last access: 2 agosto 2021. URL `https://w3.iss.it/site/RMI/influnet/Default.aspx?ReturnUrl=%2fsite%2fRMI%2finflunet%2f`.

[178] World Health Organization (WHO). Guidance on the economic evaluation of influenza vaccination, last access: 6 agosto 2021. URL `https://apps.who.int/iris/bitstream/handle/10665/250086/WHO-IVB-16.05-eng.pdf?sequence=1`.

[179] ISTAT. Rapporto annuale 2021, last access: 2 agosto 2021. URL `https://www.istat.it/it/archivio/259418`.

[180] S. Capri, M. Barbieri, C. de Waure, S. Boccalini, and D. Panatto. Cost-effectiveness analysis of different seasonal influenza vaccines in the elderly italian population. *Human Vaccines & Immunotherapeutics*, 14(6):1331–1341, 2018.

[181] S. Boccalini, A. Bechini, M. Innocenti, G. Sartor, F. Manzi, P. Bonanni, D. Panatto, P.L. Lai, F. Zangrillo, E. Rizzitelli, et al. La vaccinazione universale dei bambini contro l'influenza con il vaccino vaxigrip tetra® in italia: risultati di una valutazione di health technology assessment (hta). *Journal of Preventive Medicine and Hygiene*, 59(1 Suppl 1):E1, 2018.

[182] Ministero della Salute. Influenza, coperture vaccinali stagione 2019-2020, last access: 2 agosto 2021. URL http://www.salute.gov.it/portale/news/p3_2_1_1_1.jsp?lingua=italiano&menu=notizie&p=dalministero&id=5048.

[183] ISTAT. Demografia in cifre, last access: 2 agosto 2021. URL http://demo.istat.it.

[184] L. Fumanelli, M. Ajelli, P. Manfredi, A. Vespignani, and S. Merler. Inferring the structure of social contacts from demographic data in the analysis of infectious diseases spread. *PLOS Computational Biology*, 2012.

[185] W.E.P. Beyer, A.M. Palache, M. Boulfich, and A.D.M.E. Osterhaus. Rationale for two influenza b lineages in seasonal vaccines: A meta-regression study on immunogenicity and controlled field trials. *Vaccine*, 35(33):4167–4176, 2017.

[186] A.C. Tricco, A. Chit, C. Soobiah, D. Hallett, G. Meier, M.H. Chen, M. Tashkandi, C.T. Bauch, and M. Loeb. Comparing influenza vaccine efficacy against mismatched and matched strains: a systematic review and meta-analysis. *BMC medicine*, 11(1):1–19, 2013.

[187] R. Pebody, J. McMenamin, and H. Nohynek. Live attenuated influenza vaccine (laiv): recent effectiveness results from the usa and implications for laiv programmes elsewhere. *Archives of disease in childhood*, 103(1):101–105, 2018.

[188] S.A. Buchan, S. Booth, A.N. Scott, K.A. Simmonds, L.W. Svenson, S.J. Drews, M.L. Russell, N.S. Crowcroft, M. Loeb, B.F. Warshawsky, et al. Effectiveness of live attenuated vs inactivated influenza vaccines in children during the 2012-2013 through 2015-2016 influenza seasons in alberta, canada: a canadian immunization research network (cirn) study. *JAMA pediatrics*, 172(9):e181514–e181514, 2018.

[189] H. Caspard, R.M. Mallory, J. Yu, and C.S. Ambrose. *Live-attenuated influenza vaccine effectiveness in children from 2009 to 2015–2016: a systematic review and meta-analysis*, volume 4(3). Oxford University Press, 2017.

[190] M. Loeb, M.L. Russell, V. Manning, K. Fonseca, D.J.D. Earn, G. Horsman, K. Chokani, M. Vooght, L. Babiuk, L. Schwartz, et al. Live attenuated versus inactivated influenza vaccine in hutterite children: a cluster randomized blinded trial. *Annals of Internal Medicine*, 165(9):617–624, 2016.

[191] D. Perrotta, A. Bella, C. Rizzo, and D. Paolotti. Participatory online surveillance as a supplementary tool to sentinel doctors for influenza-like illness surveillance in italy. *PloS one*, 12(1):e0169801, 2017.

[192] S. Esposito, L. Cantarutti, C.G. Molteni, C. Daleno, A. Scala, C. Tagliabue, C. Pelucchi, C. Giaquinto, and N. Principi. Clinical manifestations and socio-economic impact of influenza among healthy children in the community. *Journal of Infection*, 62(5):379–387, 2011.

[193] A. Sessa, B. Costa, F. Bamfi, G. Bettoncelli, and G. D'Ambrosio. The incidence, natural history and associated outcomes of influenza-like illness and clinical influenza in italy. *Family practice*, 18(6):629–634, 2001.

[194] ISTAT. Prezzi al consumo.dati definitivi; maggio 2021, last access: 30 maggio 2021. URL `https://www.istat.it/it/files//2021/06/CS_Prezzi-al-consumo_Def_Maggio2021.pdf`.

[195] Struttura Interregionale Sanitari Convenzionati. Accordo collettivo nazionale per la disciplina dei rapporti con i medici di medicina generale, last access: 6 agosto 2021. URL `http://www.sisac.info/aree/www.sisac.info/resources/MEDICINA_GENERALE/ACN_testo_integrato.pdf`.

[196] M.A. Koopmanschap, F.F.H. Rutten, B.M. van Ineveld, and L. Van Roijen. The friction cost method for measuring indirect costs of disease. *Journal of health economics*, 14(2):171–189, 1995.

[197] National Health Care Institute. Guideline for economic evaluations in healthcare 2016, last access: 1 luglio 2021. URL `https://english.zorginstituutnederland.nl/publications/reports/2016/06/16/guideline-for-economic-evaluations-in-healthcare`.

[198] J. Bilcke, S. Coenen, and P. Beutels. Influenza-like-illness and clinically diagnosed flu: disease burden, costs and quality of life for patients seeking ambulatory care or no professional care at all. *PloS one*, 9(7):e102634, 2014.

[199] L. Scalone, P.A. Cortesi, R. Ciampichini, G. Cesana, and L.G. Mantovani. Health related quality of life norm data of the italian general population: results using the eq-5d-3l and eq-5d-5l instruments. *Epidemiology, Biostatistics, and Public Health*, 12(3), 2015.

[200] F.S. Mennini, C. Bini, A. Marcellusi, A. Rinaldi, and E. Franco. Cost-effectiveness of switching from trivalent to quadrivalent inactivated influenza vaccines for the at-risk population in italy. *Human Vaccines & Immunotherapeutics*, 14(8):1867–1873, 2018.

[201] R.G. Woolthuis, J. Wallinga, and M. van Boven. Variation in loss of immunity shapes influenza epidemics and the impact of vaccination. *BMC infectious diseases*, 17(1):1–11, 2017.

[202] M. Baguelin, A. Camacho, S. Flasche, and W.J. Edmunds. Extending the elderly-and risk-group programme of vaccination against seasonal influenza in england and wales: a cost-effectiveness study. *BMC medicine*, 13(1):1–13, 2015.

[203] D. Thorrington, M. Jit, and K. Eames. Targeted vaccination in healthy school children–can primary school vaccination alone control influenza? *Vaccine*, 33(41): 5415–5424, 2015.

[204] R.J. Pitman, L.D. Nagy, and M.J. Sculpher. Cost-effectiveness of childhood influenza vaccination in england and wales: results from a dynamic transmission model. *Vaccine*, 31(6):927–942, 2013.

[205] O. Damm, M. Eichner, M.A. Rose, M. Knuf, P. Wutzler, J.G. Liese, H. Krüger, and W. Greiner. Public health impact and cost-effectiveness of intranasal live attenuated influenza vaccination of children in germany. *The European Journal of Health Economics*, 16(5):471–488, 2015.

[206] H. Houweling, M. Verweij, and E.J. Ruitenberg. National immunisation programme review committee of the health council of the netherlands.criteria for inclusion of vaccinations in public programmes. *Vaccine*, 28:2924–31, 2010.

[207] H.C. Turner, G.E. Thwaites, and H.E. Clapham. Vaccine-preventable diseases in lower-middle-income countries. *The Lancet Infectious Diseases*, 18(9):937–939, 2018.

[208] World Health Organization (WHO). Immunization, last access: 3 February 2022. URL `https://www.who.int/news-room/facts-in-pictures/detail/immunization`.

[209] J. Ruiz-Aragón, Sergio Márquez-Peláez, Ray Gani, Piedad Alvarez, and Richard Guerrero-Luduena. Cost-effectiveness and burden of disease for adjuvanted quadrivalent influenza vaccines compared to high-dose quadrivalent influenza vaccines in elderly patients in Spain. *Vaccines*, 10(2):176, 2022.

[210] World Health Organization (WHO). Influenza (seasonal), last access: 3 February 2022. URL `https://www.who.int/news-room/fact-sheets/detail/influenza-(seasonal)`.

[211] Wayan CWS Putri, David J Muscatello, Melissa S Stockwell, and Anthony T Newall. Economic burden of seasonal influenza in the united states. *Vaccine*, 36 (27):3960–3966, 2018.

[212] A. García, R. Ortiz de Lejarazu, J. Reina, D. Callejo, J. Cuervo, and R. Morano Larragueta. Cost–effectiveness analysis of quadrivalent influenza vaccine in spain. *Human Vaccines & Immunotherapeutics*, 12(9):2269–2277, 2016.

[213] F.G. Sandmann, E. van Leeuwen, S. Bernard-Stoecklin, I. Casado, J. Castilla, L. Domegan, A. Gherasim, M. Hooiveld, I. Kislaya, A. Larrauri, et al. Health and economic impact of seasonal influenza mass vaccination strategies in european settings: A mathematical modelling and cost-effectiveness analysis. *Vaccine*, 40 (9):1306–1315, 2022.

[214] J. Ruiz-Aragón, R. Gani, S. Márquez, and P. Alvarez. Estimated cost-effectiveness and burden of disease associated with quadrivalent cell-based and egg-based influenza vaccines in spain. *Human Vaccines & Immunotherapeutics*, 16(9):2238–2244, 2020.

[215] A. Pérez-Rubio and J.M. Eiros. Economic and health impact of influenza vaccination with adjuvant mf59 in population over 64 years in spain. *Rev.Esp.Quim.*, 31:43–52, 2018.

[216] J. Ruiz-Aragón, A.M. Grande Tejada, S. Márquez-Peláez, and M. García-Cenoz. Estimación del impacto de la vacunación antigripal con adyuvante mf59 en población mayor de 64 años para el sistema nacional de salud: efectos y costes. *Vacunas*, 16(1):6–11, 2015.

[217] K. Haq and J.E. McElhaney. Immunosenescence: influenza vaccination and the elderly. *Current opinion in immunology*, 29:38–42, 2014.

[218] B.L. Coleman, R. Sanderson, M.D.M. Haag, and I. McGovern. Effectiveness of the mf59-adjuvanted trivalent or quadrivalent seasonal influenza vaccine among adults 65 years of age or older, a systematic review and meta-analysis. *Influenza and Other Respiratory Viruses*, 15(6):813–823, 2021.

[219] C. Boikos, M. Imran, V.H. Nguyen, T. Ducruet, G.C. Sylvester, and J.A. Mansi. Effectiveness of the adjuvanted influenza vaccine in older adults at high risk of influenza complications. *Vaccines*, 9(8):862, 2021.

[220] M. Imran, J. Puig-Barbera, J.R. Ortiz, L. Fischer, D. O'Brien, M. Bonafede, J.A. Mansi, and C. Boikos. Relative effectiveness of mf59 adjuvanted trivalent influenza vaccine vs nonadjuvanted vaccines during the 2019–2020 influenza season. In *Open forum infectious diseases*, volume 9(5), page ofac167. Oxford University Press US, 2022.

[221] P. Crepey, E. Redondo, J. Díez-Domingo, R. Ortiz de Lejarazu, F. Martinón-Torres, Á. Gil de Miguel, J.L. López-Belmonte, F.P. Alvarez, Hé. Bricout, and Mí. Solozabal. From trivalent to quadrivalent influenza vaccines: Public health and economic burden for different immunization strategies in spain. *Plos one*, 15(5): e0233526, 2020.

[222] R. Pradas-Velasco, F. Antoñanzas-Villar, and M.P. Martínez-Zárate. Dynamic modelling of infectious diseases: An application to the economic evaluation of influenza vaccination. *Pharmacoeconomics*, 26(1):45–56, 2008.

[223] M. Eichner, M. Schwehm, L. Eichner, and L. Gerlier. Direct and indirect effects of influenza vaccination. *BMC infectious diseases*, 17(1):1–8, 2017.

[224] A.T. Newall, N. Chaiyakunapruk, P. Lambach, and R.C.W. Hutubessy. Who guide on the economic evaluation of influenza vaccination. *Influenza and other respiratory viruses*, 12(2):211–219, 2018.

[225] G.E. Calabrò, S. Boccalini, D. Panatto, C. Rizzo, M.L. Di Pietro, F.M. Abreha, M. Ajelli, D. Amicizia, A. Bechini, I. Giacchetta, et al. The new quadrivalent adjuvanted influenza vaccine for the italian elderly: A health technology assessment.

International Journal of Environmental Research and Public Health, 19(7):4166, 2022.

[226] F. Trentini, E. Pariani, A. Bella, G. Diurno, L. Crottogini, C. Rizzo, S. Merler, and M. Ajelli. Characterizing the transmission patterns of seasonal influenza in italy: lessons from the last decade. *BMC public health*, 22(1):1–9, 2022.

[227] L. Redondo-Bravo, C. Delgado-Sanz, J. Oliva, T. Vega, J. Lozano, A. Larrauri, et al. Transmissibility of influenza during the 21st-century epidemics, spain, influenza seasons 2001/02 to 2017/18. *Eurosurveillance*, 25(21):1900364, 2020.

[228] Instituto Nacional de Estadistica. Population figures.latest data, last access: 10 March 2022. URL `https://www.ine.es/dyngs/INEbase/en/operacion.htm?c=Estadistica_C&cid=1254736176951&menu=ultiDatos&idp=1254735572981`.

[229] Ministerio de Sanidad. Coberturas de vacunación.datos estadísticos, last access: 10 March 2022. URL `https://www.sanidad.gob.es/profesionales/saludPublica/prevPromocion/vacunaciones/calendario-y-coberturas/coberturas/home.htm`.

[230] Ministerio de Sanidad Consumo y Bienestar Social. Recomendaciones de vacunación frente a la gripe.2021–2022, last access: 3 February 2022. URL `https://www.mscbs.gob.es/profesionales/saludPublica/prevPromocion/vacunaciones/programasDeVacunacion/docs/Recomendaciones_vacunacion_gripe.pdf`.

[231] C. Zipfel, V. Colizza, and S. Bansal. Double trouble? when a pandemic and seasonal virus collide. *MedRxiv*, 2021.

[232] European Medicines Agency. Fluad tetra.summary of product characteristics, last access: 3 February 2022. URL `https://www.ema.europa.eu/en/documents/product-information/fluad-tetra-epar-product-information_en.pdf`.

[233] Istituto Superiore di Sanità. Sorveglianza passi d'argento, last access: 3 February 2022. URL `https://www.epicentro.iss.it/passi-argento/dati/croniche#dati`.

[234] C.R. Meier, P.N. Napalkov, Y. Wegmüller, T. Jefferson, and H. Jick. Population-based study on incidence, risk factors, clinical complications and drug utilisation associated with influenza in the united kingdom. *European Journal of Clinical Microbiology and Infectious Diseases*, 19(11):834–842, 2000.

[235] C. Lucioni, B. Costa, and A. Sessa. I costi dell'influenza in italia. *Farmeconomia.Health economics and therapeutic pathways*, 2(1):11–18, 2001.

[236] M. Marchetti, U.M. Kühnel, G.L. Colombo, S. Esposito, and N. Principi. Cost-effectiveness of adjuvanted influenza vaccination of healthy children 6 to 60 months of age. *Human Vaccines*, 3(1):14–22, 2007.

[237] Ministerio de Sanidad. Acuerdo marco para la seleccion de suministradores de vacunas frente a la gripe estacional 2021–2025, last access: 3 February 2022. URL https://contrataciondelestado.es/wps/wcm/connect/7c41cd41-00c8-4c07-be3d-272d29585268/DOC20210419131140PCAP+Gripe+2021-2025.pdf?MOD=AJPERES.

[238] Consejería de Hacienda. Boletin oficial de la region de murcia.numero 54, miercoles 6 de marzo de 2019, last access: 3 February 2022. URL https://www.borm.es/services/anuncio/ano/2019/numero/1263/pdf.

[239] Departamento de Salud. Pais vasco: Gobierno vasco.osakidetza.tarifas para facturacion de servicios sanitarios y docentes de osakidetza para el año 2021, last access: 3 February 2022. URL https://www.osakidetza.euskadi.eus/servicios-on-line/-/servicios-para-empresas/.

[240] Ministerio de Sanidad. Registro de altas de los hospitales generales del sistema nacional de salud.cmbd.norma estatal.norma apr-grd 2019 v.35, last access: 3 February 2022. URL https://www.mscbs.gob.es/estadEstudios/estadisticas/cmbd.htm.

[241] R.W. Dal Negro, P. Turco, and M. Povero. Cost of influenza and influenza-like syndromes (i-lss) in italy: Results of a cross-sectional telephone survey on a representative sample of general population. *Respiratory Medicine*, 141:144–149, 2018.

[242] J. López Bastida, J. Oliva, F. Antoñanzas, A. García-Altés, R. Gisbert, J. Mar, and J. Puig-Junoy. Propuesta de guía para la evaluación económica aplicada a las tecnologías sanitarias. *Gaceta Sanitaria*, 24(2):154–170, 2010.

[243] J.A. Sacristán, J. Oliva, C. Campillo-Artero, J. Puig-Junoy, J.L. Pinto-Prades, T. Dilla, C. Rubio-Terrés, and V. Ortún. What is an efficient health intervention in spain in 2020? *Gaceta sanitaria*, 34(2):189–193, 2019.

[244] L. Vallejo-Torres, B. García-Lorenzo, and P. Serrano-Aguilar. Estimating a cost-effectiveness threshold for the spanish nhs. *Health economics*, 27(4):746–761, 2018.

[245] A. Angelis, A. Lange, and P. Kanavos. Using health technology assessment to assess the value of new medicines: results of a systematic review and expert consultation across eight european countries. *The European Journal of Health Economics*, 19(1):123–152, 2018.

[246] World Health Organization (WHO). Regional office for europe recommendations on influenza vaccination for the 2020/2021 season, last access: 3 February 2022. URL https://apps.who.int/iris/bitstream/handle/10665/335721/WHO-EURO-2020-1141-40887-55342-eng.pdf?sequence=1&isAllowed=y.

[247] A.J Leidner, N. Murthy, H.W. Chesson, M. Biggerstaff, C. Stoecker, A.M. Harris, A. Acosta, K. Dooling, and C.B. Bridges. Cost-effectiveness of adult vaccinations: A systematic review. *Vaccine*, 37(2):226–234, 2019.